POTENTIAL FLOW STUDIES

OF

LIFT-FAN INFLOW INTERFERENCE PHENOMENA

by

J. C. Wu, R. Sigman
J. Hubbartt, H. McMahon

School of Aerospace Engineering
Georgia Institute of Technology
April 1, 1973

ABSTRACT

This report presents results of a study of the lift-fan inlet problem and includes a comprehensive survey of the existing experimental data and analytical methods, an analysis of the potential flow, and a boundary layer analysis for lift-fan inlets. Numerical solutions are presented for potential flows associated with inlet ducts set in an infinite plane with and without a centerbody simulating the hub of the fan. The effects of the crossflow to mean inlet velocity ratio, of the inlet and hub lip radii to duct width ratio, of the inclination of the duct axis to the plane, and of the position of the hub relative to the plane on the flow in and near the inlet ducts are discussed utilizing a two-dimensional potential flow analysis. The maximum crossflow velocities without inlet flow separation are estimated and the effects of the various design variables on the crossflow velocity are explored by means of the boundary layer analysis.

TABLE OF CONTENTS

LIST OF TABLES

LIST OF FIGURES

A_{ij} matrix describing the normal velocity on a surface element due to a unit source density distribution on the surface.

A constant in equation (42)

B constant in equation (42)

C_f friction coefficient

D width of the duct

D_i matrix describing the boundary values of the normal velocity on a surface element

d depth of a plane across the inlet duct measured from the plane of the plate

e unit vector in the direction of the freestream velocity

F prescribed component of velocity on the body surface normal to the surface

h_{2j+1}, h_{2j-1} magnitude of the distance from P' to s_{2j+1} or s_{2j-1}

k modulus of complete elliptic integrals

L distance along a plane in the inlet duct measured from the midpoint of the plane

ℓ distance from simulated leading edge to duct centerline

M Mach number

N the body is described by $N + 1$ points

n unit vector normal to the body surface directed into the flow region

P pressure

P' general point in the flow field

p' point on the body surface

q point on the body surface in terms of dummy variables of integration

R	duct half width
R'	region of potential flow
Re_l	Reynolds number $V_d \, l/\nu$
R_{ij}	influence coefficient for the r-component of velocity at ith segment due to jth segment
r	duct lip radius
r'	radial coordinate in cylindrical coordinate system
$\tilde{r}$	distance between points p' and q
S	denotes the inlet surface
s	distance along the inlet surface
t	unit vector tangential to the body surface
u	component of the velocity in the x-direction
V	velocity
V_n	velocity normal to a plane in an inlet duct
v	component of the velocity in the y-direction
v'	component of the velocity in the r'-direction
X_{ij}	influence coefficient for the x- or x' component of velocity at ith segment due to jth segment
x	distance from the centerline of inlet in the plane of the plate
x'	distance along the centerline of the inlet measured from the plane of the plate
Y_{ij}	influence coefficient for the y-component of velocity at ith segment due to jth segment
y	distance normal to the flat plate surface
y'	distance from surface normal to surface
z	direction of the generators for two-dimensional flow
α	angle of inclination of a surface element

β angle subtended by the vectors from point P to s_{2j+1} and s_{2j-1}

γ angle of flow inclination in the duct

δ boundary layer thickness

δ^* boundary layer displacement thickness

ζ dummy integration variable in the z-direction

η dummy integration variable in the y-direction

θ circumferential coordinate in cylindrical coordinate system

θ' dummy integration variable in the θ-direction

ν kinematic viscosity

ξ dummy integration variable in the x-direction

ρ density

ρ' dummy integration variable in the r'-direction

σ surface source strength, i.e., the total outward volume flux divided by 4π per unit source surface area

τ shear stress

τ_w shear stress at wall

φ potential function

Subscripts

a   first basic solution

b   second basic solution

cs   control station

d   duct

e   at boundary layer edge

max   maximum

min   minimum

1   portion of inlet surface, S , consisting of a solid surface

2   portion of inlet surface, S , with surface suction

∞   freestream

I. INTRODUCTION

In recent years an increasing emphasis has been placed on VTOL and
STOL technology because of military and civilian needs. There are many
possible types of such aircraft, and there are several different lift systems
for achieving V/STOL capability. The lift fan concept, wherein a ducted
fan generates thrust directed downward, is suitable for high performance
fighter roles and is also applicable for transport aircraft.

At the present stage of development the lift fan aircraft suffers
from uncertainty in performance during the hovering and transition phase
of the flight. There is a need for a suitable theory for predicting the
flow field induced by a fan located in an aerodynamic surface since this
induced flow is ultimately responsible for a large portion of the thrust as
well as for the aerodynamic and dynamic behavior of the aircraft during hover-
ing and the transition to forward flight.

The overall problem of the fan-induced flow interaction is logically
divisible into two parts, namely, the efflux problem and the inflow problem.
During the past several years the efflux problem has received considerable
attention. Several analytical models are available which offer the possibility
of semi-empirically predicting the interference effects using potential flow
representations.

The lift-fan inflow problem is considered in the present work. A
literature survey was made to review the state of the art and to determine

the geometric dimensions and magnitudes of various parameters of practical interest in the fan inlet problem. These guided the choice of parameters in the analytical studies that followed. It was concluded from the survey that the best analytical method for the three-dimensional problem is that of Stockman (Ref. 42) which generates approximate three-dimensional solutions based on a succession of axi-symmetric solutions.

The present potential flow analyses were primarily directed toward: (1) finding ways of reducing the velocity peak and accompanying adverse pressure gradient on the forward inlet lip and the aft centerbody lip (since such peaks lead to boundary layer separation); (2) finding means of reducing the flow non-uniformity in the inlet duct (which causes poor fan efficiency). Solutions are presented for two types of inlet geometry: a single inlet duct set in an infinite plane and an inlet containing a centerbody simulating the hub of an inlet fan. Two-dimensional and axi-symmetric flows are considered.

The boundary layer study in this work utilizes the results of the two-dimensional potential flow analysis. The study had three objectives: (1) to establish estimates of the maximum cross-flow velocities without inlet flow separation; (2) to explore the effects of various design variables on the maximum cross-flow velocities without inlet flow separation; (3) to determine the relative magnitude of the boundary layer displacement thickness.

II. LITERATURE SURVEY

Lift for vertical takeoff can be generated by directing the thrust of a jet or propeller vertically downward. This might be accomplished by swiveling the engines, by using separate lift and cruise jet engines, by using a lifting fan mounted in the wing-chord plane, by tilting the wing-propeller combination or by using louvers to direct the thrust. The following literature survey will consider one such method - the fan mounted in the wing-chord plane, or the so-called "fan-in-wing" concept. The interaction of the flow induced by the fan located in an aerodynamic surface with the flow over that surface forms a central problem of lift-fan aircraft aerodynamics and is ultimately responsible for the aerodynamic and dynamic behavior of the aircraft during hovering and transition to forward flight. This survey will concentrate on the fan inflow problem.

The first free-flight demonstration of direct-jet-lift was made in 1954 (Ref. 1). During this period many schemes were proposed for producing lift at zero or low forward speeds by means of a fan-in-wing, but no data were available for a configuration of this type. In 1957 Hickey (Ref. 2) made a preliminary experimental investigation of a fan in wing by cutting a hole in the center of a two-dimensional wing model and mounting a six-blade propeller in the hole. No special effort was made to design the entrance shape. During

3

the same year General Electric (Ref. 3) began initial hardware testing on a lift-fan propulsion system.

Hickey and Ellis (Ref. 4) in 1959 improved on the measurements made in Reference 2. An aspect ratio 4 semispan model was used with a fan rotating in the plane of the wing. An inlet was fitted in the wing and inlet radii of 5- and 10-percent of the inlet diameter were tested. The tip clearance between the propeller tip and the duct was 0.06 propeller radius. No centerbody was fitted over the propeller hub, but an inlet and outlet cascade of vanes could be fitted as inflow and outflow guides. Total pressure surveys made just below the fan showed a considerable amount of distortion of the flow through the propeller which was reduced by using the inlet vanes. Installation of the inlet vanes caused no loss in static lift and only a slight increase in power as long as the vane angles were properly adjusted. Minimum pressure coefficients at the wing leading edge and duct inlet radius were presented as a function of propeller force coefficient for three different forward speeds.

Duvivier and McCallum (Ref. 5) studied an articulated rotor mounted in a finite wing. The rotor had a bellmouth inlet of radius 8.3% rotor diameter, which was larger than the minimum value of 6% rotor diameter which had been found necessary by other investigators (e.g., Ref. 6) to avoid inlet separation in tests of shrouded propellers in hover. Visual observation of wool tufts cemented to the wing indicated that inlet separation consistently occurred for values of the ratio flight velocity/mean inflow velocity to the rotor above about 0.40 to 0.60. These observations were verified by measurements of duct velocity distribution on the inflow side of the fan. For values of this velocity ratio greater than 1.0 the flow at the inlet showed evidence of skirting around the duct in the direction of fan rotation, with outflow at

4

the rear of the inlet. The authors concluded that a major problem with a fan in wing is the control of inlet separation in forward flight and that emphasis should be placed on the design of inlet shapes and flow control devices (e.g. vanes) for best results in forward flight. They suggested consideration of inclining the duct in the wing in the fore and aft direction as a means of alleviating inlet separation.

Some of the first detailed flow measurements just upstream and down-stream of a fan in a wing were made in England by Gregory, Raymer, and Love (Ref. 7). A 15% thick 64-in. chord, rectangular wing model was fitted with a 13-in. diameter fan with the fan axis at the 35% chord location. The 21-blade fan had a hub/diameter ratio of 0.5 and was located 0.20 duct diameters below the surface. The duct had a lip radius of 10% of the duct diameter and the fan hub had a blunt base. With the fan situated just below the inlet flare, the flow velocity into the fan had a considerable gradient from front to rear, with a speed ratio of 2:1 (high speeds at front) being observed at a value of forward velocity/mean inflow velocity of 0.55. This maldistribution was attributed to incomplete turning of the flow into the duct. When the fan was later submerged one duct diameter below the entry the underturning of the flow was largely eliminated, though at the expense of increasing the adverse effects of any flow separation on the turn of the inlet lip. In this regard, an inlet flare radius of 10% duct diameter gave rise to flow separation even under zero-forward speed conditions. A modified inlet changing continuously from a radius of 23% inlet diameter at the front of the duct to 11% at the rear eliminated flow separation up to a forward speed of 0.28 times the mean speed through the fan. A simple slat to control the boundary layer raised this

5

maximum speed ratio to 0.39. It was felt that slat design refinements or
other means of boundary-layer-control, coupled with consideration of hub
shape and location, could probably improve on these figures. A crude inlet
cascade reduced the flow divergence from the axial direction but at a large
penalty in increased drag. On the exit side of the fan the flow variations
were found to be all somewhat less than upstream and the interaction between
the efflux and the mainstream had very little upstream influence. All of this
suggested that placing the fan close to the bottom of the duct would be
benefitial if the depth of the duct is limited.

The lift fan need not be mounted in the wing but may instead be mounted
in the fuselage of the vehicle. The first large-scale wind tunnel tests of such
a configuration were performed by Maki and Hickey (Ref. 8), Trebble and
Williams (Ref. 9) and Aoyagi et al (Ref. 10). This fuselage arrangement has
the advantage that the fan can be mounted in a deep duct so that the flow has
a chance to adjust to the turn at the inlet before entering the fan. Results
of the tests of Reference 8 showed that the fan thrust was independent of
airspeed.

Analytical predictions of the potential flow behavior of an inlet
without centerbody were reported by A.M.O. Smith in Reference 11. Surface
velocity data for inlets were presented as a function of developed distance
for the pure inflow case. Smith's method, first formulated by Flügge-Lotz
(Ref. 12) and adapted to the electronic computer by Smith and Pierce (Ref. 13),
utilizes a distribution of source density on the surface of the body and solves
for the distribution necessary to meet the specific boundary conditions.
Reference 13 applies the method to arbitrary bodies of revolution whose axes
are parallel to the stream direction (i.e. axisymmetric flow) while Hess in

6

Reference 14 describes an analogous procedure for computing the flow about bodies of revolution whose axes are perpendicular to the stream direction.

The first VTOL-directed fan research at the National Research Council of Canada was reported by Fowler (Ref. 15). This work was done in support of design studies and comprised testing 12-in. diameter fans with hub/tip ratios of 1/4, 1/3, and 1/2 with symmetric inlet bellmouths having lip radius/fan diameter ratios of 1/24, 1/12, 1/6, 1/4, 1/3, and 1/2. Most tests were under static conditions; some were in crossflow. The conclusion from static tests was that for gross disc loadings up to 200 lb/ft^2 a bellmouth lip radius ratio of not less than 1/12 is advisable; for higher disc loadings the ratio should increase to 1/6 or higher. Also, the hub should be of the order of 50% of the tip diameter. Wool tuft studies in crossflow showed no pre-swirl in front of the fan.

The result that the fan thrust was independent of airspeed for a fan-in-fuselage as quoted in Reference 8 is in contrast to the results given by Hickey and Hall in Reference 16 where the fan was mounted in the wing of a large-scale model. The work of Reference 16 is a similar investigation to that at small-scale reported in Reference 4. (Full-scale wind tunnel studies of lifting-fan aircraft were begun at NASA Ames in 1960, when the General Electric X353-5 propulsion system became available (Ref. 17). A good summary of work in England to this time is found in Reference 18 . The fan in Reference 16 was mounted with the axis at 40% local chord. The fan had a 62.5 inch diameter with a single rotor of 36 blades. The inlet was fitted with three different articulated vane arrangements. The hub to fan diameter ratio was 0.42 and the lip inlet radius was 6% of the hub diameter. It was found that fan thrust decreased with increasing airspeed for all inlets tested.

Exit survey rake data indicated that fan internal performance suffered because of ineffective turning of the mainstream air. Chordwise wing surface pressure distributions through the fan axis and at several spanwise stations were presented as a function of exit-vane angle, tip-speed ratio, and wing flap deflection.

The experiment quoted above was for a shoulder-mounted wing configuration. These studies were extended by Kirk et al in Reference 19 to a model with a midmounted wing having approximately 50% larger fan-to-wing area ratio than the model reported in Reference 16. That is, the ratio of the area of the two fans to total wing area in Reference 16 was 0.10; in Reference 19 it was 0.15. In both cases the fan diameter represented about 45% of the local wing chord, and the same fan and inlet lip installation was used. No surface pressures were measured.

The work by Gregory et al (Ref. 7) was extended by the same authors in Reference 20. The research was done with the same basic model and was primarily to examine fan efflux effects, but a number of devices were examined to improve the inlet flow conditions. None were very successful. An attempt was made to "two-dimensionalize" the flow entering the duct by fitting a pair of large fins on the upper surface of the wing just outboard of the bellmouth. The resulting corner between the fin and the outer edge of the inlet flare produced separation of the fin boundary layer and consequent poor flow into the duct. The authors concluded that a closely pitched cascade would give more uniform inflow than any devices which they tested.

Turner and Sparks (Ref. 21) tested a 20-in. diameter fan (hub/tip ratio 0.5) mounted in the floor of a low-speed wind tunnel. Three inlets were tested with lip radius/tip diameter of 7%, 15%, and 25%. Previous work

8

had shown the 15% inlet to perform satisfactorily without crossflow (i.e. statically). Pressure distributions were measured at depths of 22% and 29% of duct outer diameter. The data indicated that even the intake with the smallest edge radius would give unstalled fan operation in crossflow. A maldistribution of inlet flow was noted and this had an effect on overall fan performance. With the smallest lip radius, the effect of pressure loss was greater than the maldistribution; with the largest lip radius the maldistribution effect predominated. The effects of pressure disturbances in the region of the fan attenuated rapidly in the upstream direction.

A combined analytical and experimental attack on the inlet problem was reported by Schaub and Cockshutt in 1964 (Ref. 22). A potential flow solution for crossflow into a curved bellmouth (i.e., a two-dimensional slot inlet) was obtained by using a Schwarz-Christoffel transformation. The inlet bellmouth had an approximately circular contour whose radius varied between zero (sharp corner) and 1/2 the inlet passage width. The surface contour generated by the transformation was not particularly desirable, in that discontinuities in the second derivatives of the contours generated lead to abrupt changes in pressure gradient. From the point of view of achieving an even velocity into a lifting fan, depth below the inlet surface was found to be the most valuable geometric aid, while the effects of bellmouths radius ratio are confined (in the potential flow model) to an area within one or two passage widths of the inlet. Surface velocity data comparable to that of Reference 22 for zero crossflow had been presented by Smith (Ref. 11) who used a distributed source technique. A comparison showed that the magnitude and location of the velocity peaks are very similar for the two methods; however, matching of the second derivative at the points of tangency in Smith's study resulted in a smoother

velocity curve. The two-dimensional results presented in Reference 22 show
that in the case of a crossflow velocity equal to the inlet velocity, the
velocity peak at the leading lip is about twice the value without crossflow.
The experimental results reported in Reference 22 were performed with a 14-inch
diameter suction duct attached to an 80-inch chord NACA 0015 airfoil. The
inlets tested were annular with centerbody/outside diameter ratio of 0.50
and were located at 35% wing chord. The inlet lip and centerbody top were
faired into the wing contour. Three basic inlets were tested — two were
symmetric with lip radius/outside diameter ratio of 9% and 25% and one was
asymmetric with an elliptic leading lip and circular trailing lip. The 9%
inlet was tested with four different inflow aids: a closure plate cambered
to fit the upper wing contour (to see if it would act as a ram device to
deflect air downward during forward flight), a cascade of 15 inlet guide vanes,
a perforated wall section below the leading lip lower tangent point, and a
trip fence located near the wing leading edge. The last two aids were used
for boundary layer control experiments. None of the three basic inlets gave
satisfactory inlet flows under cross-flow conditions; strong positive pressure
gradients appeared on the curved walls and caused the boundary layer to
separate. The 9% inlet performed very efficiently under static inflow condi-
tions. The closure plate was found to be an effective device for increasing
the ram recovery of the inlet and seemed especially well suited for in-flight
starting of lift fans. The trip fence showed that flow separation on the
leading edge lip may be delayed effectively by forcing the boundary layer to
become turbulent before entering the inlet (even at free stream/inflow velocity
ratio 0.5 at 12.5° angle of attack). With optimum bleed, the boundary layer
suction device completely averted separation for all test crossflow values at

zero incidence; however, the required relative mass flow to reattach the separated flow was high (10% of the suction flow at velocity ratio unity).

The work of Schaub et al in Reference 22 is further described in Reference 23. Based upon the potential flow (transformation) model the results suggest the use of a "trumpet" shaped inlet lip which would have at optimum a monotonically accelerating flow for all inlet flow velocity ratios between zero and unity. The authors propose three parameters for assessing over-all inlet performance: (1) velocity distortion index — the ratio of average velocity in the z direction based on the active flow area to the design inlet velocity (i.e. the average velocity in the z direction based on the full annulus area). As the inlet flow degenerates due to flow separation, the index value increases from a minimum value of 1.0; (2) flow misalignment angle — the angle whose tangent is the average x (streamwise) momentum divided by the average z momentum. This angle is a direct measure of distortion; (3) average total pressure loss parameter — loss in stagnation pressure divided by axial dynamic pressure. This ratio is useful as a pressure distortion index.

The experiments of Fowler (Reference 15) were continued by Schaub and Bassett (Ref. 24) in order to make a detailed performance analysis of a highly-loaded fan-in-wing configuration under static inflow conditions. A 12-inch diameter fan (hub/tip radius ratio 0.5) was mounted in a NACA 0018 airfoil with the axis at 37% chord. Inlet and centerbody fairings of $16\frac{1}{2}\%$ and 25% of fan diameter, respectively, were used. Good entry flow (no separation) was observed up to fan loadings of 500 p.s.f. It was noted that crossflow will distort the inlet flow field badly so that a fan giving satisfactory performance under static conditions will not perform as well under crossflow conditions.

Further experiments with the same fan-in-wing model as in Reference 22 are reported by Schaub in Reference 25 for a velocity ratio from zero to 1.5. He noted that this suction model gives an erroneous boundary condition in that the flow upstream of the rotating fan will be altered by the fan's ability to tolerate distortion. Measurements were made in an inlet annulus plane at a depth of 25% the annulus outer diameter. Again the author pointed out the excellent performance of the boundary layer control aids and concluded that inflow distortion, while a function of forward speed, becomes much worse only because of boundary layer separation and large positive wing incidence angles. However, even with leading lip separation prevented the velocity gradient of the inflow is not improved since the velocities at the trailing lip were substantially less than those at the leading lip. The 9% inlet exhibited a 25% gradual velocity increase from the trailing lip to the leading lip in a chordwise direction at a velocity ratio of 0.25, just prior to leading lip stall. However, contrary to the results of Reference 7, the inlet flow remained fully attached in the 9% inlet at zero forward speed. Fan performance deterioted rapidly for inflow ratios above 0.3 with a 9% (or smaller) inlet. The author noted that of the three basic inlets the 25% inlet exhibited flows that were of a more two-dimensional character than the others (the equi-velocity lines running in the spanwise direction) although there was a general tendency for the inlet plane flowfield to appear quasi-two-dimensional. The asymmetric inlet experienced large spanwise flows and therefore had the more undesirable inflow field. The distribution of such flow variables as velocity, total pressure, swirl, and inflow-to-axis angle was a strong function of inlet geometry, degree of flow separation, and wing incidence angle. Maximum local velocity and swirl angle were strongly dependent on inflow ratio

and wing incidence and were of such a magnitude as to constitute a serious problem to a fan. Leading lip separation, a function of inflow ratio, forward speed, and wall boundary condition, contributed seriously to the general problem of inflow distortion. Schaub concluded that the shuttered inlet cannot be considered a practicable inflow aid in view of the difficulty in setting the vanes individually for every new condition and its inadequate performance.

Tyson (Ref. 26) pointed out that the design requirements for lift-jets are much the same as for lift-fans. The inlet must turn the engine air flow through 90° and yet prevent excessive total and static pressure distortion. The bellmouth lip must have a reasonably small radius in order to permit close spacing of adjacent engines. A typical jet module tested had a centerbody/outside diameter ratio of 0.33 and two ratios of lip radius to outside diameter of 20% and 47%. The former exhibited unacceptable flow separation at a freestream to engine face velocity ratio of 0.6 and the latter at ratio 0.8, the engine face measuring station being one-half diameter inside the inlet. Scoops and vanes were tested and it was concluded that a scoop inlet is required for acceptable engine restart performance. The starting cycle before landing imposes a more stringent design requirement for minimizing inlet-flow distortion than does the takeoff mode since before restart the inlet behaves like a static pressure orifice and very large values of velocity ratio will be present until engine acceleration has been accomplished.

In all experiments with fan outflow there arises the question of the significance of wall effects. This was investigated in Reference 27. Significant wall effects were encountered with a model in a small test section but adequate corrections could be calculated.

Further research on the inlet problem as applied to lift jets is reported by Kuhn and McKinney in Reference 28. They found that simple

13

bellmouth inlets of adequate lip radius (about one-half the inlet throat diameter) gave reasonably high pressure recovery and low flow distortion throughout the transition region for lift engines. Scoop inlets are needed to give adequate windmilling characteristics. One of the more important results of this work was that, for this case of a lift engine in a fuselage (fuselage depth about two fan diameters) there was little or no mutual interference effect between the inlet and exit flows. This was determined by running the inlet and exit separately (by suitable auxiliary piping) and then simultaneously. This suggests that the inlet and efflux interference of the fan-in-wing combination may be attainable to good accuracy by summing the results of the two interference phenomena.

The status of lift-fan technology in 1965 is given in a paper by Dickard (Ref. 29) wherein the Army XV-5A lift-fan research vehicle, which first flew in 1964, is used as a basis for discussing improved lift-fan technology. The XV-5A employed a 62-inch diameter fan in each wing having an operating pressure ratio of 1.09, a 0.4 radius ratio, tip speed at design point 720 ft/sec. and fan discharge velocity of 405 ft/sec. The fans were driven by tip turbines (Ref. 30).

Further applications of the source-density potential flow method of solution were given by Hess and Smith in Reference 31. Calculation of flows about simple closed bodies is straightforward by this method, and extensions of the method to axisymmetric inlets, shrouds, and ducts with internal flow are discussed. A thorough review of this method (with an extensive bibliography) was given by Hess and Smith in Reference 32. Applications of the method to two-dimensional shapes, axisymmetric shapes, fully three-dimensional shapes, and extensions to nonuniform flows, unsteady flows, added mass, and

two-dimensional free surface effects are presented. In particular, a solution for a flush inlet in an infinite plane with a uniform flow parallel to the plane is given. The inlet was considered both as a two-dimensional body and as an axisymmetric body whose symmetry axis is the center line of the inlet. By superposition the flow for any ratio of inlet velocity to freestream velocity can be obtained. Data is shown for the case when the ratio is unity.

Another analytical approach to the fan-in-wing problem was given by Rubbert, et al, in Reference 33. This is a general method applicable to completely three-dimensional flows and to arbitrary wing and inlet geometry, fan inflow distribution, thrust vectoring, angle of attack and yaw, and flight speeds from hover through transition. A numerical potential flow solution is obtained by a source and vortex representation on the boundary surface composed of small source-sheet panels distributed over the exterior wing surfaces, internal vortex filaments that emanate from the wing trailing edge to provide circulation and to produce the trailing vortex sheet, and a vortex lattice across the fan face and along the periphery of the fan efflux. Source and vortex strengths are found by satisfying boundary conditions at a finite number of points on the boundary surfaces. A boundary layer theory is included to investigate the boundary layer along streamlines, particularily in the inlet region, but the aerodynamic effects of boundary layer thickening or separation are not included in the theory. The computer time needed to solve a problem is a function of the number of singularities used to represent a configuration — for a sophisticated fan-in-wing problem an hour or more of central processor time on a CDC 6600 digital computer is required. A computed case was compared with the experimental results of Hickey and Hall (Ref. 16). The theoretical force calculations depend strongly on the fan forces, which

were obtained from assumed inflow and fan exit flow distributions. The two inflow distributions investigated, uniform and with a sinusoidal variation around the fan face, produced values for lift below and above the experimental data, respectively. Comparisons of theoretical and experimental pressure distributions with the lift fans operational were in qualitative agreement, with rather large deviations near the fan inlet which were probably caused by inaccuracies in the assumed inflow distribution.

Lavi (Ref. 34) conducted full-scale tests of VTOL lift-engine and inlet/door configurations. Bellmouth radii varied from 28% to 47% of the inlet diameter. He concluded that it is unlikely that plain inlets can achieve the needed pressure recovery together with a tolerable distortion level to permit inflight engine starting. Simple doors or scoops, however, provided the required performance improvement.

An updating of the technology in the General Electric X-353-5 fans used in the XV-5A was reviewed by Przedpelski in Reference 35. The emphasis is on reduced fan dimensions, higher lift to weight ratio (at least 20:1), higher tip turbine temperatures, and improvements in cross-flow performance. Studies showed that efficient lift fans could be installed in 5% - 6% thickness ratio delta wings with 70 psf wing loading. Inlet scoops which double as fan closures could be installed with no lift penalty in hover but do not improve the fan performance in crossflow. Large fans of 30,000 pounds lift (lift/weight ratio > 21) could be built within the existing state of the art.

Data from large scale V/STOL models powered with lift fans were summarized by Hickey and Cook (Ref. 36). In particular, the effectiveness of boundary layer control on inlet performance at forward speed is discussed. One test involved an XV-5A type fan mounted in a 5% thick wing so that the

outboard portion of the fan front frame and inlet had to be removed. The outboard 180° of the inlet was replaced by a circumferential slot which supplied a jet of high velocity air over a small radius (less than one inch in some places). Over the inboard 180° the wing was thick enough for a normal XV-5A inlet. At zero forward speed the blowing provided large gains in dynamic pressure at the fan exit on the side of the fan where performance was dependent on boundary layer control. The other side of the fan also showed significant improvement when boundary layer control was applied. Thus, boundary layer control on only half the fan circumference improved flow through the whole fan. For a boundary layer control thrust of 3% of fan thrust, fan thrust was increased 30%. At forward speed, the thrust was somewhat higher with boundary layer control than with a conventional lift fan. Lift at forward speed was increased 25% with a ratio of boundary layer control to fan momentum of 8% while at a ratio of forward velocity to mean inflow velocity of 0.5.

Further tests on inlet models were reported by Schaub (Ref. 37) in 1968. Four inlets in turn were installed in an NACA 0015 profile with chord length 80 inches and aspect ratio 3/2. The inlet duct axis was at the 35% chord station, the centerbody diameter being 50% of the outer diameter of the annulus. One inlet had a constant radius (9%) lip; the second inlet had a square-edged centerbody and outer lip; the third inlet was an asymmetrically shaped trumpet, while the fourth inlet comprised an assembly of mixed vanes (radial and annular segments) in the 9% inlet. The measuring planes were at an inflow depth of one-fourth and one-eighth the outer annulus diameter. Inflow was attained by suction external to the model. It was found that inflow distance was a powerful factor in achieving flow uniformity at all forward speeds (velocity ratios of 0 - 0.7 were tested). However, near-surface

velocity peaks at the inner wall still persisted. For any given depth installation, small lipped inlets are preferrable to large lipped inlets from a flow distortion (flat velocity profile) point of view, provided that separation can be avoided; inlets with small lip radii feature large surface velocity peaks. It was observed that it was possible to extend the attached flow regime observed for circular arc lipped inlets through the use of a leading lip contour featuring a radius of curvature that increased with inflow distance. Velocity nonuniformity, the flow misalignment level, and the extent of separated flow were substantially lessened by the insertion of a radial/annular segment vane configuration, but with an associated rise in total pressure loss.

There is a lack of experimental data on two-dimensional (i.e. slot) inlets. One such test was reported by Tyler and Williamson in Reference 38. A 31.5% thick airfoil with 4-foot span and 3-foot chord was fitted with a spanwise suction slot at 65% chord. The slot width was 5% chord with an entry radius equal to the width. Air was drawn through the slot by an off-site exhauster. Pressure distributions on the basic contour and inlet lips were taken at centerspan at wing incidence of 5, 15, and 25 degrees for a range of suction coefficient from zero to 2.3. In general, relatively small levels of suction were sufficient to prevent separation upstream of the slot; a stagnation point appeared on the downstream lip. With increasing suction a strong suction peak developed on the upstream lip and the downstream stagnation point tended to move rearward.

Graham (Ref. 39) used a simple momentum theory to analyze the effect of inlet-momentum forces on aircraft in transition. The analysis is based on the addition of freestream flow with the static-induced flow at the inlet,

18

which is represented by a sink flow over a hemispherical control surface. It is shown that the lift-fan inlet develops significantly greater lift, drag, and moment than the lift-jet inlet at comparable thrust and forward speed. Results agree reasonably well with the limited amount of inlet force and moment data available; further applicable experiments were recommended.

Shumpert and Harris (Ref. 40) report an experimental investigation of lift engine total pressure recovery and total and static pressure distortion during hover and transitional flight of a full-scale Lockheed XV-4B aircraft. In this aircraft the use of ram air for in-flight engine starting was not a requirement, and the inlet configuration tested was designed to be independent of inlet closure doors. Since other investigators had found that to provide good static performance a contraction ratio of at least 33% is required, the inlet used was designed to exceed this minimum. The inlet had a forward lip radius-to-inlet diameter of 47%; the inlet was not symmetrical because of the constraints of the fuselage contour. An auxiliary lip was fitted inside the fuselage contour to give a ram scoop effect to unload the basic lip. With this arrangement, total and static pressure distortions were generally less than 10% in the VTOL operational envelope. Engine power and relative wind speed were found to exhibit independent influence on the pressure distortion.

The incompressible potential flow numerical method developed by Smith and others at Douglas (Refs. 13, 31, 32) was applied by Stockman and Lieblein (Ref. 41) to the case of axisymmetric flow in VTOL engine inlets with center-bodies in static operation (no crossflow). Example solution were given for several different inlet configurations. These differ from real inlets in that the theoretical model extends the duct far downstream, and the wing or upper

19

surface is simulated by a cone (in the limit a flat plate) tangent to the bellmouth and extending far into the free stream, and the ideal inlet is axisymmetric over the entire length whereas the real one may not be in the upper bellmouth region because it would have to fair into the wing or fuselage surface. The solution requires that the average inlet velocity be specified at a control station which is generally taken at the inlet plane of the fan. As a preliminary, a two-dimensional solution was obtained from the Douglas planar program (Refs. 13 and 32) and compared with the axisymmetric result for a simple hub and shroud. The surface velocities agree well on the shroud but not on the hub because the radius is small. The agreement of the velocity profiles near the hub is poor and probably inadequate for rotor blade design. The axisymmetric program was next applied to a range of geometric configuration variables such as bellmouth curvature, centerbody location (axial depth) and ratio of hub radius to tip radius. Comparison with available experiments indicated that the analysis adequately predicted results for compressible flow, providing there is no boundary layer separation. For the range of inlet variables covered, a trumpet shaped inlet was best for minimizing surface velocity gradients, while increased depth was best for reducing radial velocity variations. The hub surface-velocity gradients were small compared with the shroud surface velocity gradients.

In Reference 42, Stockman extended the above analytical work to operation of the inlet in crossflow. This was accomplished by superposition of three basic solutions: one with pure crossflow and two axisymmetric solutions for the case of the inlet duct extension closed and open (these being necessary because the basic solution for zero free-stream velocity cannot be obtained directly). The method of solution was based on the assumptions of

incompressible flow and an axisymmetric configuration. However, several

techniques were discussed that minimize the effect of compressibility in the

incompressible flow solution. Also, it is shown that an approximate solution

for unsymmetrical inlets can be obtained from a succession of solutions based

on several discrete profiles at key circumferential locations (e.g. the forward,

aft, and spanwise inlet profiles) and then fairing the plot of the flow

parameters of interest against circumferential angle. Several comparisons

with experiments for inlets operating with and without crossflow are given.

·Agreement of surface pressure and velocity contours for static and crossflow

cases with symmetric annular inlets is excellent, even when the inlet Mach

number is high subsonic. Agreement with results for an unsymmetric XV-4B

inlet is reasonably good.

A 1970 perspective on VTOL propulsion is given by Cockshutt in

Reference 43. The paper reports on experiments to answer the question of

whether the fan itself has a significant influence on the flow into it. This

was done by running a true fan-in-wing configuration using a 12-inch diameter

fan in a 40-inch chord two-dimensional wing and comparing the inlet flow surveys

with earlier experimental work by Schaub, et al, (Refs. 22, 25, 37) where the

flow was sucked through a test inlet in a wing by a remote exhauster. A

comparison was made at the fan inlet face (1/4 fan diameter below the top

surface). At low crossflow ratio (freestream/fan axial velocity of 0.20)

the fan model data showed the same general trend as the suction model data,

with high velocities near the leading lip and lower velocities at the trailing

lip. In addition, there was a definite skewing of the velocity pattern

opposite to the sense of fan rotation which was absent in the suction tests.

Both flows were substantially without total pressure loss. At a velocity

ratio of 0.50 (typical of transition to horizontal flight) the presence of the fan significantly changed the flow pattern and effectively prevented separation. At both velocity ratios the fan operated very powerfully on the inlet velocity distribution, converting a distorted inlet velocity field fore and aft into a basically radial distortion in the efflux plane. The normal assumption in fan design of uniform outlet static pressure was deemed invalid for shallow installations.

An overview of VTOL propulsion systems is also given by Lieblein in Reference 44. The author concluded that there is no superior lift propulsion concept. The lift-fan low-pressure ratio propulsion system has desirable features of good potential for noise reduction, provision for safe management of power plant failure, capability for high cruise speed, and good passenger appeal. There is no clear advantage between fans having integral power systems (i.e. powered by a coaxial gas turbine) and those having remote drives (i.e. fan and drive turbine separate from the power plant, with the turbine drive being a tip turbine or coaxial with the hub). The author cited inflow distortion and fan noise as primary lift-fan problems. He noted that, besides loss of symmetry in the inlet flow, which may lead to flow separation, there is incomplete turning of the inflow into the fan passage, resulting in an "advancing-retreating" orientation for the rotating fan blades. The circumferential variation in approach angle in conjunction with the circumferential variation in meridional velocity then produces a circumferential variation in change of incidence angle of the rotor. The result is the deterioration of fan thrust and efficiency as airspeed increases, plus the possibility of increased noise during transition.

As pointed out in the introduction to this review, fan-in-wing installations also present novel aerodynamic problems associated with interaction of the inlet flow field with adjacent vehicle surfaces. This interaction is most important during flight modes for which the inlet velocity is much larger than the forward speed of the aircraft. The two-dimensional theory of airfoils with arbitrarily strong inlet flow into the upper surface was examined by Serdengecti and Marble (Ref. 45) with the aim of developing a thin airfoil theory which is valid for this condition. The results showed that airfoil theory, in the conventional sense, breaks down at very large ratios of inlet to free-stream velocity. This occurs when the strong induced field of the inlet dominates the free-stream flow so much that the flow no longer leaves the trailing edge but flows toward it. For the example treated, this breakdown occurred at a ratio of inlet to free-stream velocity of about ten. This suggests that for ratios in excess of the critical value, the flow separates from the trailing edge and the circulation is dominated by conditions at the edges of the inlet.

The severe inlet design condition of lift-engine starting and acceleration at the beginning of a decelerating transition has been mentioned previously. A configuration which eliminates this problem is discussed by Kirk and Barrack in Reference 46. Here the engine is rotated into the airstream at the beginning of the transition for starting, thereby eliminating the high crossflow angle and the necessity of the inlet decelerating the crossflow and turning this flow 90°. Once started, the engines can be accelerated and rotated toward the vertical position as the transition proceeds. Inlet distortion and total-pressure recovery during transition were studied using a large-scale lift-engine fighter model powered by J-85 engines. The maximum inlet distortion

23

was less than 4% and inlet pressure recovery greater than 95% throughout a velocity ratio range of 0 to 0.7 at engine angles of 90° and 75°. As the engines were swiveled toward horizontal, inlet distortion decreased until at an engine angle of 30° there was little measurable distortion.

The application of a tip-turbine driven lift-fan to thin wings (5% thickness) for supersonic performance reported by Hickey and Cook (Ref. 36) was discussed further by Hodder, et al, in Reference 47. Recall that in Reference 36 an X-353-5B lift-fan was mounted in a 5% thick wing, necessitating the removal of the conventional bellmouth inlet from the outboard 180° of the fan. This inlet section was then replaced by an inlet of varying radius which would blend in with the local contours of the wing and a blowing nozzle for boundary-layer control (BLC) was incorporated in the inlet. While the BLC effect was to increase fan thrust at zero airspeed, an exploratory investigation indicated that BLC in this type application is probably effective only when a limiting inlet depth to diameter ratio is not exceeded; BLC could be ineffective in a deeper duct. Lift with BLC was considerably larger at forward speed than without BLC, but it was thought that flow separation may have occurred in the conventional fan discharge stator, since dimensionless performance with forward speed of the modified fans, with and without BLC, was better than that of the conventional fan. The authors concluded that V/STOL capability provided by lift fans for this supersonic fighter configuration appears feasible.

Although the present review is concerned with the inflow problem during transition, it should be noted that exhaust gas ingestion and the recirculating flow field while in proximity to the ground is an important design problem for VTOL aircraft, particularily for those with jet lift.

Some typical results are given by Hall in References 48 and 49. Also, noise presents an important problem which may have an influence on inlet design. Some results of a recent noise-reduction test program are given by Benzakein and Kazin in Reference 50.

A fan propulsion system study by Bland (Ref. 51) pointed up the fact that the best lift-fan VTOL aircraft results when the basic lift system performs the multiple functions of lift, cruise, and control. The optimum fan pressure ratio was found to be 1.3 to 1.4 and it was noted that fans should not be too large so that response to command (which should be about 0.2 seconds) becomes unacceptably long. Another general study on the application of high bypass turbofan lift engine technology to V/STOL aircraft design is given by Hill in Reference 52. A system study by Dugan, et al.,(Ref. 53) considers two fuselage lift fans each delivering 15,000 lb. thrust at takeoff. An average inlet Mach number of 0.6 is considered, with an inlet hub/tip radius ratio of 0.5. The authors concluded that remote lift-fan propulsion systems for VTOL transports are feasible.

A summary of results obtained from crossflow tests of a 15-inch diameter lift fan installed in a wing was reported by Lieblein, et al., in References 54 and 55. The basic objective of the study was to determine lift fan behavior in the crossflow environment and to define the principal factors affecting fan performance. The wing tested was a two-dimensional model with maximum thickness ratio of 17%. The axis of the model lift fan was at the 40% chord location. The fan rotor was driven by a compact supersonic turbine located in the hub section of the assembly. High-pressure air to drive the turbine was supplied through six equally-spaced struts spanning the fan passage. The ratio of inlet depth to rotor tip diameter was 0.16. Four

25

louver vanes for aft flow deflection were attached to the wing. The inlet
bellmouth was designed according to the methods of Reference 41 to avoid
velocity peaks on the outer shroud during static (no crossflow) operation.
The fan stage was designed for a pressure ratio of 1.28. Two forms of
inlet flow distortion were present in crossflow: (1) - increased inflow
velocity over the forward portion of the bellmouth and decreased velocity
over the aft portion coupled with an advancing/retreating blade motion with
respect to the incoming air caused by incomplete turning of the inlet air, and
(2) - local boundary layer separation at the rotor inlet caused by pronounced
accelerating and decelerating flows on the forward portion of the outer shroud
and the aft portion of the nosepiece resulting from the surface curvatures.
Boundary layer separation appeared to be restricted to a relatively small
area of the forward portion of the bellmouth. The average loss in total
pressure in the localized separated flow region was less than 1%, so that the
viscous loss associated with this particular bellmouth design did not seem
likely to pose any serious problem for crossflow operation. The fan was found
to experience a wide variation in back pressure over the test range of
operations, i.e., the static pressure at the exit of the duct was not equal
to the ambient pressure. Detailed pressure and flow direction measurements
are presented in the work. The data appeared to point to two major ingredients
that determine fan thrust variations in crossflow: the effects of inflow
distortion and stage back pressure variations induced by the crossflow. Inflow
distortion affected fan performance primarily by losses in total pressure
across the rotor and stator blade rows arising from circumferential variations
in local blade inlet flow angle. Fan stage back pressure (fan duct static

26

pressure) was found to decrease with increasing rotor tip speed and increasing crossflow velocity, and to increase with increasing vectoring louver angle. Fan back pressure decrease with tip speed was established to be the result of the turbine base flow effect. Fan back pressure decrease with crossflow was conjectured to be the result of some interaction effect between the fan assembly discharge streams and the crossflow stream. Force data from this fan-in-wing experiment are reported in Reference 56.

The wing used in these single 15-in. lift fan tests was also used in an experimental program in which the individual performance of multiple model lift fans was measured. The results are reported in Reference 57. The model consisted of three 5.5 -in. diameter tip-turbine driven model lift fans mounted chordwise in a two-dimensional wing to simulate a pod-type array. Tests were performed over a range of crossflow velocities from zero to 170 mph. Individual fan thrust performance was measured under static and crossflow conditions with inlet and exit cover doors of various designs installed on the basic model. Tests were also performed with a large panel simulating an aeroplane fuselage mounted next to the fans at two lateral positions. Further data were obtained for a simulated gas generator failure to a single fan. Fan performance was measured in terms of exit total and static pressures, speed, and gross thrust for each fan. Overall model lift, drag, and moment coefficients were also determined. The thrust of the upstream fan decreased significantly more than the two downstream fans, while the thrust of the downstream fan increased slightly over the entire range of crossflow velocities tested. The algebraic sums of the thrust for all three fans decreased only about 4% over the test range of crossflow velocity.

27

Thus there is probably no difficulty in terms of total thrust loss but the differences in thrust between the upstream and downstream fans cause adverse pitching moments. Tests showed that static thrust losses introduced by the use of inlet and exit cover doors can be significant. The effect of proximity of the fuselage simulator panel to the fan on static thrust was also significant. It was concluded that measured thrust variations caused by the presence of adjacent fans, inlet and exit cover doors, and adjacent fuselage panels were of sufficient magnitude to warrant consideration in the determination of installed thrust for takeoff and for individual fan thrust control during transition. The experiments also indicated that for valid results, lift fan test models should provide a close scaling or simulation of the complete real installation.

III. THEORETICAL ANALYSIS OF THE POTENTIAL FLOW

GENERAL CONSIDERATIONS

The equations describing the steady flow of an inviscid, incompressible fluid are the Euler equation:

$$(\vec{V} \cdot \vec{\nabla})\vec{V} = \frac{1}{\rho} \vec{\nabla}P \tag{1}$$

and the continuity equation:

$$\vec{\nabla} \cdot \vec{V} = 0 \tag{2}$$

where $\vec{V}$ is the velocity of the fluid at any point, P is the fluid pressure and ρ is the constant fluid density. Equations (1) and (2) hold throughout the region R' of the flow.

For flows external to a surface S, the boundary conditions are that the velocity infinitely far from the surface, V_∞, and the component of the fluid velocity normal to the surface, F, on S are known functions of position. The condition on S is written

$$\vec{V} \cdot \vec{n}\big|_s = F \tag{3}$$

where $\vec{n}$ is the unit normal vector directed from the surface S into the region R'. If the surface is the boundary of a solid, then the normal velocity component, F, is zero.

For the flows to be considered in this report, the velocity can be expressed as the sum of two velocities

$$\vec{V} = \vec{V}_\infty + \vec{v} \tag{4}$$

where $\vec{V}_\infty$ is the freestream velocity, or the velocity that would exist if the surface were absent, and $\vec{v}$ is the disturbance velocity produced by the surface. The disturbance velocity is assumed to be irrotational and thus can be expressed as the negative gradient of a potential function φ, i.e.,

$$\vec{v} = - \vec{\nabla}\varphi \tag{5}$$

Since the freestream flow represents an incompressible flow, V_∞ satisfies equation (2) and is solenoidal. Consequently, from equations (2) and (4), $\vec{v}$ is also solenoidal. The potential function φ therefore satisfies the Laplace equation

$$\nabla^2 \varphi = 0 \tag{6}$$

in the region R'. The boundary conditions on φ are obtained by inserting equations (4) and (5) into (3) giving

$$\vec{\nabla}\varphi \cdot \vec{n}\big|_S = \frac{\partial \varphi}{\partial n}\bigg|_S = \vec{V}_\infty \cdot \vec{n}\big|_S - F \tag{7}$$

and the condition at infinity

$$\left|\vec{\nabla}\varphi\right| \longrightarrow 0 \tag{8}$$

Equations (6), (7), and (8) form a properly posed Neumann problem for the solution of φ.

The approach to this Neumann problem as developed by A. M. O. Smith et al, (Ref. 11, 13, 31 and 32) is to reduce this problem to an integral

30

equation over the surface of the body. This approach is adopted for the study of the inlet flow problem and is summarized below for clarity.

The surface of the body is represented by a continuous source distribution of local intensity $\sigma(q)$ where $q(\xi,\eta,\zeta)$ is a general point on the body surface. The potential at a general point $P'(x,y,z)$ in the region R' due to this surface is given by

$$\varphi = \iint \frac{\sigma(q)}{\tilde{r}(P',q)} \, dS \tag{9}$$

where $\tilde{r}$ is the distance between the points P' and q, that is,

$$\tilde{r} = \sqrt{(x - \xi)^2 + (y - \eta)^2 + (z - \zeta)^2}$$

The potential defined by equation (9) satisfies the Laplace equation (6) as well as the boundary condition (8) for any arbitrary bounded source distribution σ. The unknown source distribution is obtained by requiring the boundary condition (7) to be satisfied. Equation (7) requires that the spatial derivatives of equation (9) be evaluated at points on the body surface S. As the general point P' approaches the surface, the normal derivative of the integral in equation (9) becomes singular and the principal value must be extracted. Kellogg (Ref. 58) has shown that the limit of $- \partial\varphi/\partial n$ as the point P' approaches a point p' located on the surface S is

$$- \frac{\partial\varphi}{\partial n} = 2\pi\sigma(p') - \iint \sigma \frac{\partial}{\partial n} \left(\frac{1}{r(p',q)} \right) dS \tag{10}$$

It should be emphasized that equation (10) applies on the surface S. When combined with equation (7), it enables the solution of three-dimensional

31

problems by numerical quadrature of a double integral and the solution of two-dimensional or axi-symmetric problems by numerical quadrature of a simple integral.

Hess and Smith (Ref. 32) present a qualitative review of the limitations of equation (10) with regard to existence and uniqueness of solutions. The only restriction of importance to the study of the inlet problem is the requirement that the normal vector $\vec{n}$ be continuous on the surface. Since an exact solution of equation (10) for an arbitrary surface is beyond present capability, it is necessary to resort to a numerical approximation. For the two classes of problems studied in this report; that is, two-dimensional and axi-symmetric flows, the body profile can be described in a single plane - z = 0 or θ = 0. The surface is then described by N + 1 points spaced along the surface profile. The actual surface profile is then approximated by the chords between the N + 1 points. Thus, the integral in equation (10) is broken into N integrals over each of the N segments representing the surface. The source density on each segment is assumed to be constant over the segment and thus can be taken outside of the integral. The remaining integral is a function only of the surface geometry and can be evaluated for a given surface. Thus, the normal velocity at a point p′, say the mid-point of a segment, can be written in terms of the N unknown values of the source density. By requiring equation (10) to hold at the mid-point of each of the N segments, a system of N linear algebraic equations is obtained. Thus, the problem reduces to an N x N linear matrix equation of the form

$$A_{ij}\ \sigma_j = D_i \qquad\qquad (11)$$

32

It should be noted that the tangential velocities on the surface must also be evaluated at the mid-point of the segment. However, there is no principal value to be extracted for the tangential component.

A. FORMULATION FOR TWO-DIMENSIONAL FLOW

The two-dimensional body is defined in the plane z = 0 by an x - y cartesian coordinate system. The surface extends from z = - ∞ to Z = + ∞, but the profile is the same in any plane z = const. The point at which the potential is to be evaluated is denoted $P'(x,y,z)$ and the integration is over the surface S in the space $q(\xi,\eta,\zeta)$. The potential at point P', then is given by

$$\varphi_{P'} = \int_s \int_{-\infty}^{+\infty} \frac{\sigma(s)d\zeta ds}{[(x - \xi)^2 + (y - \eta)^2 + \zeta^2]^{1/2}} \tag{12}$$

where s is the distance along the profile of the surface in the plane z = 0.

Since the integral equation involves normal derivatives, it is convenient to first evaluate the x and y derivatives of φ

$$\left(\frac{\partial \varphi}{\partial x}\right)_{P'} = - 2 \int_s \int_0^{\infty} \frac{\sigma(s)(x - \xi)d\zeta ds}{[(x - \xi)^2 + (y - \eta)^2 + \zeta^2]^{3/2}} \tag{13}$$

and

$$\left(\frac{\partial \varphi}{\partial y}\right)_{P'} = - 2 \int_s \int_0^{\infty} \frac{\sigma(s)(y - \eta)d\zeta ds}{[(x - \xi)^2 + (y - \eta) + \zeta^2]^{3/2}} \tag{14}$$

It is apparent that the ζ integration can be performed immediately to reduce the problem to the two-dimensional form

33

$$\left(\frac{\partial\varphi}{\partial x}\right)_{P'} = -2\int_s \frac{\sigma(s)(x-\xi)ds}{(x-\xi)^2 + (y-\eta)^2} \tag{15}$$

$$\left(\frac{\partial\varphi}{\partial y}\right)_{P'} = -2\int_s \frac{\sigma(s)(y-\eta)ds}{(x-\xi)^2 + (y-\eta)^2} \tag{16}$$

In order to avoid difficulties with multiple values and indeterminate forms, the integration is performed in terms of s, which is the distance along the body profile. The profile is broken up into N linear segments with the source density considered constant on each segment. These segments are numbered consecutively so that the flow region R' is on the left as the surface is transversed. The end points of the segment J are designated by the odd numbers s_{2J-1} and s_{2J+1}. The mid-point is designated by the even sub-script s_{2J}. Using these notations and noting that $\sigma(s)$ is a constant for each segment J, equations (15) and (16) give the velocity at the point P'(x,y) induced by the source element J as

$$\left.\frac{\partial\varphi}{\partial x}\right|_{P',J} = -2\sigma_J \, X_{P',J}(x,y) \tag{17}$$

$$\left.\frac{\partial\varphi}{\partial y}\right|_{P',J} = -2\sigma_J \, Y_{P',J}(x,y) \tag{18}$$

where

$$X_{P',J} = \int_{s_{2J-1}}^{s_{2J+1}} \frac{(x-\xi)ds}{(x-\xi)^2 + (y-\eta)^2} \tag{19}$$

34

$$Y_{P',J} = \int_{s_{2J-1}}^{s_{2J+1}} \frac{(y - \eta)ds}{(x - \xi)^2 + (y - \eta)^2} \qquad (20)$$

The quantities $X_{P',J}$ and $Y_{P',J}$ depend only on the relative positions of the points $P'(x,y)$, $s_{2J-1}(\xi_{2J-1}, \eta_{2J-1})$, and $s_{2J+1}(\xi_{2J+1}, \eta_{2J+1})$. It can be shown that, if P' is not on the segment J, then

$$X_{P',J} = \beta_J \sin \alpha_J + \cos \alpha_J \, \ln(h_{2J+1}/J_{2J-1}) \qquad (21)$$

$$Y_{P',J} = -\beta_J \cos \alpha_J + \sin \alpha_J \, \ln(h_{2J+1}/h_{2J-1}) \qquad (22)$$

where β_J is the angle subtended at the point P' by the segment extending from the point s_{2J-1} to the point s_{2J+1}, and h_{2J+1} and h_{2J-1} are the magnitude of the distances from P' to s_{2J+1} and s_{2J-1}, respectively.

The velocity components induced by the N source segments at the point P' in the region R' are therefore

$$-\frac{\partial \varphi}{\partial x}\bigg|_{P'} = 2 \sum_{J=1}^{N} \sigma_J X_{P',J} \qquad (23)$$

$$-\frac{\partial \varphi}{\partial y}\bigg|_{P'} = 2 \sum_{J=1}^{N} \sigma_J Y_{P',J} \qquad (24)$$

In the limit as the point P' approaches the mid-point, s_{2i}, of the segment i, equations (19) and (20) simplify to

$$X_{ii} \longrightarrow \pi \sin \alpha_i \qquad (25)$$

35

$$Y_{ii} \longrightarrow - \pi \cos \alpha_i \qquad (26)$$

The normal and tangential velocity components at s_{2i} are therefore

$$-\left.\frac{\partial \varphi}{\partial n}\right|_i = 2\pi\sigma_i + \sum_{j \neq i} \sigma_j (X_{i,j} \sin \alpha_i - Y_{i,j} \cos \alpha_i) \qquad (27)$$

$$-\left.\frac{\partial \varphi}{\partial t}\right|_i = \sum_{j \neq i} \sigma_j (- X_{i,j} \cos \alpha_i - Y_{i,j} \sin \alpha_i) \qquad (28)$$

It is noted that equation (27) is in agreement with equation (10). Using equations (7) and (27), the boundary condition on the surface is written

$$2\pi\sigma_i + \sum_{j \neq i} \sigma_j (X_{i,j} \sin \alpha_i - Y_{i,j} \cos \alpha_i) = -\vec{V}_\infty \cdot \vec{n}_i + F_i \qquad (29)$$

Equation (29) is a system of N linear algebraic equations and permits the computation of the N values of σ_i's. Once the values of σ_i's are computed, the velocities at every point of the flow field R′ can be calculated explicitly using equations (23) and (24).

B. FORMULATION FOR AXI-SYMMETRIC FLOW

The analysis for axi-symmetric flow is similar to the analysis for two-dimensional flow. In a cylindrical coordinate system (x', r', θ) where the x-axis is the axis of symmetry, the potential at point $P'(x', r', \theta)$ in the region R′ is given by

$$\varphi_{P'} = \int_s \int_{\theta'=0}^{2\pi} \frac{\rho' \sigma(s) d\theta' ds}{[(x' - \xi)^2 + r'^2 + \rho'^2 - 2r'\rho' \cos (\theta - \theta')]^{1/2}} \qquad (30)$$

36

where s is the distance along the profile of the surface in a meridian plane, and the integration is over the surface in the space $q(\xi, \rho', \theta')$. Since the problem is independent of the azimuthal coordinate θ, θ may be taken to be zero without losing generality and the integration with respect to θ' in equation (30) can be performed immediately. Alternatively, the derivatives of φ_p can be taken in order to obtain the axial and radial velocity components; u and v

$$u = -\frac{\partial \varphi}{\partial x'} = \int_s \int_{\theta'=0}^{2\pi} \frac{\rho' \sigma(s)(x-\xi) \, d\theta' ds}{[(x' - \xi)^2 + r'^2 + \rho'^2 - 2r'\rho' \cos \theta']^{3/2}} \quad (31)$$

$$v' = -\frac{\partial \varphi}{\partial r'} = \int_s \int_{\theta'0}^{2\pi} \frac{\rho' \sigma(s)(r' - \rho \cos \theta') \, d\theta' ds}{[(x' - \xi)^2 + r'^2 + \rho'^2 - 2r'\rho' \cos \theta']^{3/2}} \quad (32)$$

Integrating with respect to θ' then gives

$$u = \int_s \frac{4\rho'(x' - \xi) \sigma(s) E(k) \, ds}{\sqrt{(r' + \rho')^2 + (x' - \xi)^2} \left[(r' - \rho')^2 + (x' - \xi)^2\right]} \quad (33)$$

and

$$v' =$$

$$\int_s \frac{2\rho' \sigma(s)}{r'\sqrt{(r' + \rho')^2 + (x' - \xi)^2}} \left[K(k) + \frac{r^2 - \rho^2 - (x' - \xi)^2}{(r' - \rho')^2 + (x' - \xi)^2} E(k)\right] ds \quad (34)$$

where $K(k)$ and $E(k)$ are complete elliptic integrals of the first and second kinds, respectively. The modulus k is given by

$$k^2 = \frac{4r'\rho'}{(r' + \rho')^2 + (x' - \xi)^2}$$

37

The profile S is broken up into N linear segments with the source density considered constant on each segment. The end points of the segment j are designated as s_{2j-1} and s_{2j+1}. The mid-point is designated s_{2j}.

The velocity components induced by the source segment j at the ith segment (the point s_{2i}) are expressed in terms of geometric coefficients X_{ij} and R_{ij} as follows:

$$\left(\frac{\partial \varphi}{\partial x}\right)_{i,j} = \sigma_j \, X_{i,j} \qquad (35)$$

$$\left(\frac{\partial \varphi}{\partial r}\right)_{i,j} = \sigma_j \, R_{i,j} \qquad (36)$$

For a point p' at the mid-point of the ith segment, the coefficients due to the jth segment are given by

$$\substack{X_{ij}\\i\neq j} = -4 \int_{s_{2j-1}}^{s_{2j+1}} \frac{\rho'(x'_{2i} - \xi) \, E(k) \, ds}{\sqrt{(r'_{2i} + \rho')^2 + (x'_{2i} - \xi)^2} \left[(r'_{2i} - \rho')^2 + (x'_{2i} - \xi)^2\right]} \qquad (37)$$

$$\substack{R_{ij}\\i\neq j} = -4 \int_{s_{2j-1}}^{s_{2j+1}} \frac{\rho'}{r'_{2i} \sqrt{(r'_{2i} + \rho')^2 + (x'_{2i} - \xi)^2}} \left[K(k)\right.$$

$$\left. + \frac{r'^2_{2i} - \rho'^2 - (x'_{2i} - \xi)^2}{(r'_{2i} - \rho')^2 + (x'_{2i} - \xi)^2} \, E(k)\right] ds \qquad (38)$$

where

$$k^2 = \frac{4 \, r'_{2i} \, \rho'}{(r'_{2i} + \rho')^2 + (x'_{2i} - \xi)^2} \tag{39}$$

For each segment j, which in this case is in the form of a frustrum of a cone, the integral in equations (37) and (38) must be evaluated to obtain the effect of the segment on the point p'. Each segment is divided into a number of subelements and the integration is performed by Simpson's rule. The number of subelements used on the jth segment is determined by the formula $16 \Delta s_j / d_{min}$, where d_{min} is the shortest distance from the point p' to a point on segment j, and Δs_j is the length of the jth segment. This number is rounded off to the nearest even integer greater than zero. This formula, as proposed by Smith and Pierce (Ref. 13) is simply a device to introduce a large number of subelements (as many as 32) when p' is very close to the subelement and the integrand varies considerably over the subelement; and a small number of subelements when the segment j is far from the segment i and the integrand is nearly constant over the range of integration. This procedure insures good numerical accuracy while keeping the number of computations reasonably small.

The above procedure is used for computing the velocities induced by the segment j at the segments other than j. When the segments i and j coincide with each other, the integrand contains a singularity and a special procedure is employed. The segment is broken up into 3 divisions from s_{2i-1} to $s_{2i} - s'$, from $s_{2i} - s'$ to $s_{2i} + s'$ and from $s_{2i} + s'$ to s_{2i+1}. The integrals from s_{2i-1} to $s_{2i} - s'$ and from $s_{2'} + s'$ to s_{2i+1} contain no singularities and are evaluated using Simpson's rule with 16 subelements on each division. For the singular subelement which consists of the portion of the frustrum between

39

$s_{2i} - s'$ and $s_{2i} + s'$, where s' is very small, the integrand is expanded in a series about the mid-point s_{2i}. With the series expanded about the mid-point s_{2i}, the singularity is of the order s^{-1}. The singularity is odd and is eliminated by the "even" integration. The results are combined with the terms $- 2\pi \sin \alpha_i$ and $2\pi \cos \alpha_i$ supplied by Kellogg's theorem, equation (10), to provide the geometric coefficients X_{ii} and R_{ii}. Using these expressions, the boundary condition on the normal component of the velocity, equation (7), is written

$$2\pi\sigma_i + \sin \alpha_i \sum_{j=1}^{N} \sigma_j X_{ij} - \cos \alpha_i \sum_{j=1}^{N} \sigma_j R_{ij} = \vec{V}_\infty \cdot \vec{n}\bigg|_i - F_i \qquad (40)$$

The tangential component of the velocity at the point i is written

$$V_{t,i} = - \cos \alpha_i \sum_{j=1}^{N} \sigma_j X_{ij} - \sin \alpha_i \sum_{j=1}^{N} \sigma_j R_{ij} + \vec{V}_\infty \cdot \vec{t} \qquad (41)$$

The solution of equation (40) gives the values of σ_i. Once σ_i values are computed, velocity components at each point in R' can be calculated. In particular, the tangential velocity components at the surface can be computed using equation (41).

C. BASIC SOLUTIONS

Since the Laplace equation, (6), is linear, the principle of super-position can be utilized to obtain solutions for various freestream velocities and inlet flow rates from two basic solutions, one with zero inlet flow rate and the other with zero freestream velocity. The velocity potential φ is written in terms of two basic solutions φ_a and φ_b

$$\varphi = A\varphi_a + B\varphi_b \tag{42}$$

The first basic solution φ_a is the solution of

$$\nabla^2 \varphi_a = 0 \tag{43}$$

with the boundary conditions

$$\vec{\nabla}\varphi_a \longrightarrow 0 \qquad \text{infinitely away from S} \tag{44}$$

and

$$\frac{\partial \varphi_a}{\partial n} = \vec{e} \cdot \vec{n} \quad \text{on S} \tag{45}$$

where S is the surface of an inlet with closed ducts, shown in solid lines in Figure 1; $\vec{e}$ is a unit vector giving the direction of freestream velocity, $\vec{V}_\infty$. The second basic solution, φ_b, is the solution of

$$\nabla^2 \varphi_b = 0 \tag{46}$$

with the boundary conditions

$$\vec{\nabla}\varphi_b \longrightarrow 0 \qquad \text{infinitely away from S} \tag{47}$$

$$\frac{\partial \varphi_b}{\partial n} = 0 \qquad \text{on } S_1 \tag{48}$$

$$\frac{\partial \varphi_b}{\partial n} = 1 \qquad \text{on } S_2 \tag{49}$$

41

where S_1 is the surface of an inlet with open ducts, shown in solid lines in Figure 1, and S_2 is the floor of the ducts shown in dotted lines. Physically, the first basic solution is that for a flow over a closed duct. the second basic solution is for a flow induced by suction in the duct with no crossflow over the inlet.

It is easy to show that φ as given by equation (42) satisfies equation (6) and the boundary conditions (7) and (8) provided $A = V_\infty$ and $B = -F$.

The velocities corresponding to φ_a and φ_b are respectively $v_a = -\vec{\nabla}\varphi_a$ and $\vec{v}_b = \vec{\nabla}\varphi_b$. The total velocity corresponding to a given freestream velocity $\vec{V}_\infty$ and a given mean inlet duct velocity V_d is

$$\vec{V} = V_\infty \, (\vec{v}_a + \vec{e}) - V_d \vec{v}_b \qquad (50)$$

It should be noted that the basic solutions $\vec{V}_a$ and $\vec{v}_b$ contain no reference velocity. They depend only on the inlet geometry and need to be computed only once for each specified inlet configuration. Once $\vec{v}_a$ and $\vec{v}_b$ are computed, the solution for $\vec{V}$ for any specified values of V_∞ and V_d follows from (5).

Recalling the requirement that the normal vector $\vec{n}$ be continuous on the surface, it is anticipated that some numerical difficulty will be encountered at the corner formed by the duct and the floor of the duct. In particular, for the second basic solution, due to numerical errors described above, there exists a region near the corner where "leakage" through the sides of the ducts is significant. As a consequence, the volume flow rate through the control station located some distance above the floor differs

from that through the floor. In actual computations, the floor is placed at least one inlet width below the inlet lip. The velocity at the control stations, placed approximately midway between the floor and the lip, is found to be uniform, although the magnitude of the velocity is smaller than the specified velocity normal to the floor. The numerical results for the second basic solution are corrected by letting

$$\vec{V}_b' = \vec{V}_b \left(\frac{1}{V_{cs}}\right) \tag{51}$$

where V_{cs} is the averaged velocity at the control station. The total velocity corresponding to the given velocity $\vec{V}_\infty$ and the given inlet velocity V_d is still given by (50).

NUMERICAL RESULTS

Two types of inlet geometry were studied. The first type consists of a single inlet duct set in an infinite plate. The second type contains a centerbody simulating the hub of an inlet fan. Both types are shown in Figure 2, for the case where the axis of the inlet duct is perpendicular to the flat plate surface, and the top of the centerbody coincides with the plane of the plate. Variations from these basic geometries are examined for an inclined inlet axis case and both raised and lowered centerbodies.

The velocity component parallel to the inlet axis and the angle of inclination of the velocity vector from the inlet axis are presented for several planes perpendicular to the inlet axis. The tangential velocity profile along the flat plate, the inlet lip, the duct, and the hub surfaces are also presented. Surface distances, s, are measured from the point where

43

the inlet lip joins the flat plate. For the centerbody, surface distances are measured from the mid-point of the top of the centerbody. The sign conventions used are depicted in Figure 2.

A. INLETS WITHOUT THE CENTERBODY

The inlet geometry is shown in Figure 2a. The flat plate and the inlet duct are joined by circular arcs of radius r, with r = 0.1D where D is the width of the duct.

1. TWO-DIMENSIONAL RESULTS

Inlet Duct Perpendicular to the Flat Plate

The two basic solutions for this geometry are shown in Figures 3 and 4 where the distances, s, are non-dimensionalized by D. Figure 3a shows the tangential velocities on the forward portion of the inlet surface. It is seen that for the first basic solution, i.e., a flow over the inlet with closed duct, the tangential velocity increases from the freestream value far upstream to a maximum value of about 1.84 times the freestream value a short distance after the point where the inlet lip joins the plate. The tangential velocity then drops rapidly. At a depth of 1D below the flat plate, the velocity is nearly zero. For the second basic solution, i.e., the flow with suction but zero crossflow, the tangential velocity far upstream is zero. The velocity increases and reaches a peak value of about 1.80 times the mean inlet flow velocity shortly downstream of the velocity peak location for the first basic solution. It also drops rapidly after the peak and approaches the mean inlet flow velocity approximately at a depth of 0.6 D below the flat plate.

Figure 3a also shows the tangential velocity for the case where the crossflow velocity is equal to the mean inlet flow velocity. For this particular case, the tangential velocity, non-dimensionalized with respect to either the mean inlet flow or the freestream velocity, is simply the sum of the two basic solutions. The peak velocity is now about 3.48 times the mean inlet flow velocity. The peak is now somewhat spread out since the peak velocities of the two basic solutions do not occur at the same streamwise location. The large velocity gradient produced by the addition of the two basic solutions is responsible for the experimentally observed boundary layer separation on the forward inlet lip.

The tangential velocities over the aft section of the inlet are illustrated in Figure 3b. The tangential velocity on the inlet surface for the first basic solution, i.e., crossflow over a closed duct, is symmetric with respect to the centerline of the duct. The tangential velocity for the second basic solution is anti-symmetric about the axis of the inlet since it describes an inflow into the duct and the sign convention is positive for flow into the duct on the forward section but is negative for flow into the duct on the aft section. Also shown in Figure 3b is the tangential velocity for the case where the freestream velocity is equal to the mean inflow velocity in the duct. This solution, again non-dimensionalized by the mean inflow velocity, contains neither a velocity peak nor a resulting large velocity gradient since it represents the difference between the two basic solutions. Note that a stagnation point occurs on the circular arc portion of the aft inlet lip. The slight bump is due to the difference in peak-velocity locations of the two basic solutions.

For flows with smaller values of the ratio of the freestream velocity to the mean inlet velocity, a peak velocity is found on the aft inlet surface. The magnitude of this peak, however, is always much less than the magnitude of the peak velocity on the forward inlet surface.

Figure 4 shows the magnitude of the normal velocity component (in the direction of the duct-axis) and the angle of inclination of the velocity vector relative to the axis of the duct on a plane perpendicular to the axis of the duct at depths of 0.15 D and 0.20 D below the surface of the plate. A positive normal velocity results from a flow into the duct. A positive angle of inclination results when the velocity in the duct has a component directed into the duct and a component directed from the front to the rear of the duct. For the first basic solution, the normal velocity over the forward half of the plane is positive indicating flow into the duct, with the flow angle increasing from 0 to 90 degrees. Over the aft portion of the plane, the normal velocity is negative and the angle increases from 90 to 180 degrees, indicating flow out of the duct. The normal velocity is seen to the anti-symmetric about the duct axis, giving the anticipated result of no net mass flow into the closed duct. The second basic solution for suction in the duct gives a net inflow velocity which is symmetric about the duct axis. The magnitude of the velocity on the duct surface is larger than the mean inflow. The flow inclination angle indicates that the flow is directed toward the center-line of the duct.

The case of the freestream velocity equal to the mean inflow velocity is also presented in Figure 5. The velocity normal to the plane

is seen to be quite non-uniform. The angle of inclination, however, is very nearly symmetric and is positive over the entire plane. An examination of the numerical results for the case where the freestream velocity is equal to the mean inlet velocity reveals two causes of flow non-uniformity in the duct. The flow near the surface of the inlet is strongly affected by flow acceleration and subsequent deceleration around the inlet lip. This effect is evident near the inlet duct walls. The rapid change in the velocity profiles in the region within 0.3 D from each wall between the depths of 0.15 D and 0.20 D results from this flow acceleration and subsequent deceleration around the inlet lip. The flow over the center 40 percent is approximately a straight line at both depths representing the effect of the crossflow on the flow in the duct. This non-uniformity will be referred to as crossflow non-uniformity and extends into the duct for several duct widths. The non-uniformity near the walls represents the deviation of the normal velocity profile from a straight line drawn through the center 40 percent of the normal velocity profile and will be referred to as curvature non-uniformity. The curvature non-uniformity extends several lip radii into the duct.

It should be noted that the location of the fan plane in a fan-in-wing installation is restricted by the thickness of the wing. Although the curvature non-uniformity can be alleviated by maximizing the depth of the fan plane location, the crossflow non-uniformity is expected to prevail in actual fan-in-wing installations.

Inlet Duct Inclined to the Flat Plate

Following the suggestion of Durvivier and McCallum (Ref. 5), an inlet with a duct inclined 10° to the perpendicular of the plate was studied. The intersections of the duct and flat plate are faired by circular arcs of radius 0.1D. A comparison of the tangential velocity of the inclined inlet with that over the previously discussed perpendicular inlet shows that, for the first basic solution of a crossflow over a closed duct, the velocity profiles are very nearly equal. For the second basic solution, i.e., the flow with suction but zero crossflow, the tangential velocity profiles are compared with those for the perpendicular inlet in Figure 5. The comparison shows that the peak tangential velocity on the forward section of the inlet lip is smaller for the inclined inlet than that for the perpendicular inlet (1.62 times the mean inlet flow velocity vs 1.84). On the aft section, the velocity peak for the inclined inlet is higher (1.95). The tangential velocity profile on the inlet surface with an inclined duct is compared to that for the perpendicular duct in Figure 6 for the case where the freestream velocity is equal to the mean inflow velocity. Over the front half of the inlet (Figure 6a) the tangential velocity profile for the inclined duct is nearly identical to the velocity profile for the perpendicular duct. The reduction in the peak velocity for the case of suction in the duct but no crossflow is lost when the effect of crossflow is included. The comparison of the tangential velocities over the rear half of the inlet (Figure 6b), shows that the previously mentioned bump caused by the difference in the velocity-peak locations of the two basic solutions is more pronounced for the inclined inlet.

In order to compare the flow nonuniformity in the duct, the normal velocities and flow inclination angles were calculated for two planes. Both planes were perpendicular to the axis of the duct. The first plane intersected the aft wall of the duct at a depth of 0.15D and intersected the front duct wall at a depth of .288D, where the depths are measured parallel to the duct axis. The second plane intersects the aft wall at a depth of .20D and intersects the front wall at a depth of .376D. For comparison purposes, normal velocities and flow inclination angles were computed for an inlet with a perpendicular duct at four planes at depths corresponding to the maximum and minimum depths of the inclined duct planes, i.e. 0.15D, 0.20D, 0.288D, and .376D. The results are compared in Figure 7 for the case where the freestream velocity is equal to the mean inlet flow velocity. The flow nonuniformity over the planes of the inclined duct is almost identical to that of the perpendicular duct at depths corresponding to the maximum depths of the inclined planes, and is significantly less severe than that of the perpendicular duct at depths corresponding to the minimum depths of the inclined planes.

2. AXI-SYMMETRIC RESULTS

In Figure 8a, tangential surface velocities over half of the inlet for the second basic solution, i.e. mass flow through the duct but no crossflow as calculated for a two-dimensional inlet and an axi-symmetric inlet are compared. Both inlets have lip radii of 0.10D and the velocities are non-dimensionalized by the mean inlet flow velocity. The magnitude of the velocity peak for the axi-symmetric inlet is about 1.58 times the mean inlet flow as compared to 1.80 for the two-dimensional inlet. The

peak velocity in the axi-symmetric duct occurs slightly deeper in the inlet than that in the two-dimensional inlet. In fact, the magnitude of the velocity tangential to the inlet surface for the axi-symmetric inlet is always less than the tangential velocity on the surface of the two-dimensional inlet, at equal streamwise stations. The velocities normal to planes perpendicular to the axis of the duct at depths of 0.15D and 0.20D are compared for the two geometries in Figure 8b. At equal depths, the flow in the axi-symmetric duct is more nearly uniform than the flow in the two-dimensional duct.

Although the flow associated with an axi-symmetric inlet is quantitatively dissimilar to that associated with a two-dimensional inlet, there is a qualitative similarity between the two. It is expected that any trends observed for two-dimensional inlets should be found in axi-symmetric or even nearly axi-symmetric inlets. Practical inlet configurations often do not lend themselves to axi-symmetric analyses. For example, the inclined inlet case discussed earlier would require a full three-dimensional study. The numerical solution of the full three-dimensional problems requires very large amounts of computational effort and may not yield highly accurate results. The two-dimensional analysis requiring a minimum amount of computational effort can offer useful information regarding the general flow features.

B. INLETS WITH CENTERBODY

The geometry of an inlet with a centerbody simulating the hub of a fan is shown in Figure 2b for the case where the top of the centerbody is in the plane of the flat plate. The distances are non-dimensionalized by the half-width of the inlet, R. The half-width of the hub is taken to be .5R.

The inlet duct and flat plate, and the centerbody sides and top surface are joined by circular arcs of radius r. All inlet ducts studied are perpendicular to the flat plate and the sides of all centerbodies are parallel to the duct walls.

1. TWO-DIMENSIONAL RESULTS

Variation of Velocities with the Freestream/Mean Inlet Flow Velocity Ratio.

Figures 9 and 10 compare the tangential surface velocities over the front and rear halves of the inlet/centerbody combination with lip radii of 0.1R for the freestream to mean inlet velocity ratios of 0.0, 0.2, 0.5, and 1.0. This family of velocity profiles represents a series of velocity profiles on the inlet as the crossflow velocity is increased while maintaining a constant mean inlet velocity in the duct, i.e. it represents the transition of a fan in wing inlet from hovering to forward flight. The first basic solution corresponds to the case $V_\infty/V_d = \infty$ and is symmetric with respect to the centerline of the inlet. The second basic solution corresponds to the case $V_\infty/V_d = 0$ and is anti-symmetric with respect to the centerline of the inlet.

The velocities over the forward part of the plate and duct surface are similar to the velocities found in the inlet without a centerbody. As seen in Figure 9, a stagnation point is found on the centerline of the centerbody for $V_\infty/V_d = 0.0$, corresponding to the second basic solution of inflow but no crossflow. This stagnation point moves upstream as the crossflow velocity increases and at a velocity ratio of $V_\infty/V_d = 0.46$ the stagnation point moves onto the circular arc portion of the centerbody.

51

Over the rear half of the hub, Figure 10, the magnitude of the velocity peak is less than the peak on the front part of the inlet (2.6 as compared to 2.9 at $V_\infty/V_d = 1.0$).

A stagnation point appears on the aft section of the inlet surface for $V_\infty/V_d > 0$. This stagnation point also moves upstream with increasing V_∞/V_d, and, at a freestream to mean inlet velocity ratio of .73 V_d, the stagnation point moves onto the circular arc portion of the inlet lip.

In Figure 11, the normal velocities and angles of flow inclination across a plane located at a depth of 0.20R are presented for values of the velocity ratio of $V_\infty/V_d = 0.0, 0.2, 0.5,$ and 1.0. The solutions show a mild amount of curvature nonuniformity. The crossflow nonuniformity increases with increasing crossflow to mean inlet velocity ratio.

Variation of Surface Velocities with the Height of the Centerbody

Calculations were made for the inlet with the top of the centerbody raised 0.1R (equal to the inlet lip radius) above the plane of the plate; and lowered 0.1R below the plane of the plate. For the first basic solution of crossflow over a closed duct, the peak velocity on the inlet lip increases from the value of $1.6V_\infty$ for the normal centerbody to $1.72V_\infty$ for the case where the centerbody is lowered below the plane of the plate, and decreases to $1.48V_\infty$ for the case of a raised centerbody. However, the peak velocity on the centerbody lip decreases from the value of $1.60V_\infty$ for the normal centerbody location to $1.40V_\infty$ for the lowered centerbody and increases to the value $1.79V_\infty$ for the raised centerbody. For the second basic solution of suction in the duct but no crossflow the opposite trend is observed. The peak velocity on the inlet lip decreases from $1.57V_d$ for the normal

52

centerbody to $1.50V_d$ for the lowered centerbody and increases to the value $1.63V_d$ for the raised centerbody. On the centerbody lip the peak velocity increases from $1.35V_d$ for the normal centerbody to $1.45V_d$ for the lowered centerbody and decreases to $1.28V_d$ for the raised centerbody. For intermediate values of the freestream/mean inlet velocity (0.2 - 0.7) the surface velocities over the forward section of flat plate, inlet lip and duct are nearly identical for all three centerbody locations. Similarly, the surface velocities over the aft portion of the centerbody including the aft centerbody lip and duct are nearly identical for all three centerbody locations. These results indicate that the height of the hub is not expected to significantly influence the flow separation that may occur on the forward inlet lip and the aft centerbody lip resulting from the large velocity gradients near the velocity peaks.

The tangential velocity over the upstream portion of the centerbody surface and the aft portion of the inlet surface are somewhat influenced by the hub height. The profiles near the velocity peaks, however, are not strongly influenced by the hub height and the overall effect of the hub height on the flow is expected to be small.

The normal velocities and flow inclination angles on a plane at a depth of 0.2R for the raised, normal and lowered hub are compared in Figure 12 for the case $V_\infty/V_d = 0.5$. The normal velocity for the lowered hub exhibits a strong curvature nonuniformity near the centerbody, since the plane intersects the centerbody at the point where the circular arc section joins the centerbody duct wall. The normal velocities for the raised and normal centerbodies are nearly equal over the front half of the

53

plane. Over the aft half of the plane, the flow nonuniformity is less severe with the raised hub. The use of a raised hub is, thus, expected to be beneficial in reducing the flow nonuniformity at the flow plane.

Variation of Velocities with Lip Radius

Additional solutions were obtained for the basic inlet, with the top of the centerbody in the plane of the flat plate, with lip radii of 0.08R and 0.15R. The radii of the circular arcs joining the centerbody, top and sides, were taken to be the same as the radii of the circular arcs joining the flat plate and duct walls. Figures 13 and 14 compare the velocities on the inlet and centerbody surfaces at a velocity ratio of V_∞/V_d = 0.5 for inlet/centerbodies with lip radii of 0.08R, 0.10R, and 0.15R. It is apparent that increasing the lip radius has a substantial effect on reducing both the magnitude of the velocity peak and the surface velocity gradient with respect to the streamwise distance. For example, for V_∞/V_d = 0.5, the peak velocity for a lip radius of 0.08R is 2.35 V_d as compared to a peak velocity of 1.90 V_d for a lip radius of 0.15R. In Figure 15 the normal velocities and angles of flow inclination across a plane in the duct located at a depth of 0.20R are compared for the three geometries. The freestream to mean inlet velocity ratio, V_∞/V_d,is 0.50. Since the plane intersects the duct walls much closer to the circular arc section in the case where the lip radius is 0.15R, there is more curvature nonuniformity in the duct for this geometry.

2. AXI-SYMMETRIC RESULTS

Surface velocities on the surface of an inlet and centerbody with lip radii of 0.1R as calculated for an axi-symmetric inlet and a two-dimensional inlet are compared in Figure 16 for the second basic solution of suction in

the inlet but no crossflow. Although there is a slight difference in
the velocities on the centerbody, the velocities on the inlet surface
are very nearly equal. A comparison of the solutions for different lip
radii indicate that this good agreement is independent of the lip radius.
The normal velocity and angle of flow inclination across a plane at a
depth of 0.20D are compared in Figure 17 for the axisymmetric and two-
dimensional inlets. Again the agreement is very good.

IV. BOUNDARY LAYER ANALYSES

Boundary layer analyses were made to

1. Establish estimates of the maximum cross-flow velocities without inlet flow separation.

2. Explore the effects of the various design variables on the maximum cross-flow velocities without inlet flow separation.

3. Determine the relative magnitude of the boundary layer displacement thickness.

Only the two-dimensional inlet flows were considered. In addition, because of the limitations of existing boundary layer theories, emphasis was placed on establishing trends rather than on making numerous detailed calculations leading to "precise" theoretical results. The boundary layer theory employed in these analyses and the results obtained are discussed in the next two sections.

ANALYTICAL PROCEDURES

Over fifty methods of predicting the development of turbulent boundary layers in low speed flow may be found in the literature. Most of the commonly used methods for incompressible flow were recently compared in considerable detail at the 1968 AFOSR-IFP-Stanford Conference.[59] These methods extended from the relatively simple and fast integral solutions to extremely detailed finite difference solutions which utilize turbulent transport equations. Seven of the total of twenty-eight methods were selected as superior by an evaluation committee. The seven included a finite difference method which has been developed over a number of years by A.M.O. Smith and his associates at McDonnell Douglas Corporation. This finite difference solution was selected for the present analyses since it is apparently as accurate as any

56

existing method, it has been extended to include compressible flow, and a computer listing of the numerical solution was available in the literature. The method is described in complete detail in Ref. 60. Reference 61 lists the computer program and gives a detailed description of its use. Only a brief description of this method will be given herein.

The differential continuity, momentum and energy equations are basically solved numerically along both the normal and streamwise directions. The shear stresses are related to the mean flow velocity gradients using the eddy-viscosity model. The boundary layer is subdivided into an inner and an outer layer, each of which uses a separate expression for the eddy viscosity. In the inner layer the eddy viscosity is specified by the Prandtl mixing layer theory with the mixing length modified to account for the viscous sublayer and for pressure gradient effects. The corresponding shear stress in the inner layer is then given by the expression

$$\tau = 0.16 \ \rho y^2 \left\{ 1 - \exp\left[- \frac{y}{26\nu} \left(\frac{\tau_w}{\rho} + \frac{dP}{dx} \frac{y}{\rho} \right)^{\frac{1}{2}} \right] \right\}^2 \left(\frac{\partial V_t}{\partial y'} \right)^2$$

The exponential factor represents the correction due to the viscous sublayer and the transition region. The constant coefficient is the square of the Karman constant, which is taken to be 0.4.

In the outer layer the eddy viscosity is determined by specifying a constant value of the turbulent Reynolds number based on the edge velocity V_e (i.e., the scaling velocity) and the displacement thickness δ^* (i.e., the scaling length). However, the eddy viscosity is assumed to vary in the normal direction in accordance with the intermittency factor. The corresponding shear stress is given by the expression

$$\tau = 0.0168 \, \rho v_e \delta^* \left[1 + 5.5 \left(\frac{y}{\delta} \right)^6 \right]^{-1} \frac{\partial v_t}{\partial y}$$

The constant coefficient represents the reciprocal of the turbulent Reynolds number (i.e., $Re_T = 59.5$) and the bracketed term represents the correction factor for intermittency.

The inner and outer layers are matched at the point where the shear stresses are equal.

The heat conduction is related to the mean enthalpy gradient using an eddy-conductivity model. The eddy conductivity is then determined from the eddy viscosity by assuming a constant value of the turbulent Prandtl number.

In the present analysis the free stream static conditions are taken as the standard atmospheric conditions (i.e., $T_\infty = 519^\circ R$ and $P_\infty = 2116 \, \#/ft^2$). In addition, the laminar and turbulent Prandtl numbers are taken as 0.7 and 0.9, respectively.

The geometric model used in the present boundary layer calculations is shown in Fig. 18. As in the case of the potential flow analyses, the fan duct is assumed to be imbedded in an infinite plate parallel with the freestream flow. However, for the boundary layer analyses, which depend upon the Reynolds number and the Mach number, it is necessary to specify a length and a velocity scale. The velocity is selected as the uniform-flow, duct velocity V_d. The length is selected as the distance ℓ from the simulated wing leading edge to the duct centerline. The boundary layer on the forward section of the wing surface is assumed to begin at the simulated leading edge. For the hub and the rear wing surface, the boundary layer development begins at the stagnation points, as indicated on the sketch. In all cases, the local velocities on the surfaces are obtained from the potential flow solutions.

All boundary layer calculations were made using

$$R/\ell = 0.5$$

For a duct located at the wing mid-chord, this corresponds to a total duct width which is 50 percent of the wing chord. The reference Reynolds number used in the boundary layer analyzer is defined as

$$Re_\ell = \frac{V_d \ell}{\nu_d}$$

. where ν_d is the kinematic viscosity of the air at the velocity V_d. The reference Mach number is defined as

$$M_d = \frac{V_d}{C_d}$$

where C_d is the speed of sound at the velocity V_d.

Boundary layer separation was assumed to occur when the shear stress at the wall was zero since a majority of the experts believe that this is the most suitable indicator of separation. The conditions for zero shear stress at the wall were obtained by extrapolating the friction coefficients to zero using relatively few data points, rather than employ a lengthy and wasteful process of progressively approaching zero shear stress. Enough calculations were made, however, to establish convincing evidence for the extrapolations. Although the prediction of separation is highly debatable, it is believed that for these flows the approach to separation is very rapid, and the conditions for separation are, correspondingly, relatively insensitive to the criterion. In any event, the consistency of the analyses should provide for meaningful, relative comparisons.

RESULTS AND DISCUSSIONS

Typical variations in the surface friction coefficients with distance along the surface and freestream to duct velocity ratios are shown in Fig.19. The Reynolds number of $Re_\ell = 14.8 \times 10^6$ and Mach number of $M_d = 0.46$ correspond to a duct velocity of $V_d = 500$ ft/sec and a characteristic length of $\ell = 5$ ft for standard, freestream air conditions. Most of the present calculations were made for these practical design conditions.

As illustrated in Fig.19 the friction coefficient reaches a peak near the beginning of the inlet lip curvature as a result of a gradual flow acceleration. The rapid flow acceleration induced by the lip curvature then causes the friction coefficient to decrease rapidly until a relatively flat velocity peak is reached. Thereafter, the friction coefficient again decreases rapidly in the presence of the adverse pressure gradients which rob momentum from boundary layer flow near the wall. The friction coefficient reaches a minimum value slightly downstream of the inlet lip radius where the deceleration is diminishing and uniform duct flow conditions are being approached. Downstream of this minimum, the boundary layer profile gradually fills as turbulent mixing effects dominate the pressure gradient effects and, correspondingly, the friction coefficient increases. As the freestream to duct velocity ratio increases, the minimum value of the friction coefficient decreases as a result of the increasing peak velocities and the subsequent increases in the adverse pressure gradients. In this particular case, separation exists with $V_\infty/V_d = 0.6$ and the maximum value of V_∞/V_d without separation is clearly between 0.5 and 0.6. Extrapolation of the minimum value of C_f (i.e., $C_{f_{min}}$) to zero yields $V_\infty/V_d = 0.555$ for incipient separation.

Typical plots of the minimum friction coefficients are shown on Fig. 20. Extrapolation of these curves to $C_{f_{min}} = 0$ yields the value of V_∞/V_d for incipient separation. The curve for $r/R = 0.15$ in Fig.20a corresponds to the results shown on Fig. 19. The values of Re_ℓ and M_d of Fig.20b correspond to $V_d = 100$ ft/sec and $\ell = 5$ ft for standard, freestream conditions. However, for this low Mach number the flow is essentially incompressible and only the Reynolds number is significant. Consequently, the results of Fig.20b are applicable for any combination of u_d and ℓ with incompressible flow which give $Re_\ell = 3.17 \times 10^6$. As will be demonstrated later, the effects of M_d is apparently negligible, at least within the range considered herein, and, consequently, only Re_ℓ is significant even in Fig. 20a.

The results in Fig.20 demonstrate the smooth and consistent extrapolation to $C_{f_{min}} = 0$. It should be pointed out that, in all cases, C_f distributions were calculated at values of V_∞/V_d somewhat greater than those for $C_{f_{min}} = 0$ (i.e., for V_∞/V_d greater than the values established for incipient separation) in order to confirm that separation had occurred. For example, for the case of $r/R = 0.15$ in Fig. 20b, calculations of the C_f distribution for $V_\infty/V_d = 0.4$ confirmed that incipient separation would occur at V_∞/V_d slightly below 0.4. In general, the results of Fig.20 demonstrate that the freestream to duct velocity ratio must be decreased to avoid separation if the lip to duct radius ratio r/R is decreased, as one would expect. Surprisingly, however, the results of Fig. 20a indicate that this is not necessarily the case since V_∞/V_d for incipient separation is essentially the same for $r/R = 0.1$ and $r/R = 0.08$. The reason for this is not clear and may indicate a deficiency in the theory. Perhaps, for these particular flow conditions with $r/R = 0.08$, the rapid acceleration during the initial part

of the inlet bend increases the momentum in the boundary layer near the surface tending to offset the effects of the increased pressure rise downstream of the peak velocity. In any event, this aspect is worthy of additional studies.

Table I demonstrates the relatively small effect of Mach number on the computed values of $C_{f_{min}}$ for values of $C_{f_{min}}$ near zero (i.e., for conditions near incipient separation). The first four rows compare values of $C_{f_{min}}$ for duct Mach numbers of 0.46 and 0.09 with a constant Reynolds number of $Re_{\ell} = 14.8 \times 10^6$. The differences in the computed values of $C_{f_{min}}$ for these two Mach numbers with the same values of V_{∞}/V_d are insignificant (i.e., extrapolations to $C_{f_{min}}$ would yield insignificant differences in V_{∞}/V_d for incipient separation). In fact, the effect of M_d reverses as V_{∞}/V_d is changed from 0.30 to 0.32. These differences are probably well within the differences due to the numerical inaccuracies. The last four rows are included to illustrate this point. These entries present comparisons for constant values of Re_{ℓ} but at low Mach numbers. In these cases, the Mach numbers are well within the incompressible flow range where Mach number effects must be small. Nevertheless, the effects of these small Mach number changes on $C_{f_{min}}$ is of the order of those obtained when the Mach number changes should be significant. It must be emphasized, however, that these results are based on boundary layer edge velocities computed using incompressible flow. Compressibility is included in the sense that the pressures and the temperatures are computed using compressible flow equations with these incompressible flow velocities. Perhaps the effects of Mach number would be significant if the edge velocities also accounted for compressibility effects. Within the limitations of the incompressible, potential flow solutions for the edge velocities it is concluded, therefore, that M_d is not an important flow parameter for the present boundary

layer analyses. The only significant flow parameter other than the velocity ratio is the Reynolds number.

A summary plot of the freestream to duct velocity ratios for incipient separation on the rear hub and forward inlet sections is presented in Fig. 21. For the range of flow conditions considered herein, separation does not occur on either the front hub or the rear inlet sections. As shown in Fig. 21 the velocity ratios for incipient separation on the rear hub are approximately 0.2 higher than that for incipient separation on the forward inlet section. Consequently, the flow over the forward inlet section is considerably more critical than that over any other portion of the inlet. This is also consistent with experimental observations. For the rear hub section, this critical velocity ratio decreases consistently and sharply with decreasing r/R at $Re_{\ell} = 14.8 \times 10^6$. In contrast, however, the critical velocity ratio for the forward inlet section decreases as r/R is decreased from 0.15 to 0.10 but then remains constant as r/R is decreased from 0.10 to 0.08. As mentioned previously in connection with Fig. 20, this unexpected anomaly needs further study. In fact, it was at first suspected that this might have been caused by numerical inaccuracies due to a relatively course numerical grid. However, subsequent reductions in the grid spacing resulted in no significant changes. The critical velocity ratios were not calculated for $r/R = 0.08$ at the low Reynolds number.

Figure 21 also illustrates that the Reynolds number has a relatively strong effect on the velocity ratio for incipient separation. Figures 22 and 23 have been included to emphasize this effect of Reynolds number. In Fig. 22 the minimum value of the friction coefficient for several constant values of the velocity ratio is plotted against the Reynolds number. These results are for the forward inlet section with $r/R = 0.1$. The circular points identify calculated points or points obtained by extrapolations to $C_{f_{min}} = 0$, as

63

previously described. The dashed lines indicate qualitative extrapolations which are believed to be reasonably accurate and are included in order to more completely illustrate the general trends. These results show that the minimum value of the friction coefficient is very sensitive to the Reynolds number as separation is approached. Or, conversely, the velocity ratio for incipient separation (i.e., the velocity ratios along the line for $C_{f_{min}} = 0$) is sensitive to the Reynolds number. Apparently this can be attributed to the relatively large increase in the turbulent shear stresses as the Reynolds number is increased.

Figure 23 shows the variation of the critical velocity ratio for incipient separation with Reynolds number. The curve for $r/R = 0.10$ represents the intercepts of the constant velocity ratio curves of Fig. 22 with the abscissa, where $C_{f_{min}} = 0$ (i.e., the condition for incipient separation). The solid symbols indicate the intercept obtained using the extrapolated curves of Fig. 22. Consequently, these points are only qualitative. Nevertheless, they complete a consist trend and are believed to be relatively accurate. The curve for $r/R = 0.15$ is faired consistently through the two computed points. These results clearly show that the Reynolds number has a significant influence on the critical velocity ratio. Correspondingly, one must expect that the location of the duct inlet relative to the leading edge (which is specified by $R/\ell = 0.5$ in the present study), the velocity distribution over a finite wing (as opposed to the infinite plate in the present study), and the three-dimensional flow for an axisymmetric duct (as opposed to the two-dimensional flow in the present study) would significantly affect the critical velocity ratios. For these reasons, it is believed that additional parametric studies for the flow geometries considered herein would be of little or no value for establishing the critical velocity ratios for practical configurations.

64

Table II presents the results of an endeavor to find a relatively simple, approximate criterion for the velocity ratio for incipient separation. The last column lists the ratio of the maximum value of the inlet lip velocity, V_{max}, to the duct velocity for the various conditions at which incipient separation existed. The next-to-the-last column lists the corresponding critical freestream to duct velocity ratios. These correspond to the nine points shown on Fig. 21. These results show that the variation of V_{max}/V_d for the various lip radii and the two inlet sections is not large for a fixed Reynolds number. In fact, for $r/R = 0.10$ and 0.15, V_{max}/V_d is very nearly 2.0 and 1.8 for $Re_d = 14.8 \times 10^6$ and 3.2×10^6, respectively. These values are undoubtedly within the accuracy of the present results. The deviation from $V_{max}/V_d = 2$ for $r/R = 0.08$ at $Re_d = 14.8 \times 10^6$ will significantly affect the critical velocity ratio, however. In addition, the Reynolds number effect is again significant and, therefore, the generality of these results is doubtful.

The computed values of the boundary layer displacement thicknesses prior to incipient separation were always less than one percent of the duct radius R. The effects of this small a displacement thickness on the potential flow results should be well within the accuracy of the present analyses.

V. CONCLUSIONS

1. The method developed by A.M.O. Smith, et al., (Refs. 11, 13, 31, and 32) for the solution of potential flow equations is highly effective for predicting flows about two-dimensional and axi-symmetric inlets. During the present research, closed form analytical solutions have been developed for velocities induced by uniform surface distributions of source-sink elements over finite circular cylinders. The solutions are expressed in terms of complete elliptical integrals and the Heuman's Lambda function and are presented in the Appendix of this report. The availability of these analytical expressions contributes to the efficient and accurate computation of flows about axi-symmetric inlets.

2. The results of a review of existing literature on fan inlets indicate that the method of N. Stockman (Ref. 43), which gives approximate potential flow solutions for three-dimensional inlets from a succession of solutions for axi-symmetric shapes, effectively circumvents the difficulties of large computer time and of inaccuracy encountered in the numerical solution of many three-dimensional inlet problems. Stockman's method utilizes a computer program developed by Smith et al. to generate solutions for axi-symmetric shapes. The analytical expressions presented in the Appendix are of significance in the further development of numerical methods applicable to three-dimensional problems.

3. For inlet configurations that do not lend themselves to "axi-symmetric" analyses, the two-dimensional approach, which requires a minimum amount of computational effort, offers useful information regarding the general flow features. In particular, the trends regarding flow separation on the forward portion of the inlet can be predicted by a parametric study of the inlet flow using the two-dimensional approach. It is observed that for the limiting case of zero crossflow, the two-dimensional potential flow solution is in good numerical agreement with that for axi-symmetric flow. Thus, for cases of small freestream to mean inlet flow velocity ratio, two-dimensional results are expected to yield good quantitative predictions. The potential flow computer program developed during the course of this research is sufficiently general to allow any conceivable two-dimensional inlet geometry to be treated. The computation is reasonably rapid. For the inlet with a centerbody, the computer time used to generate the two basic solutions is under 30 seconds on the UNIVAC 1108 computer. With the basic solutions, each solution for a given combination of freestream and mean inlet velocities was obtained in less than 1 second. The potential flow solutions provided the needed input for boundary layer calculations.

The following observations, derived from the two-dimensional analyses, are expected to be valid for three-dimensional inlets.

4. Within the accuracies of the present analyses, the effects of the boundary layer displacement thickness on the potential flow solutions are negligible for all inlet configurations studied.

5. With an increasing crossflow to mean inlet velocity ratio, separation occurs first on the forward portion of the inlet lip and next on the aft portion of the hub. The velocity ratio is about 0.2 higher for separation to occur on the aft portion of the hub than on the forward portion of the inlet lip. For the range of conditions considered, separation does not occur on either the aft portion of the inlet lip or the forward portion of the hub.

6. Of the several parameters studied, the most significant parameter influencing the magnitude of the peak velocity, and hence also the maximum adverse pressure gradient, is the ratio of the radius of the circular arcs forming the lips of the inlet duct and the hub to the inlet width. Decreasing the ratio of the lip radius to the inlet width increases the velocity peak. This increase is accompanied by a moderate reduction in flow non-uniformity across the duct. In general, the critical velocity ratio at which flow separation begins to occur on the forward inlet lip decreases sharply with decreasing lip radius, as expected. However, in one case no change in the critical velocity was observed with a twenty percent decrease in the lip radius. This anomaly is worthy of further study.

7. The inclined duct does not offer a significant advantage over the perpendicular duct in terms of minimizing the adverse pressure gradient that exists on the forward position of the inlet lip.

8. Raising or lowering the hub has little effect on the magnitude of the peak velocity for intermediate values of freestream to mean inlet velocity ratio (between 0.2 and 0.7). For high values of the velocity ratio, a raised hub gives a lower peak velocity on the inlet lip and a higher peak velocity on the hub. For low values of the velocity ratio, the converse is true.

The trends for a lowered hub are opposite to that for a raised hub. The flow non-uniformity is severe for a lowered hub at planes in the duct near the top surface of the hub.

9. An increase in the Reynolds number can result in a relatively large increase in the critical velocity ratio. This suggests that additional parametric studies must include less restricted flow geometries than considered here.

10. For duct Mach numbers up to 0.5 the critical velocity ratios for separation were not influenced by Mach number. However, these compressible flow boundary layer analyses were based on edge velocities determined from incompressible, potential flow solutions. The effects of compressibility might become important with compressible, potential flow solutions.

11. In some cases, a simple criterion on the ratio of the maximum inlet lip velocity to the duct velocity is sufficiently accurate for estimating the critical velocity ratio at which flow separation begins.

REFERENCES

1.   Tryckare, Tre, <u>The Lore of Flight</u>, Time-Life Books, 1970.

2.   Hickey, D. H., "Preliminary Investigation of the Characteristics of a
     Two-Dimensional Wing and Propeller with the Propeller Plane of Rotation
     in the Wing-Chord Plane," NACA RM A57F03, Aug. 1957.

3.   Russell, H., True, H., "Phase I Flight Testing Results of the Lift Fan
     Propulsion System," 10th Annual ASME Gas Turbine Conference and Pro-
     ducts Show, Washington, D. C., 1965.

4.   Hickey, D., Ellis, D., "Wind-Tunnel Tests of A Semispan Wing with a
     Fan Rotating in the Plane of the Wing," NASA TN D-88, Oct. 1959.

5.   Duvivier, J., McCallum, R., "Investigation of Tilting Duct and Fan-
     Wing in Transition Flight," MIT ASRL Tech. Rept. 90-1, Dec. 1960.

6.   Partlett, L., "Aerodynamic Characteristics of a Small-Scale Shrouded
     Propeller at Angles of Attack from 0° to 90°," NACA TN 3547, Nov. 1955.

7.   Gregory, N., Raymer, W., Love, E.,"The Effect of Forward Speed on the
     Inlet Flow Distribution and Performance of a Lifting Fan Installed in
     a Wing," A. R. C. R & M 3388, June, 1962.

8.   Maki, R., Hickey, D., "Aerodynamics of a Fan-in-Fuselage Model," NASA
     TN D-789, May, 1961.

9.   Trebble, W., Williams, J., "Exploratory Wind-Tunnel Investigations on
     a Bluff Body Containing a Lifting Fan," A.R.C. C.P. 597, April 1961.

10. Aoyagi, K., Hickey, D., de Savigny, R., "Aerodynamic Characteristics
     of a Large-Scale Model with a High Disc-Loading Lifting Fan Mounted in
     the Fuselage," NASA TND-775, Oct. 1961.

11. Smith, A. M. O., "Incompressible Flow About Bodies of Arbitrary Shape,"
     IAS Paper 62-143, June 1962.

12. Lotz, I., "Calculation of Potential Flow Past Airship Bodies in Yaw,"
     NACA TM 675, July, 1932.

13. Smith, A. M. O., Pierce, J., "Exact Solution of the Neumann Problem.
     Calculation of Non-Circular Plane and Axially Symmetric Flows About
     or Within Arbitrary Boundaries," Douglas Aircraft Co., Report ES-26988,
     April, 1958.

14. Hess, J., "Calculation of Potential Flow about Bodies of Revolution
     having Axes Perpendicular to the Free-Stream Direction," JAS, Vol. 29,
     No. 6, June 1962.

15. Fowler, H., "Some Tests of 12-in. Diameter Model VTOL Ducted Fans," National Research Council of Canada Aeronautical Report LR-367, 1962.

16. Hickey, D., Hall, L., "Aerodynamic Characteristics of a Large-Scale Model of Two High Disc-Loading Fans Mounted in the Wing," NASA TN D-1650, Feb. 1963.

17. Goldsmith, R., Hickey, D., "Characteristics of Lifting-Fan V/STOL Aircraft," Astronautics and Aerospace Engineering, Vol. 1, No. 9, p. 70, Oct. 1963.

18. Williams, J., "Some British Research on the Basic Aerodynamics of Powered Lift Systems," Jour. Royal Aero. Soc., Vol. 64, p. 413, July 1960.

19. Kirk, J., Hickey, D., Hall, L., "Aerodynamic Characteristics of a Full-Scale Fan-in-Wing Model Including Results in Ground Effect with Nose-Fan Pitch Control," NASA TN D-2368, July 1964.

20. Gregory, N., Raymer, W., Love, E., "Wind Tunnel Tests of a Wing Fitted with a Single Lifting Fan," ARC R & M 3457, Dec. 1964.

21. Turner, R., Sparkes, D., "Tests on a Simulated Lifting Fan System with Inlet Cross Flow," ARC R & M 3461, Aug. 1964.

22. Schaub, U., Cockshutt, E., "Analytical and Experimental Studies of Normal Inlets, with Special Reference to Fan-in-Wing VTOL Powerplants," Proceedings of the 4th Congress of the International Council of the Aeronautical Sciences, Aug. 1964; Spartan Books, Inc., 1965, p. 519.

23. Schaub, U., Bassett, R., Cockshutt, E., "An Investigation of the Aero-dynamics of Inlets in the Upper Surface of a Wing," Quar. Bull. of Div. of Mech. Eng. and N.A.E., National Research Council of Canada, Dec. 1966.

24. Schaub, U., Bassett, R., "Analysis of the Performance of a Highly-Loaded 12-inch VTOL Z-Axis Fan-In-Wing at Zero Forward Speed," National Research Council of Canada Aeronautical Report LR-439, Sept., 1965.

25. Schaub, U., "Experimental Studies of VTOL Fan-In-Wing Inlets," Agardograph 103, Pt. II, Oct. 1965, p. 715.

26. Tyson, B., "Tests to Establish Flow Distortion Criteria for Lift Engines," AIAA Journal of Aircraft, Vol. 2, No. 5, Sept.-Oct. 1965.

27. Davenport, E., Kuhn, R., "Wind-Tunnel-Wall Effects and Scale Effects on a VTOL Configuration with a Fan Mounted in the Fuselage," NASA TN D-2560, Jan. 1965.

28. Kuhn, R., McKinney, M., NASA Research on the Aerodynamics of Jet VTOL Engine Installations," Agardograph 103, Part II, Oct. 1965, p. 689.

29. Dickard, H., "Lift-Fan V/STOL Propulsion and Airframe Integration," Agardograph 103, Part II, Oct. 1965.

30. Beeler, E., "Lift Fan V/STOL," General Electric Company Advanced Engine and Technology Department, 1965.

31. Hess, J., Smith, A., "A General Method for Calculating Low Speed Flows About Inlets," Agardograph 103, Part I, Oct., 1965, p. 345.

32. Hess, J., Smith, A., "Calculation of Potential Flows About Arbitrary Bodies," Progress in Aeronautical Sciences, Vol. 8, Pergamon Press, p. 1-138, 1967.

33. Rubbert, P., Saaris, G., Scholey, M., Standen, N., Wallace, R., "A General Method for Determining the Aerodynamic Characteristics of Fan-In-Wing Configurations," The Boeing Company, USAAVLABS Tech. Report 67-61A and 67-61B, Dec. 1967. See also NASA SP218, Sept. 1969.

34. Lavi, R., "An Experimental Investigation of VTOL Lift-Engine Inlet," AIAA Jour. Aircraft, Vol 4, No. 2, March-April, 1967.

35. Przedpelski, Z., "Lift Fan Technology Studies," NASA CR-761, April 1967.

36. Hickey, D., Cook, W., "Aerodynamics of V/STOL Aircraft Powered by Lift Fans," Paper presented at a Specialists Meeting of the Fluid Dynamics Panel of AGARD, Goettingen, Sept. 1967 (N68-22498).

37. Schaub, U., "Experimental Investigation of Flow Distortion in Fan-In-Wing Inlets," AIAA Jour. Aircraft Vol. 5, No. 5, Sept.-Oct. 1968. See also AIAA Paper No. 67-746.

38. Tyler, R., Williamson, R., "Experimental Investigation of Slotted Engine Intakes in the Upper Surface of a Thick Wing," National Research Council of Canada, Aeronautical Report LR-526, Dec. 1968.

39. Graham, W., "Aerodynamic Effects of Lift-Jet and Lift-Fan Inlets in Transition Flight," AIAA Jour. Aircraft, Vol. 6, No. 2, March-April 1969.

40. Shumpert, P. Harris, A., "Full-Scale Development of Lift Engine Inlets for the XV-4B Aircraft," AIAA Jour. Aircraft, Vol. 6, No. 4, July-Aug. 1969.

41. Stockman, N., Lieblein, S., "Theoretical Analysis of Flow in VTOL Lift Fan Inlets Without Crossflow," NASA TN D-5065, Oct. 1968.

42. Stockman, N., "Potential Flow Solutions for Inlets of VTOL Lift Fans and Engines," NASA SP-228, Oct. 1969.

43. Cockshutt, E., "VTOL Propulsion - 1970 Perspective," Canadian Aeronautics and Space Journal, April, 1971.

44. Lieblein, S., "A Review of Lift-Fan Propulsion Systems for Civil VTOL Transports," NASA TM-X-52829, June 1970. (See also AIAA Paper No. 70-670).

45. Serdengecti, S., Marble, F., "A Theory of Two-Dimensional Airfoils with Strong Inlet Flow on the Upper Surface," USAF ARL 70-0139, Aug. 1970.

46. Kirk, J., Barrack, J., "Reingestion Characteristics and Inlet Flow Distortion of V/STOL Lift-Engine Fighter Configurations," NASA TN D-7014, Dec. 1970.

47. Hodder, B., Kirk, J., Hall, L., "Aerodynamic Characteristics of a Large-Scale Model with a Lift Fan Mounted in a 5-Percent-Thick Triangular Wing, Including the Effects of BLC on the Lift-Fan Inlet," NASA TN D-7031, Dec. 1970.

48. Hall, G., "Recirculation Characteristics of A Small-Scale VTOL Lift Engine Pod," NASA CR-1774, May 1971.

49. Hall, G., "Model Tests of Concepts to Reduce Hot Gas Ingestion In VTOL Lift Engines," NASA CR-1863, July, 1971.

50. Benzakein, M., Kazin, S., "Some Experimental Results on Lift Fan Noise Reduction," AIAA/SAE 7th Propulsion Joint Specialists Conference, AIAA Paper No. 71-743, June 1971.

51. Bland, A., "Fan Propulsion System Influence on VTOL Transport Design," AIAA/SAE 7th Propulsion Joint Specialists Conference, AIAA Paper No. 71-744, June 1971.

52. Hill, T., "All Turbofan VTOL or STOL," AIAA Jour. of Aircraft, Vol. 8, No. 4, April, 1971.

53. Dugan, J., Krebs, R., Civinskas, K., Evans, R., "Preliminary Study of an Air Generator-Remote Lift Fan Propulsion System for VTOL Transports," NASA TM-X-67916, Aug. 1971.

54. Lieblein, S., Yuska, Jr., Diedrich, J., "Wind Tunnel Tests of a Wing-Installed Model VTOL Lift Fan With Coaxial Drive Turbine," NASA TM-X-67854, 1971. See also AIAA Paper No. 71-742, June 1971.

73

55. Lieblein, S., Yuska, J., Diedrich, J., "Performance Characteristics of a Model VTOL Lift Fan in Crossflow", AIAA Journal of Aircraft, Vol. 10, No. 3, March, 1973.

56. Yuska, J., Diedrich, J., "Fan and Wing Force Data from Wind-Tunnel Investigation of a 0.38 Meter (15-in.) Diameter VTOL Model Lift Fan Installed in a Two-Dimensional Wing", NASA TN D-6654, 1972.

57. Diedrich, J., Clough, N., Lieblein, S., "Installation Effects on Performance of Multiple Model V/STOL Lift Fans", NASA TM X-68138, 1972.

58. Kellogg, Oliver D., Foundations of Potential Theory, Dover Publications, N. Y., 1953.

59. Kline, S. J., Morkovin, M. V., Sovran, G., and Cockrell, D. J., "Computation of Turbulent Boundary Layers," Proceedings of the 1968 AFOSR-IFP- Stanford Conference, Stanford University Press, 1969.

60. Cebeci, Tuncer, Smith, A.M.O., and Wang, L. C., "A Finite-Difference Method for Calculating Compressible Laminar and Turbulent Boundary Layers," Part I, McDonnell Douglas Report No. DAC-67131, March 1969.

61. Cebeci, Tuncer, Mosinskis, G., and Wang, L. C., "A Finite-Difference Method for Calculating Compressible Laminar and Turbulent Boundary Layers," Part II, McDonnell Douglas Report No. DAC-67131, May 1969.

Table I. Effect of Duct Mach Number on the Minimum Friction Coefficient

$\dfrac{V_\infty}{V_d}$	Re_ℓ	M_d	$c_{f_{min}}$
0.32	14.8×10^6	0.09	0.184×10^{-3}
0.32	14.8×10^6	0.46	0.197×10^{-3}
0.30	14.8×10^6	0.09	0.292×10^{-3}
0.30	14.8×10^6	0.46	0.287×10^{-3}
0.20	4.44×10^6	0.090	0.303×10^{-3}
0.20	4.44×10^6	0.126	0.316×10^{-3}
0.175	2.54×10^6	0.072	0.113×10^{-3}
0.175	2.54×10^6	0.090	0.121×10^{-3}

Table II. Peak to Duct Velocity Ratio for Incipient Separation

$\dfrac{r}{R}$	SECTION	Re x 10^{-6}	$\dfrac{V_\infty}{V_d}$	$\dfrac{V_{max}}{V_d}$
0.15	FORWARD INLET	14.8	0.56	1.98
0.10	FORWARD INLET	14.8	0.36	2.00
0.08	FORWARD INLET	14.8	0.36	2.17
0.15	REAR HUB	14.8	0.76	1.99
0.10	REAR HUB	14.8	0.60	2.03
0.08	REAR HUB	14.8	0.49	2.08
0.15	FORWARD INLET	3.2	0.39	1.80
0.10	FORWARD INLET	3.2	0.21	1.80
0.15	REAR HUB	3.2	0.60	1.79
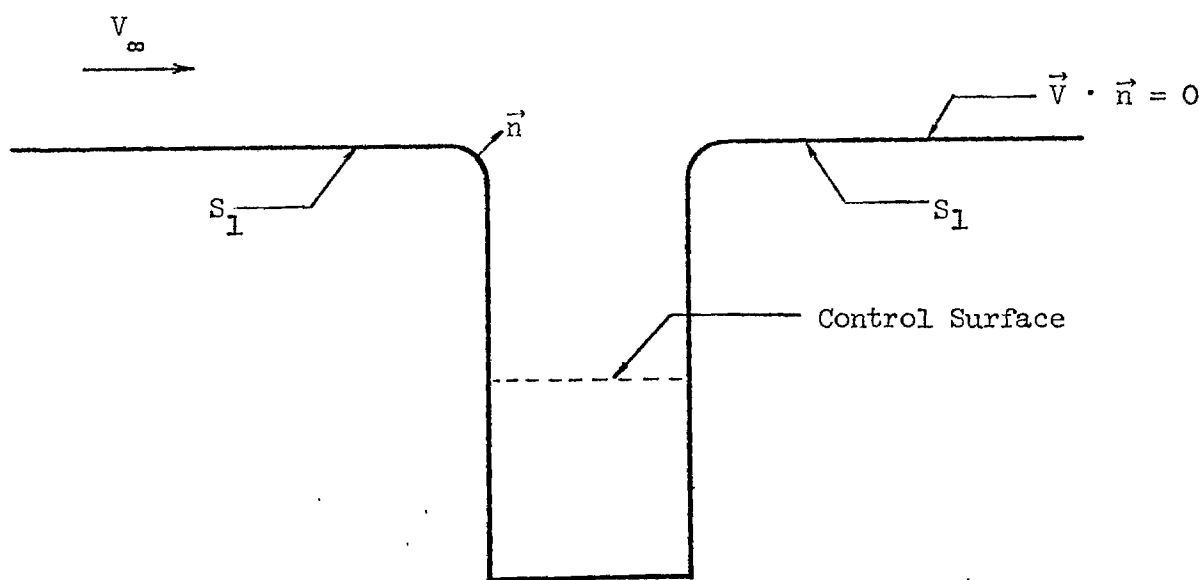
a. First Basic Solution
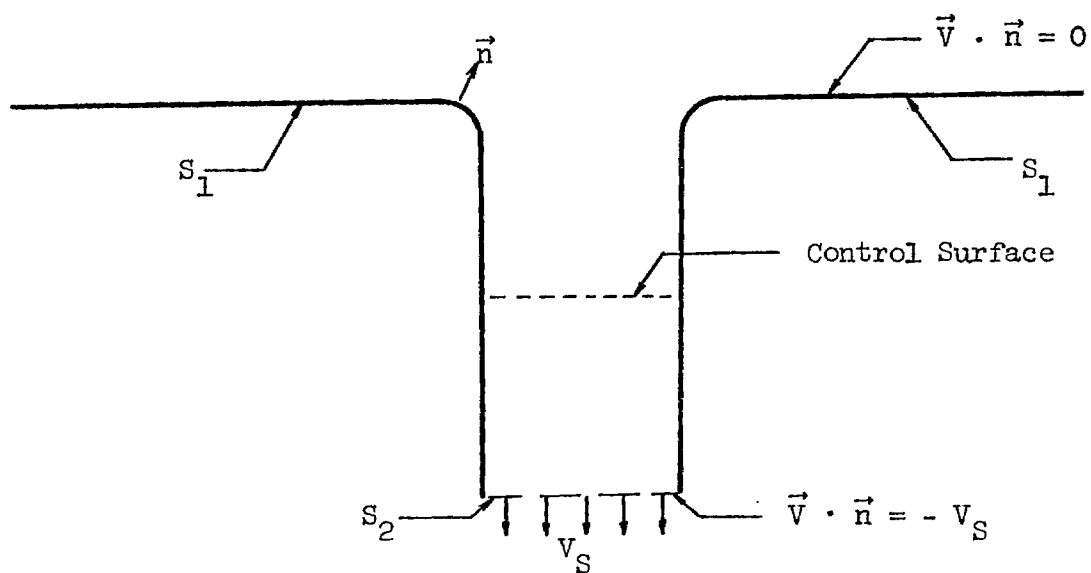
b. Second Basic Solution

FIGURE 1. Boundary Conditions for the Two Basic Solutions
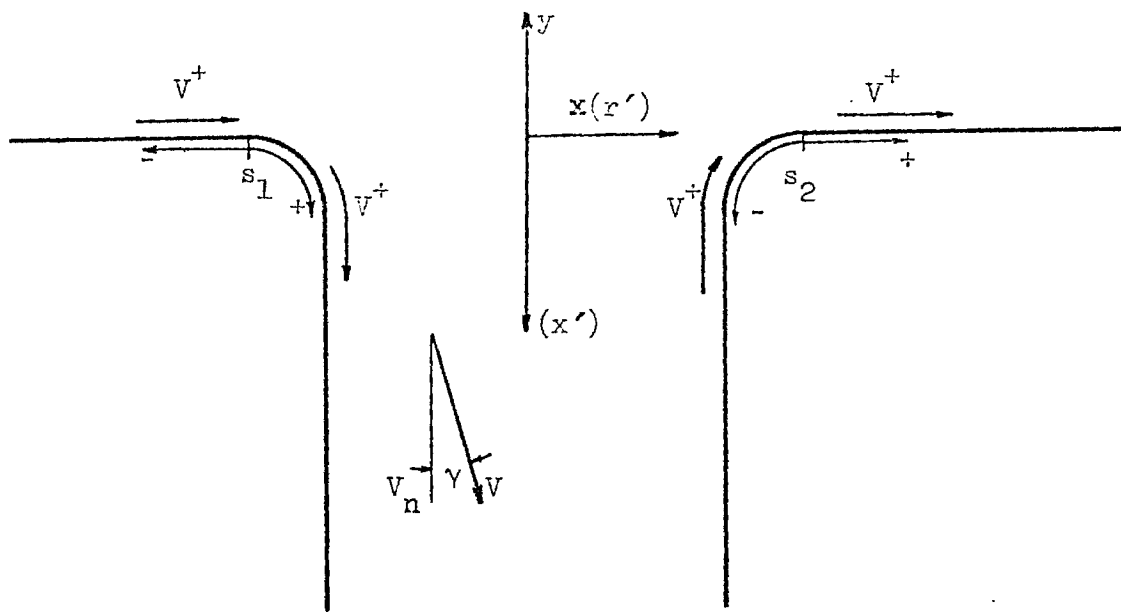
a. Inlet Without Centerbody
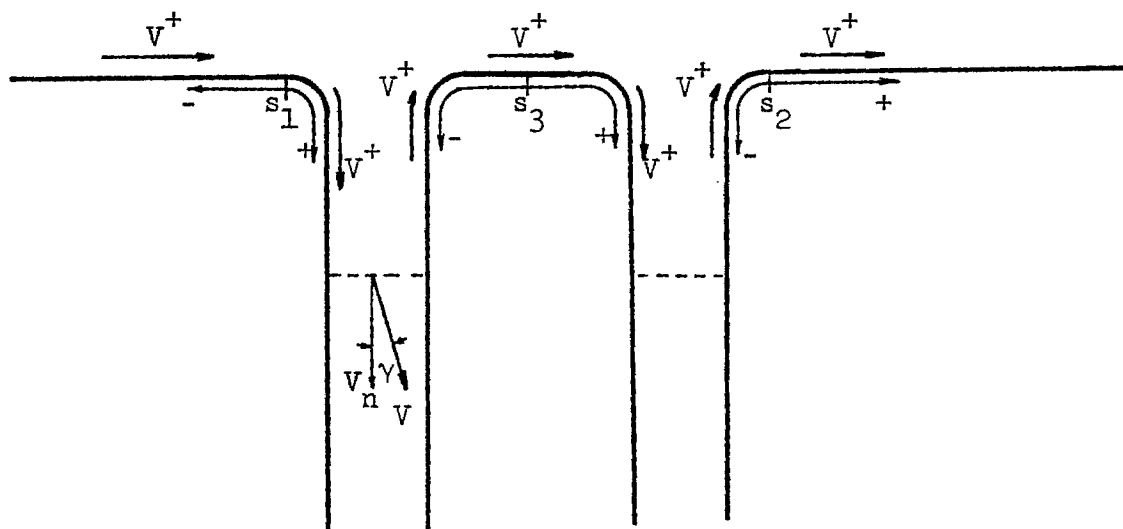
b. Inlet With Centerbody

FIGURE 2. Body Geometries and Sign Conventions.
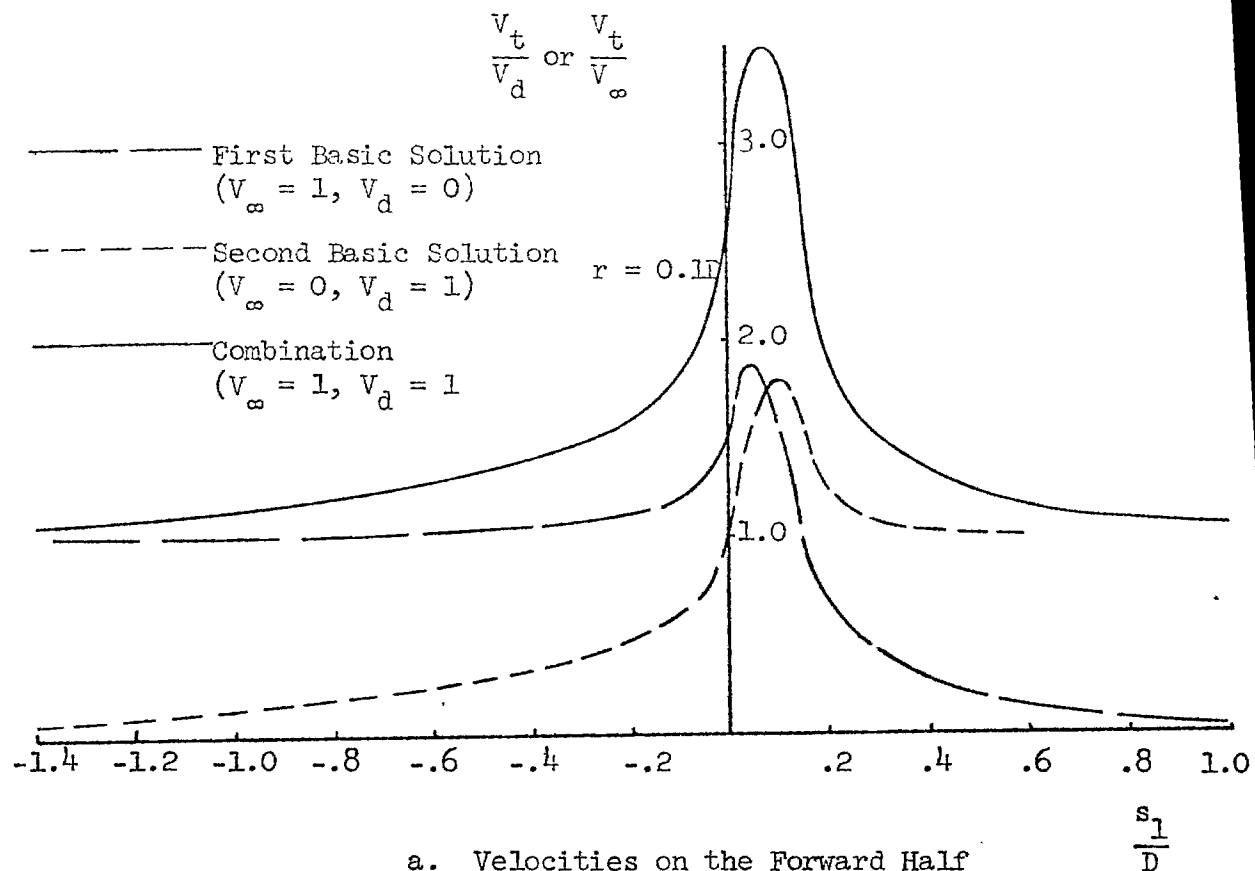
78

a. Velocities on the Forward Half of the Inlet
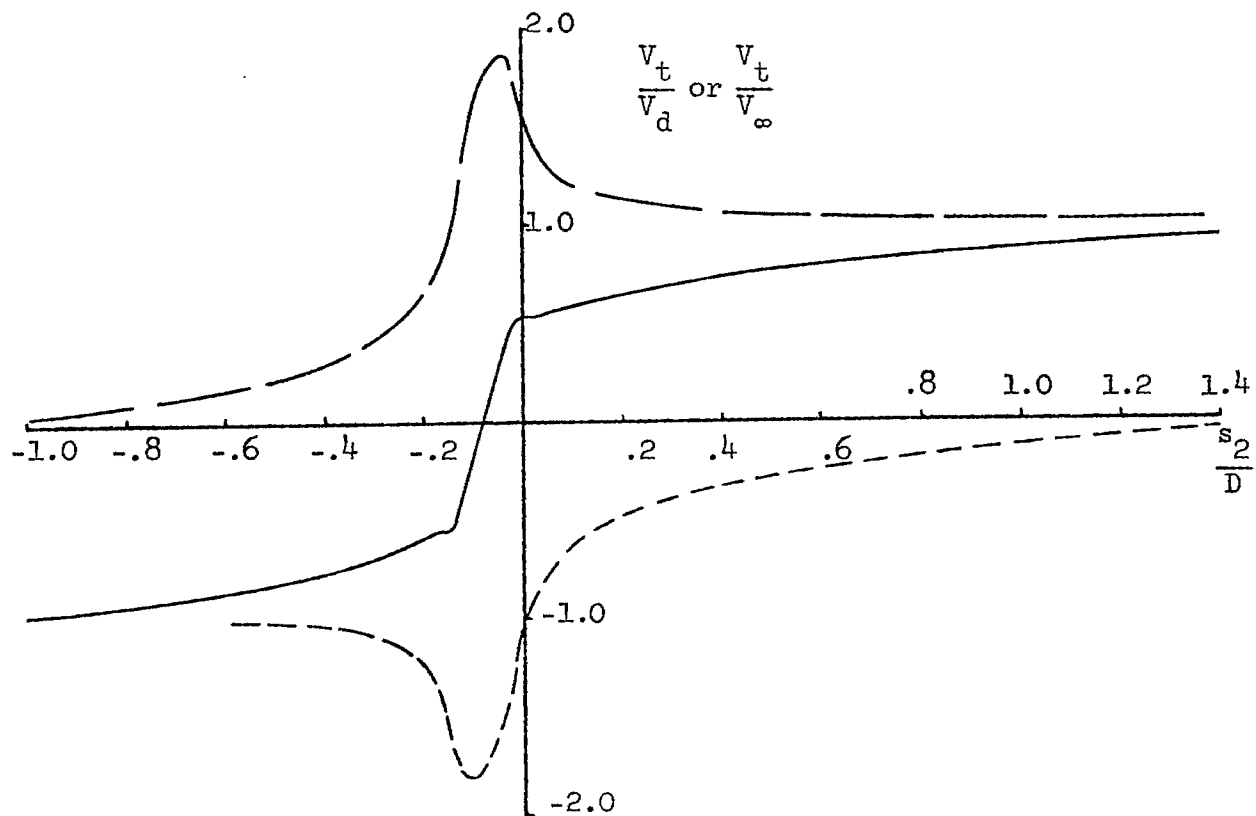
b. Velocities on the Aft Half of the Inlet

FIGURE 3. Tangential Velocities on the Surface of an Inlet

First Basic Solution $(V_\infty = 1, V_d = 0)$ ——O—— d = .15   ——O—— d = .20

Second Basic Solution $(V_\infty = 0, V_d = 0)$ ——△—— d = .15   ——△—— d = .20   r = 0.1D

Combined Solution $(V_\infty = 1, V_d = 1)$ ——◇—— d = .15   ——◇—— d = .20
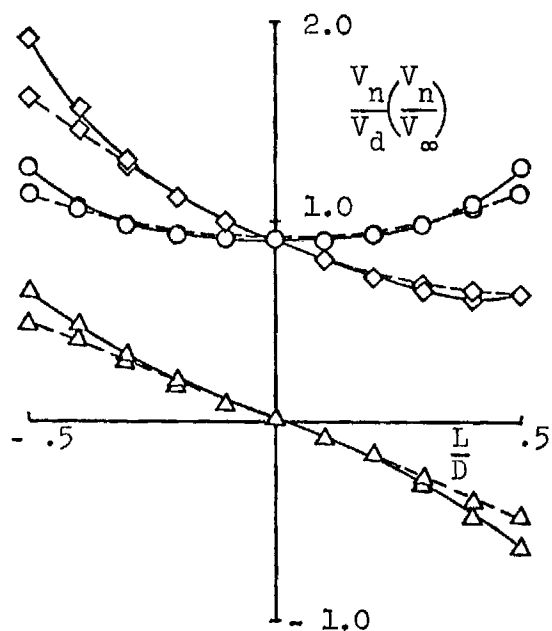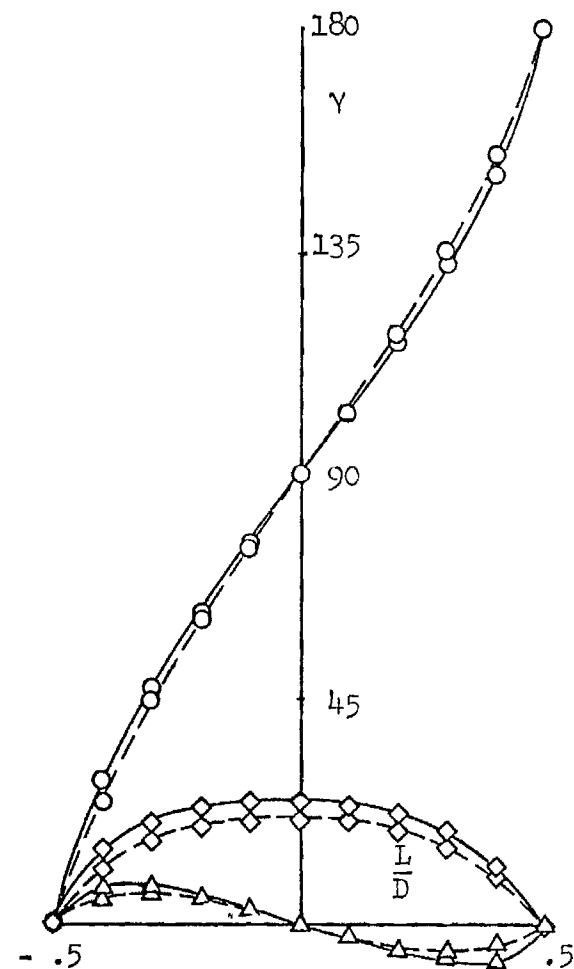
a. Normal Velocities in the Duct   b. Flow Inclination Angle in the Duct

FIGURE 4.   Flow Non-Uniformity Across Two Planes in the Inlet Duct

a. Velocities on the Forward Half of the Inlet

b. Velocities on the Aft Half of the Inlet
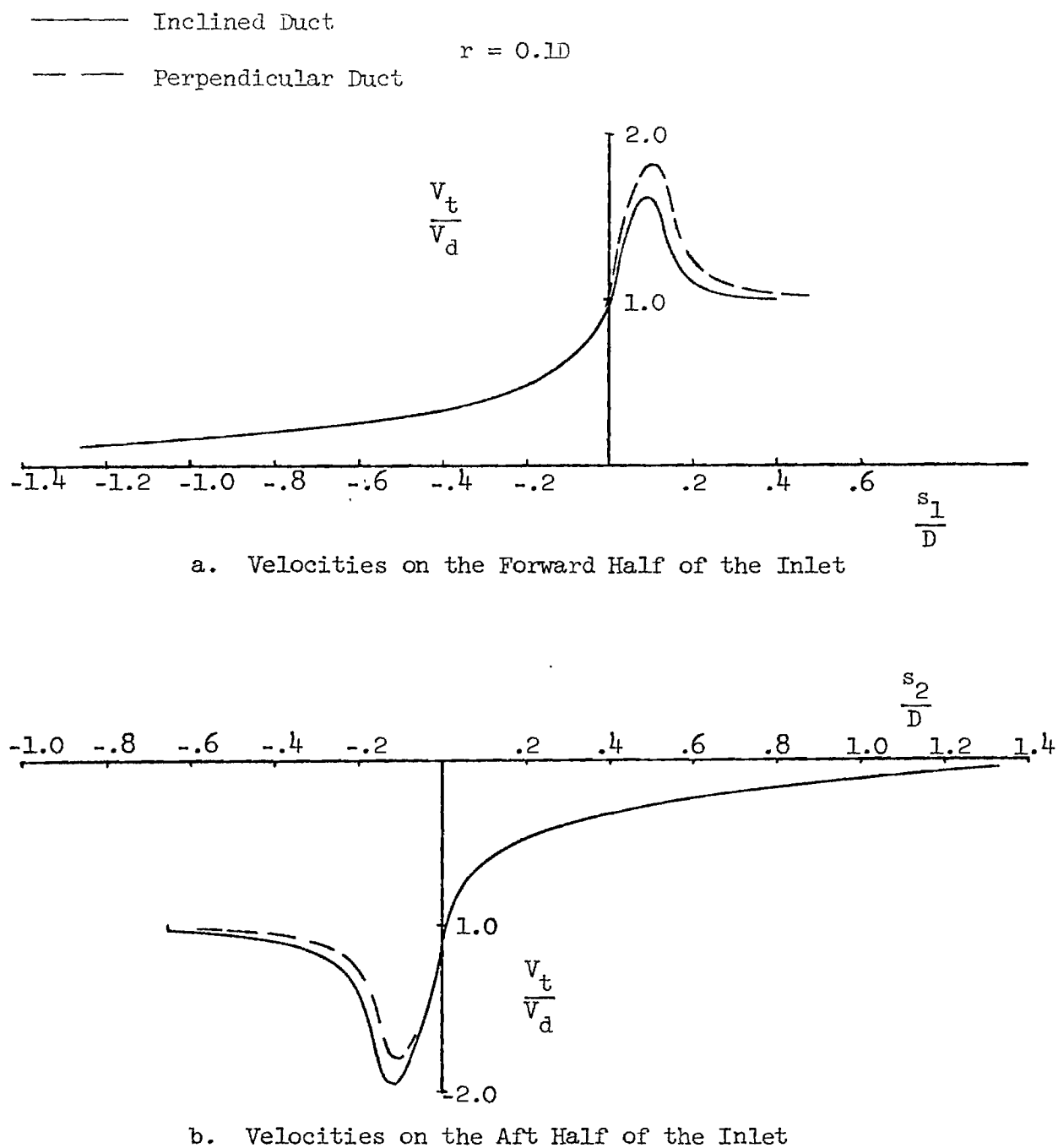
FIGURE 5. Tangential Velocities for an Inclined Duct Compared to Those for a Perpendicular Duct - Second Basic Solution ($V_\infty = 0$, $V_d = 1$).

81

——— Inclined Duct

— —Perpendicular Duct

$r = 0.1D$ $\dfrac{V_t}{V_d}$

a. Velocities on the Forward Half of the Inlet $\dfrac{s_1}{D}$

b. Velocities on the Aft Half of the Inlet
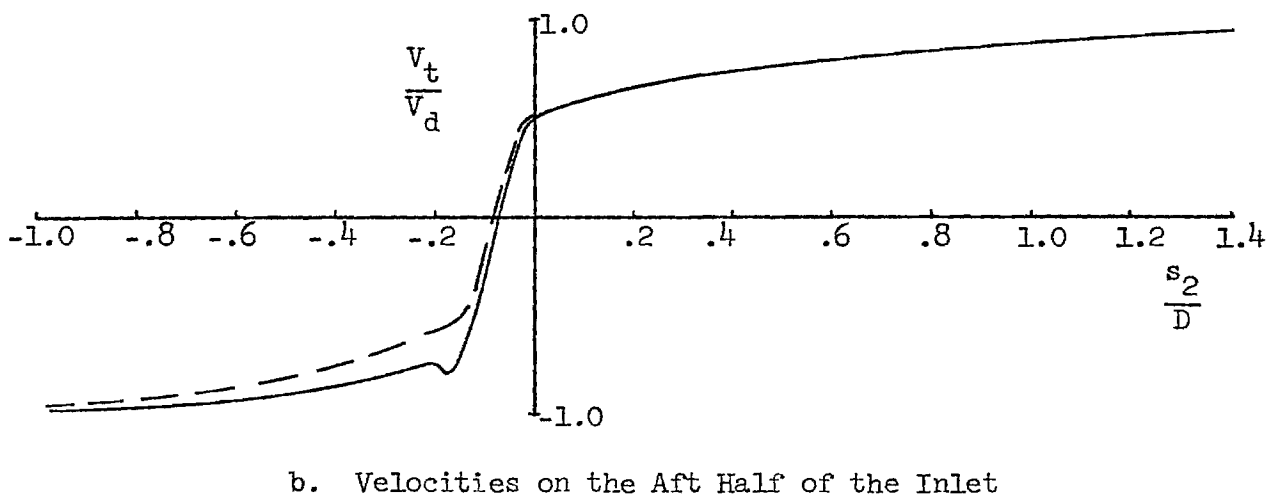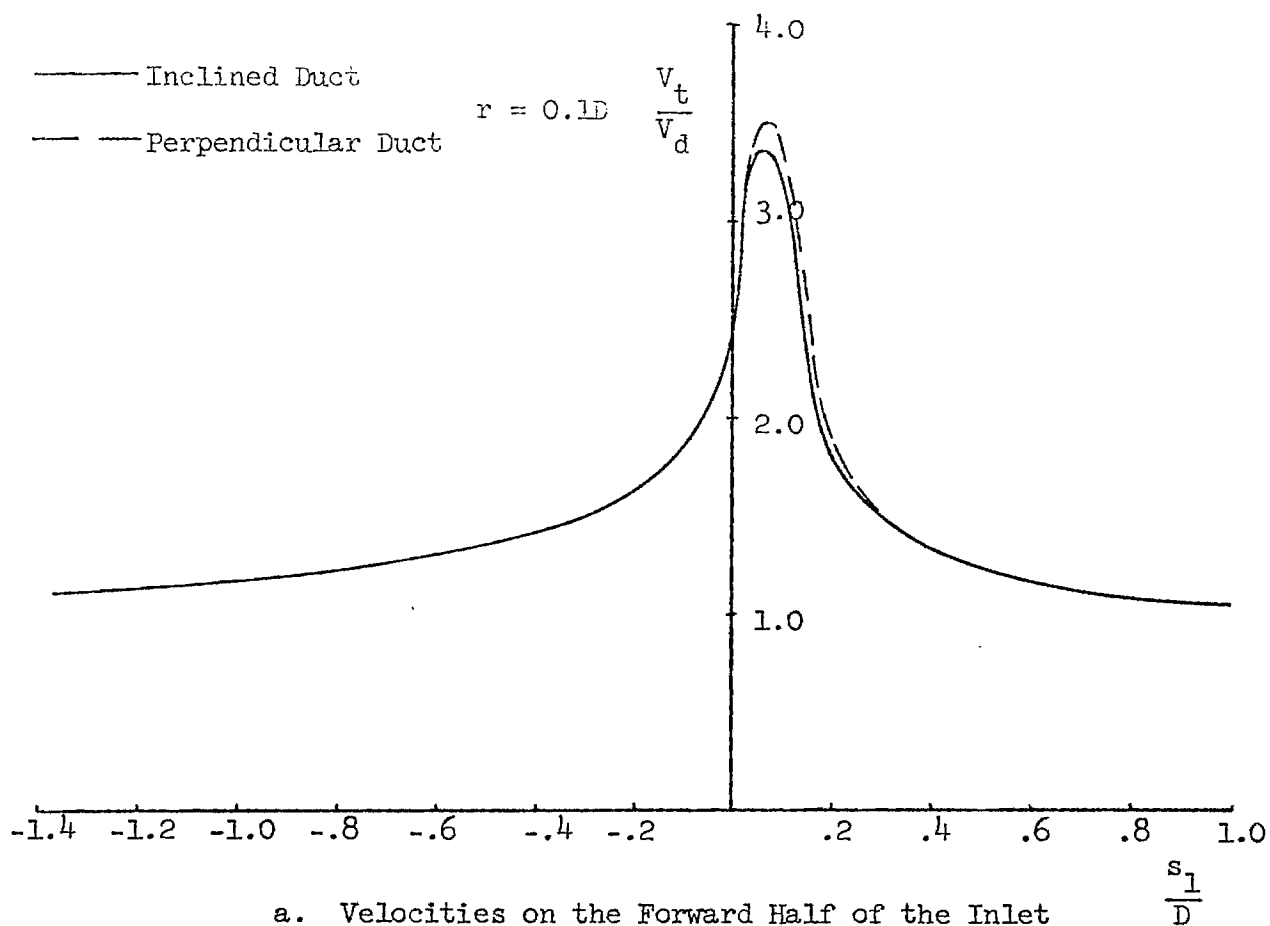
FIGURE 6. Tangential Velocities for an Inclined Duct Compared to Those for a Perpendicular Duct - Combined Solution ($V_\infty = 1$, $V_d = 1$).

82
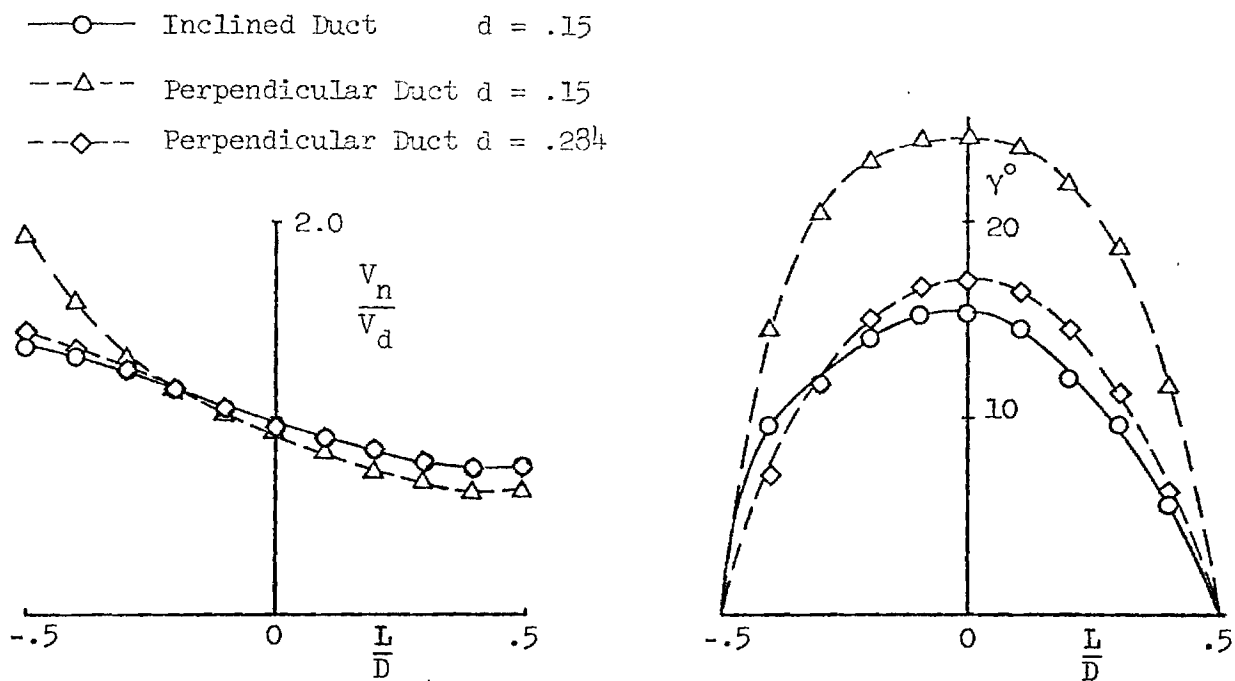
a. Shallower Plane
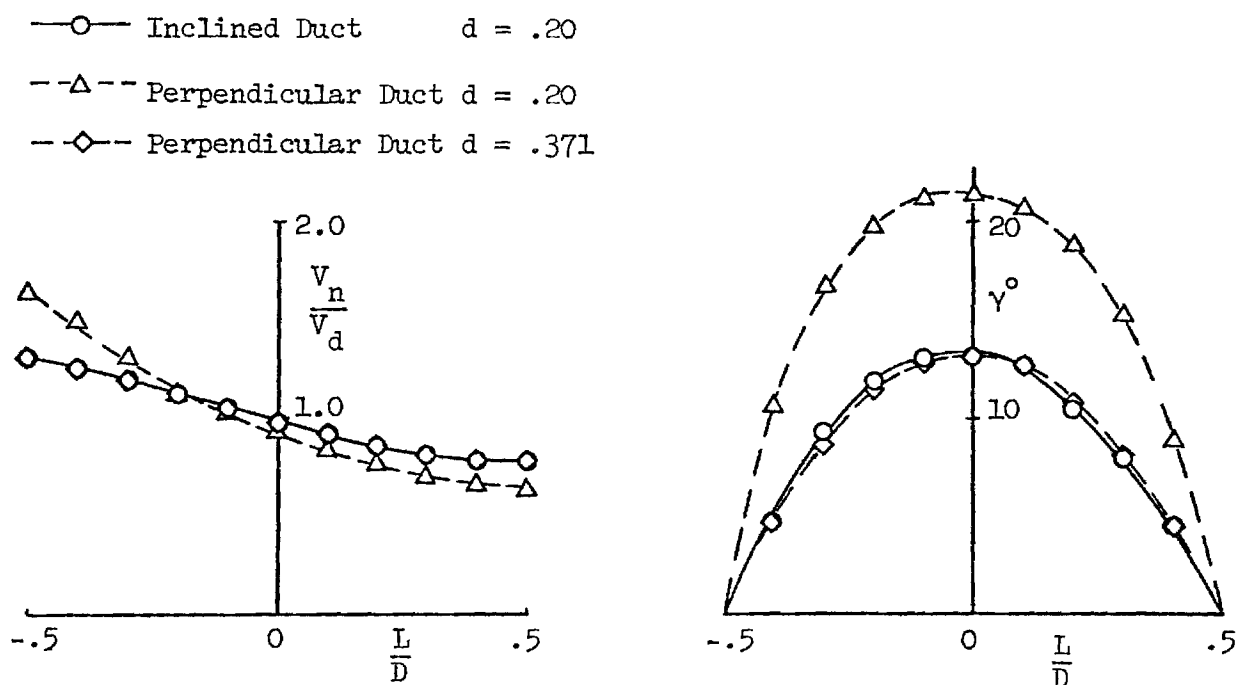
b. Deeper Plane

FIGURE 7. Flow Non-Uniformity Across an Inclined Duct Compared to That
for a Perpendicular Duct - Combined Solution $(V_\infty = 1, V_d = 1)$.

83
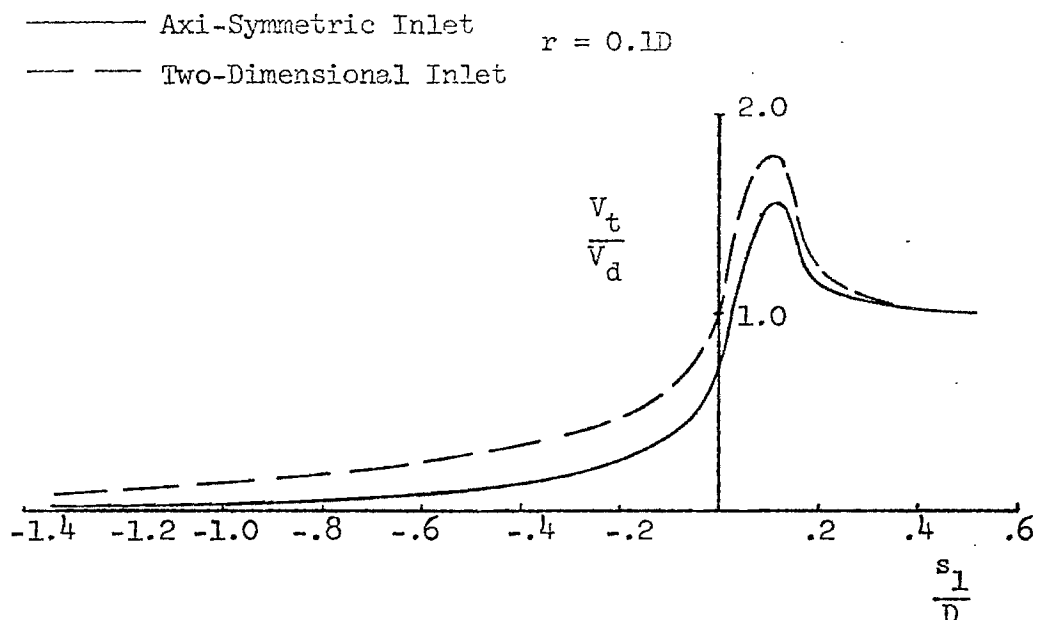
a. Velocities on the Front Half of the Inlet
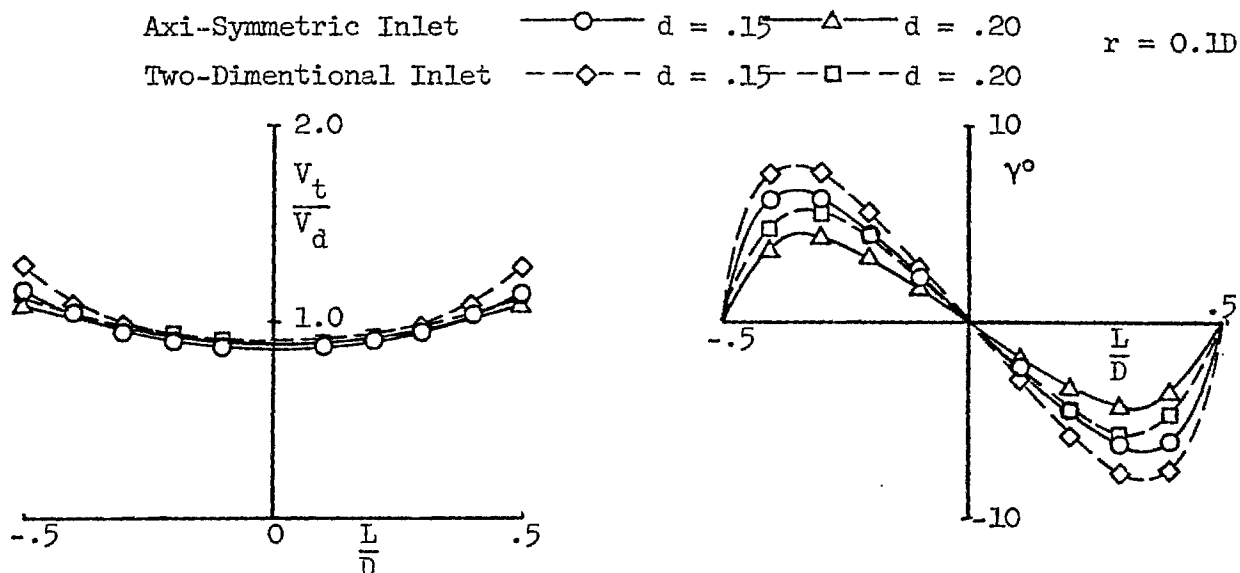
b. Normal Velocities and Flow Inclination Angle across Two Planes in the Ducts

FIGURE 8. Surface Velocities and Flow Non-Uniformity Across the Duct for an Axi-Symmetric Inlet Compared to Those for a Two-Dimensional Inlet - Second Basic Solution ($V_\infty = 0$, $V_d = 1$).
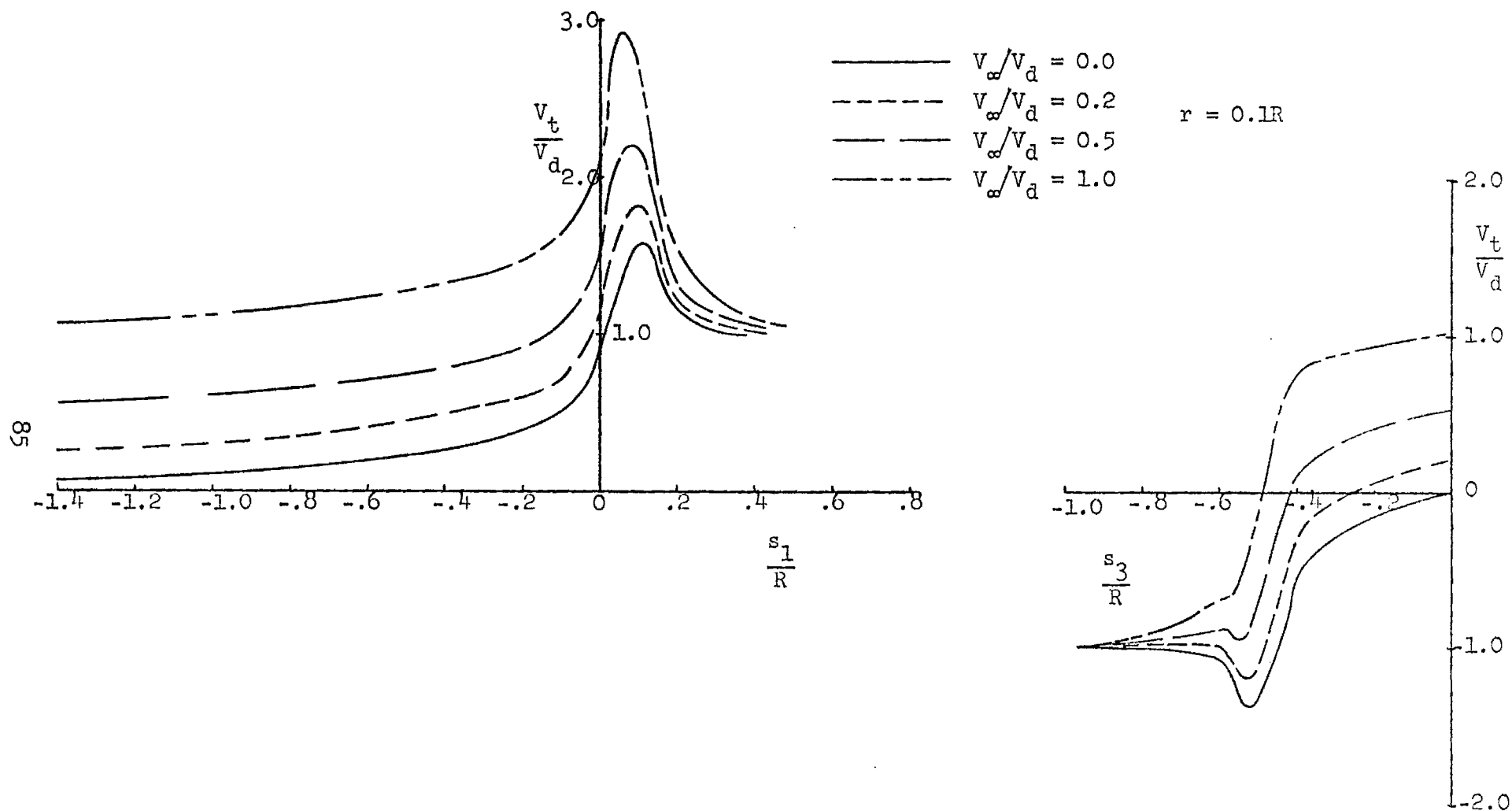
FIGURE 9.   Tangential Velocities on the Forward Half of an Inlet with Centerbody for V_∞/V_d = 0.0, 0.2, 0.5, and 1.0.
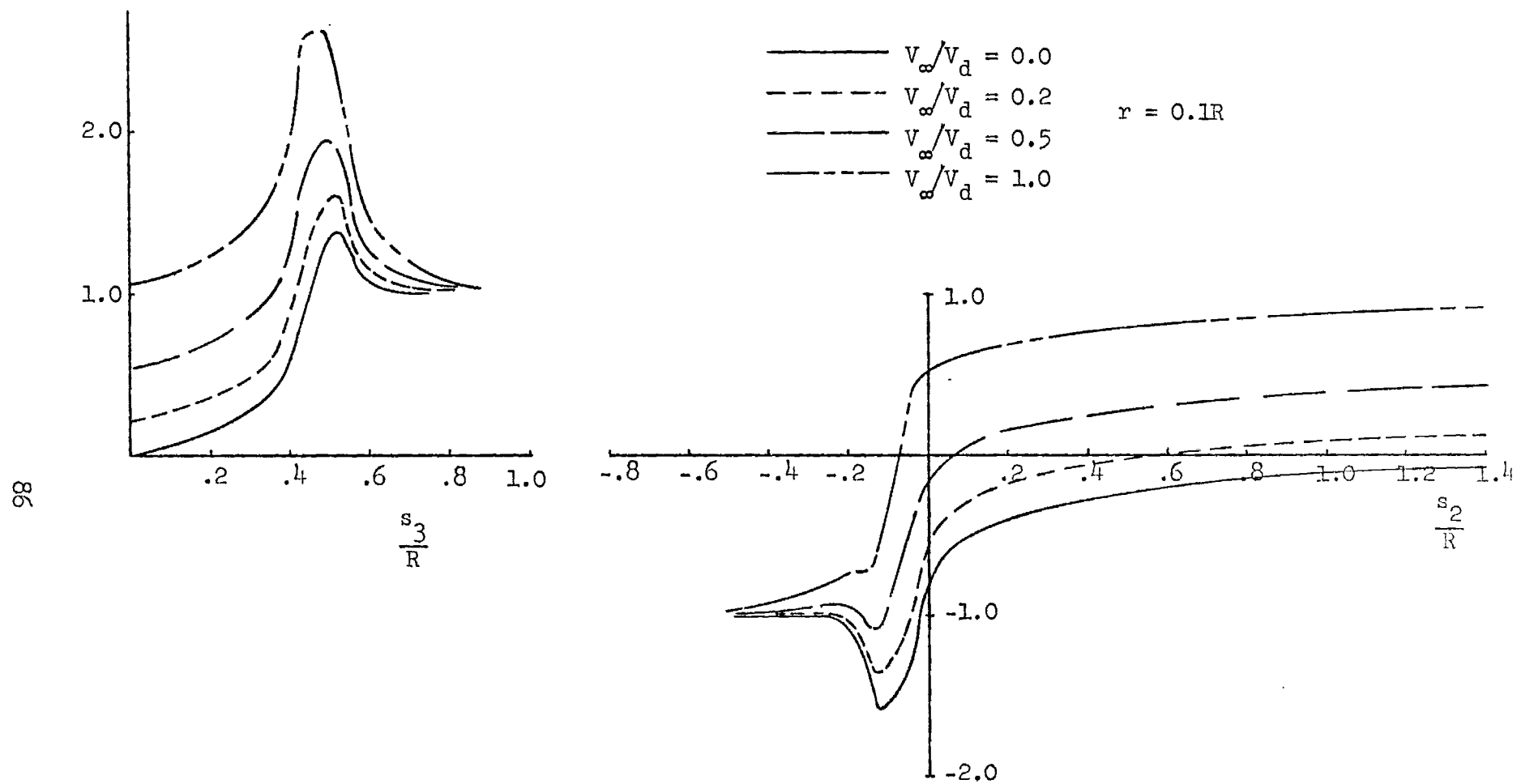
FIGURE 10. Tangential Velocities on the Aft Half of an Inlet with Centerbody for $V_\infty/V_d = 0.0$, 0.2, 0.5, and 1.0.
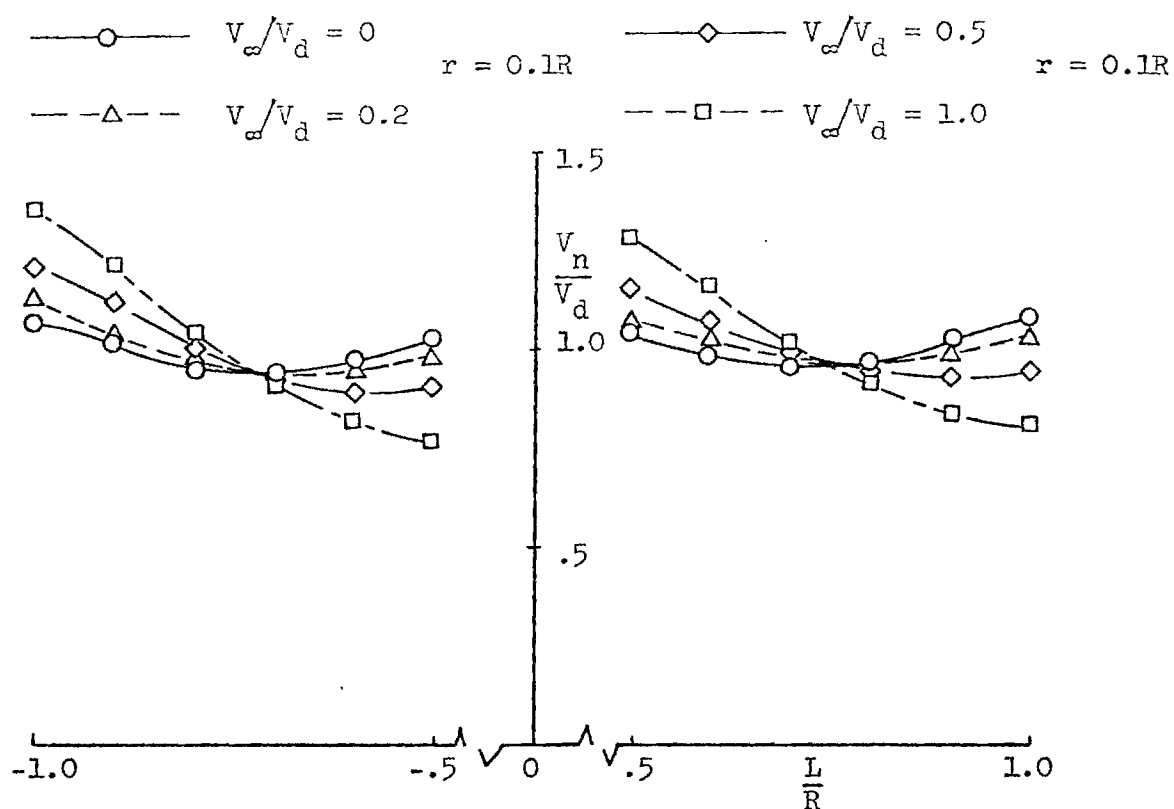
a. Normal Velocities in the Ducts
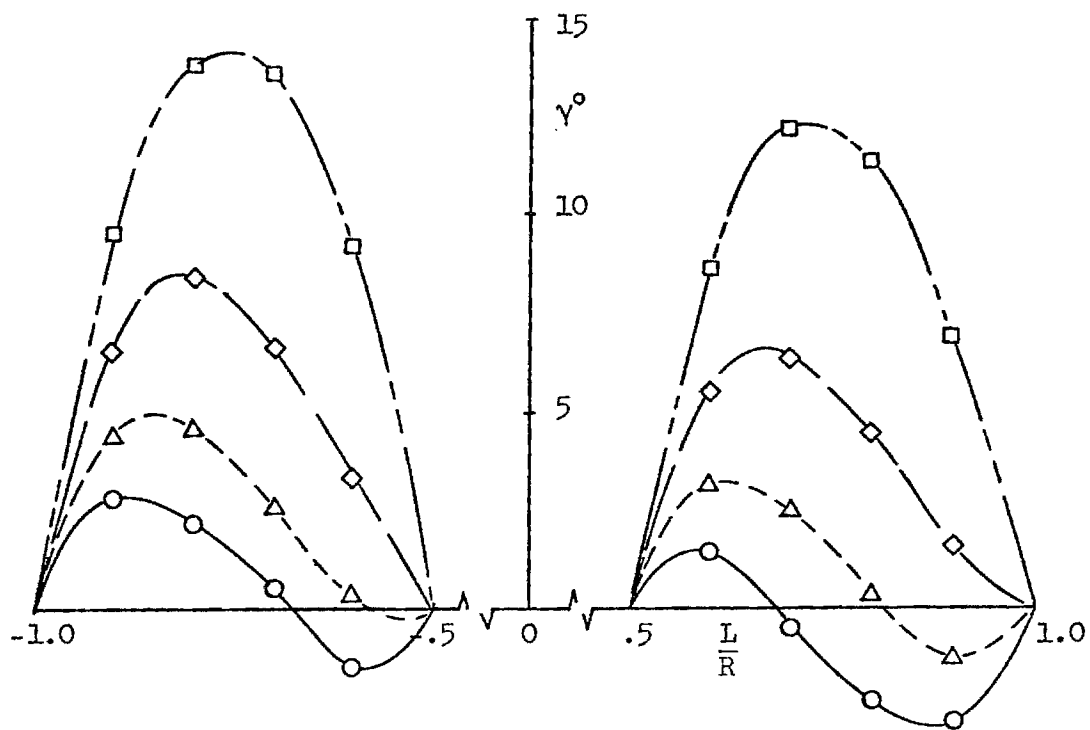
b. Flow Inclination Angles in the Ducts

FIGURE 11. Flow Non-Uniformity Across the Ducts of an Inlet with Centerbody
for V_∞/V_d = 0.0, 0.2, 0.5, and 1.0.

87
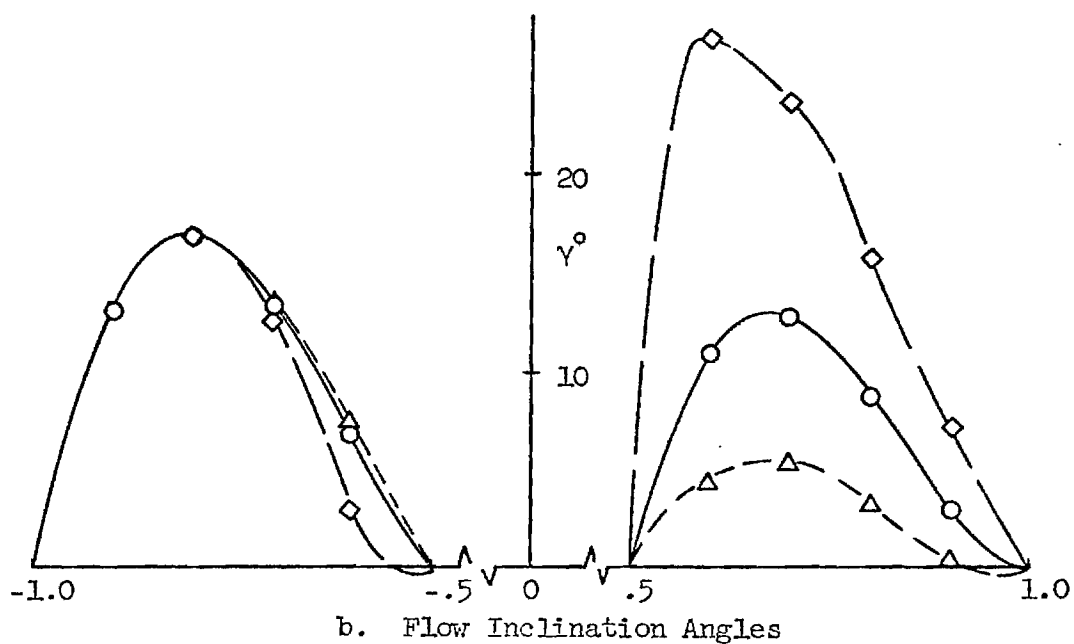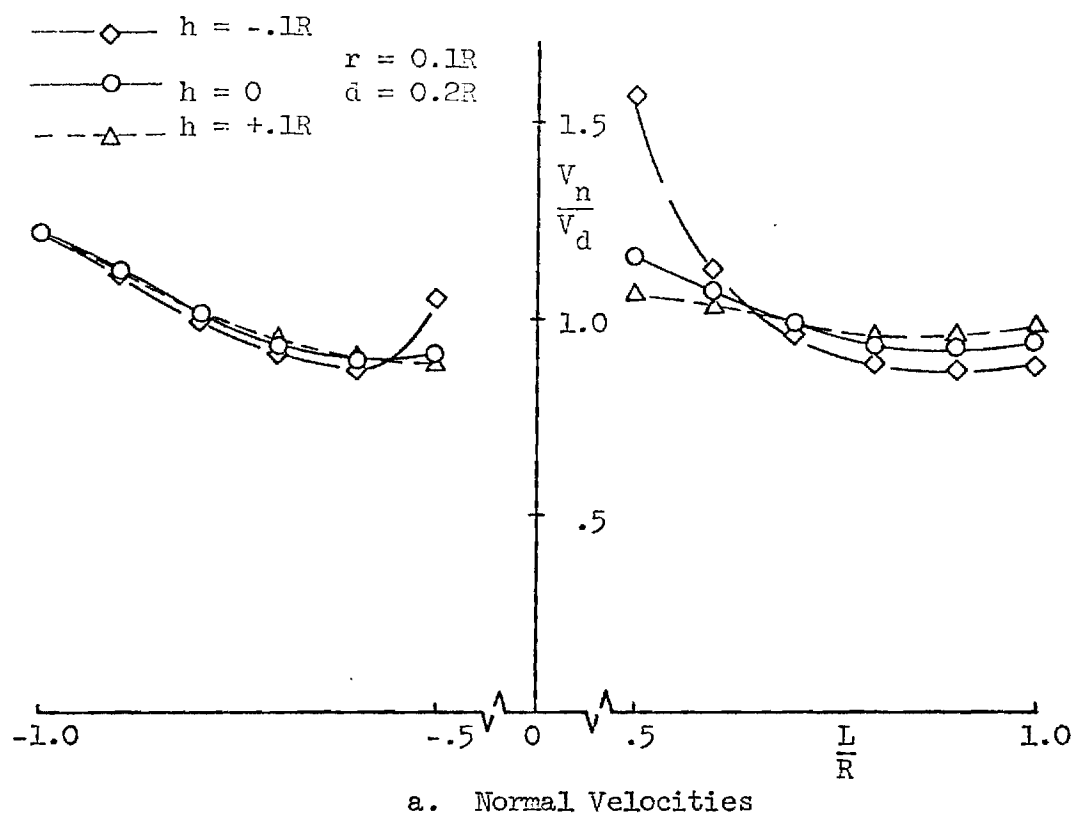
FIGURE 12. Flow Non-Uniformity Across the Ducts of an Inlet with Raised and Lowered Centerbody $(V_\infty/V_d = 0.5)$.

88
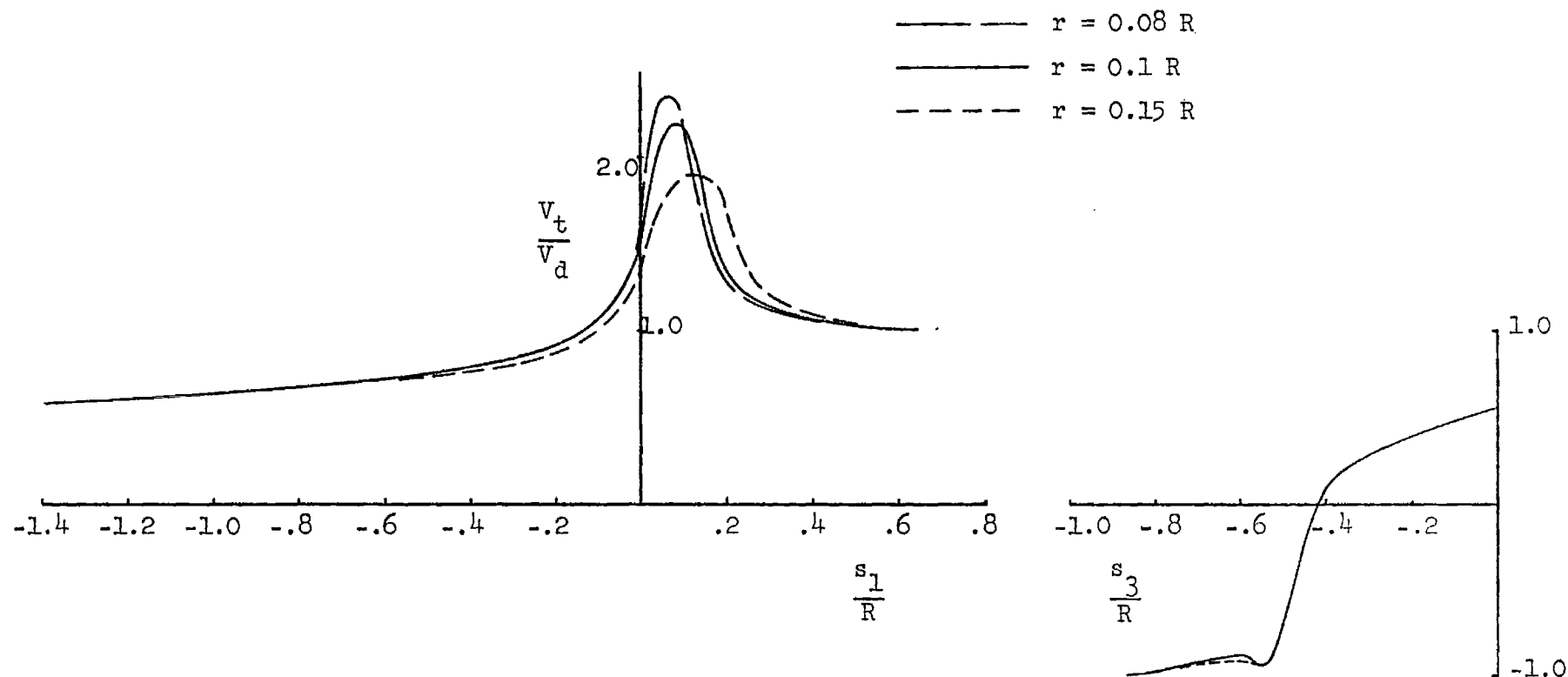
FIGURE 13. Tangential Velocities on the Surface of the Forward Half for Inlets with Inlet and Centerbody Lip Radii of 0.08R, 0.1R, and 0.15R ($V_\infty/V_d = 0.5$).
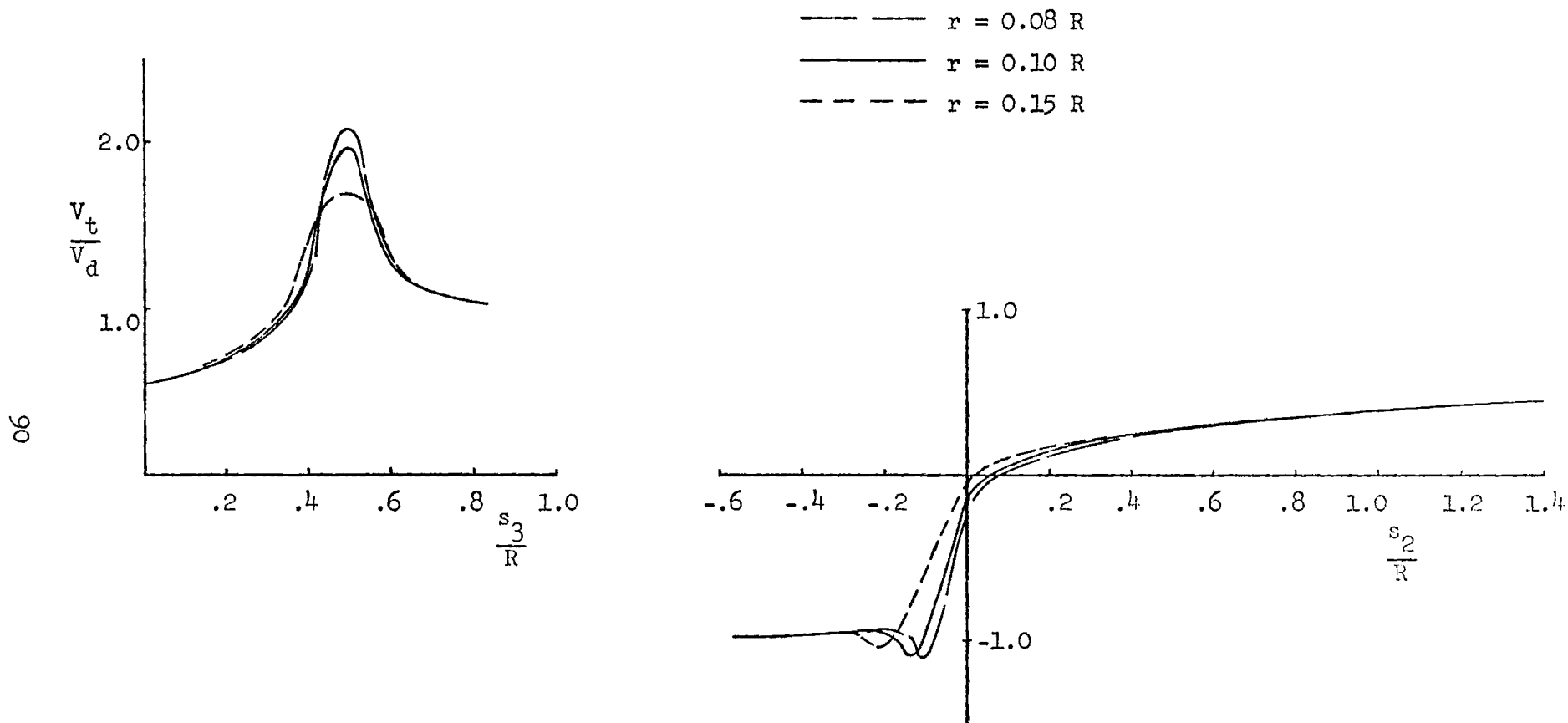
FIGURE 14. Tangential Velocities on the Surface of the Aft Half for Inlets with Inlet and Centerbody Lip Radii of 0.08R, 0.10R, and 0.15R ($V_\infty/V_d = 0.5$).
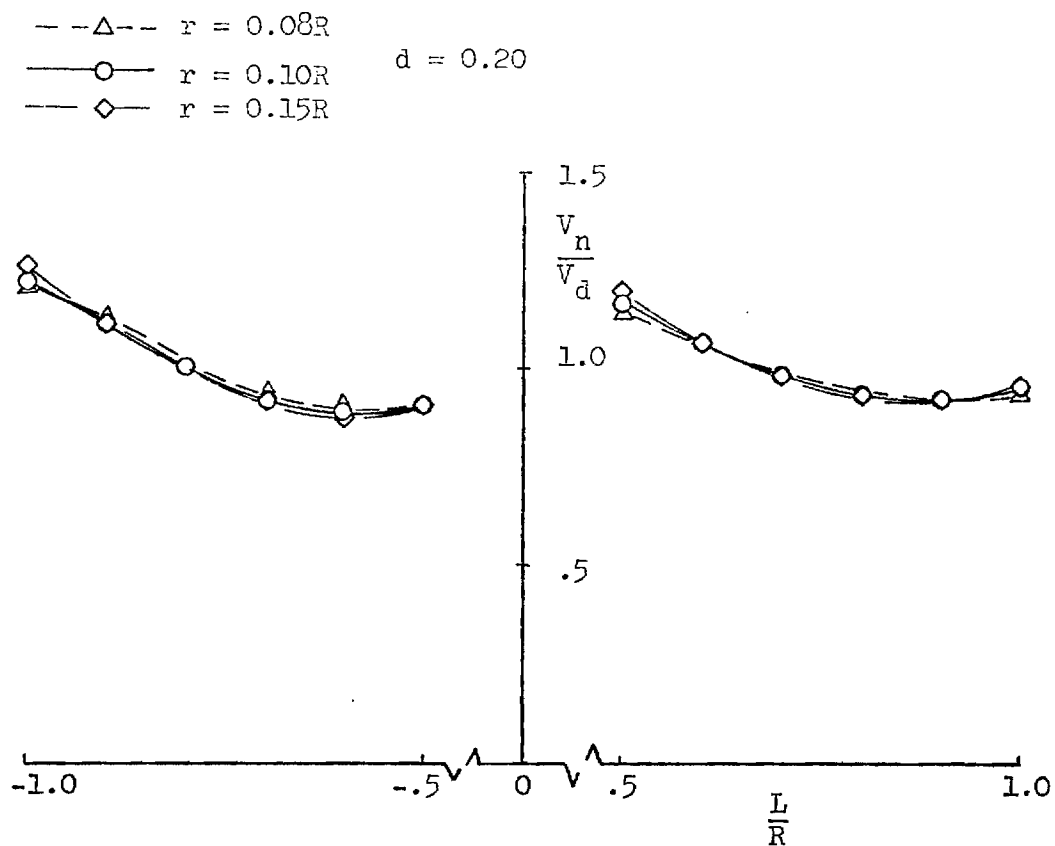
a. Normal Velocities
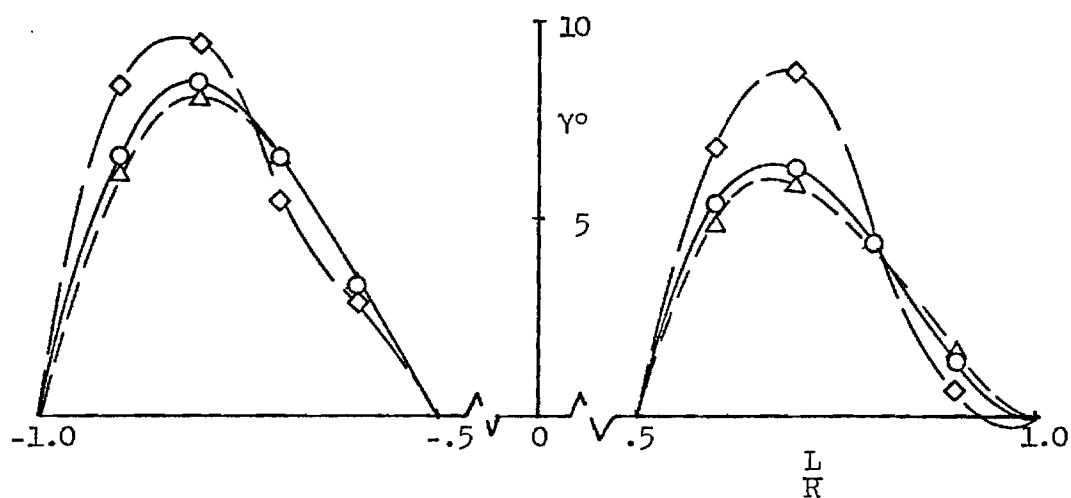
b. Flow Inclination Angle

FIGURE 15. Flow Non-Uniformity Across the Ducts of Inlets with Inlet and Centerbody Lip Radii of 0.08R, 0.10R, and 0.15R (V_∞/V_d = 0.5).
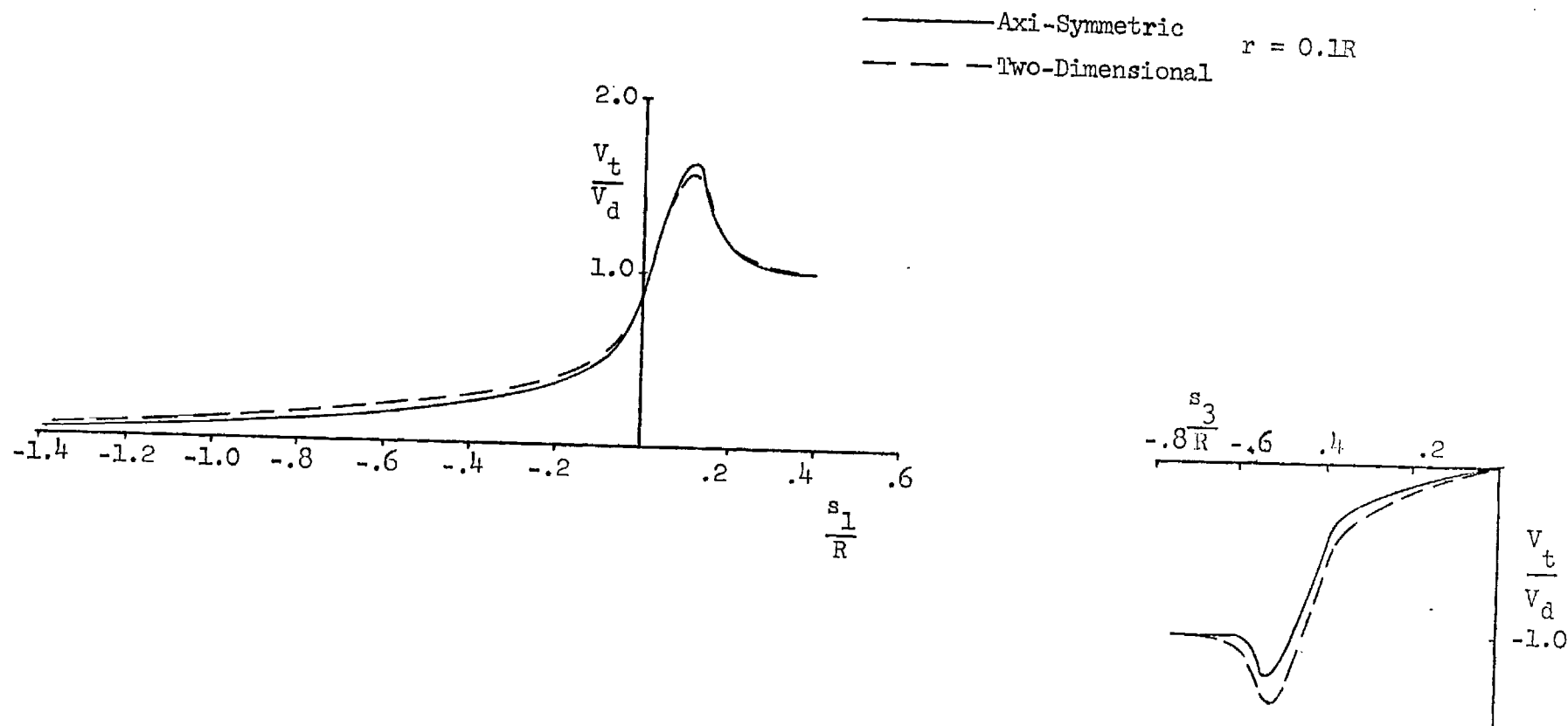
FIGURE 16.   Tangential Velocities on the Surface for an Axi-Symmetric Inlet Compared to Those on a Two-Dimensional Inlet - Second Basic Solution ($V_\infty = 0$, $V_d = 1$).

———○——— Axi-Symmetric   r = 0.1R

— —△— — Two-Dimensional   d = 0.2R
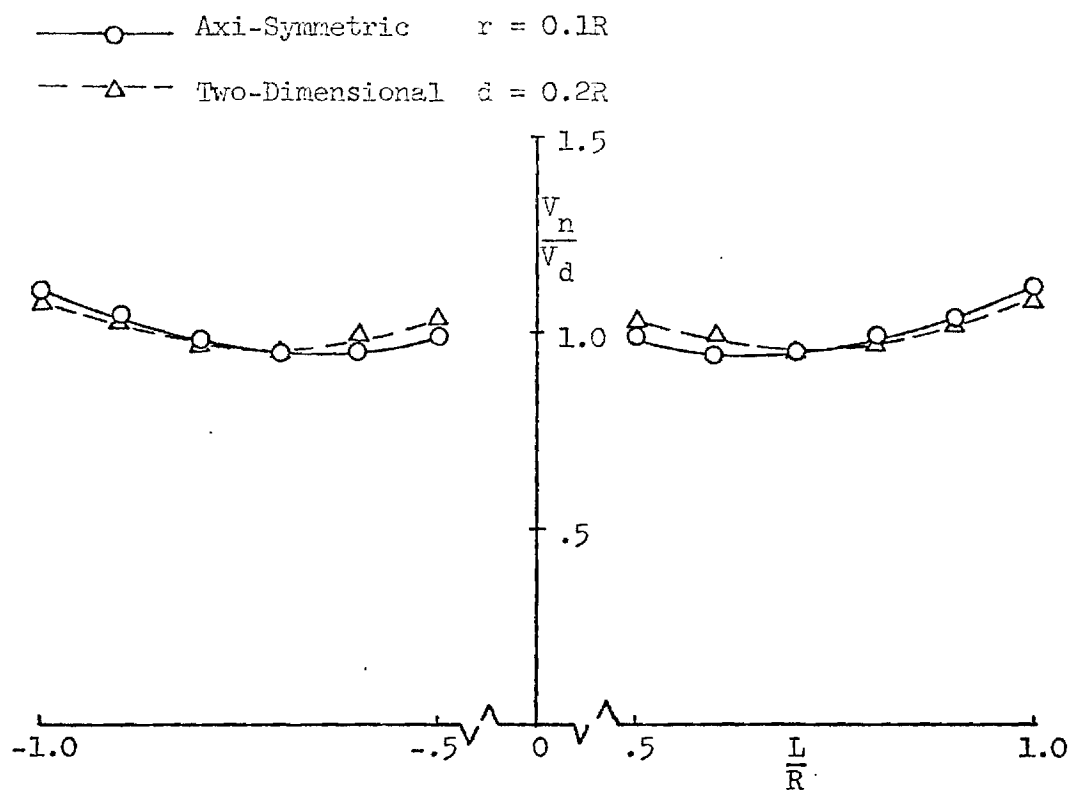
a. Normal Velocities
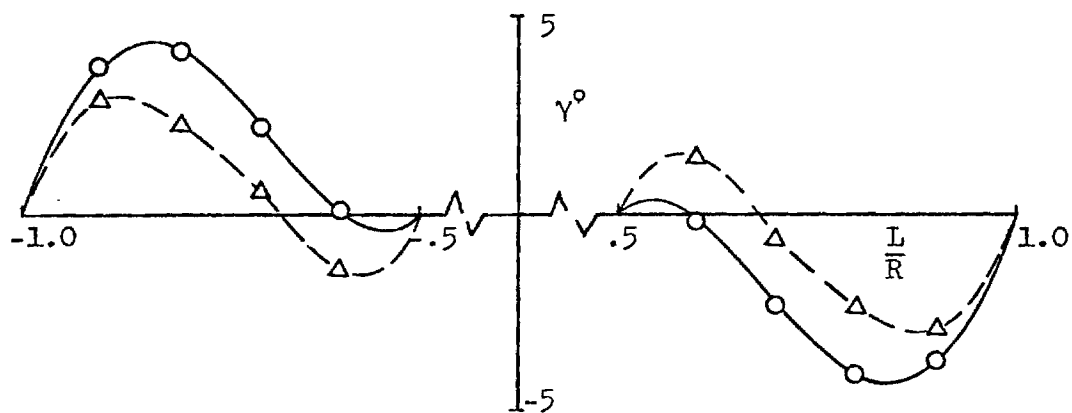
b. Flow Inclination Angles

FIGURE 17. Flow Non-Uniformity Across the Ducts of an Axi-Symmetric Inlet Compared to That of a Two-Dimensional Inlet - Second Basic Solution $(V_\infty = 0, V_d = 1)$.

93
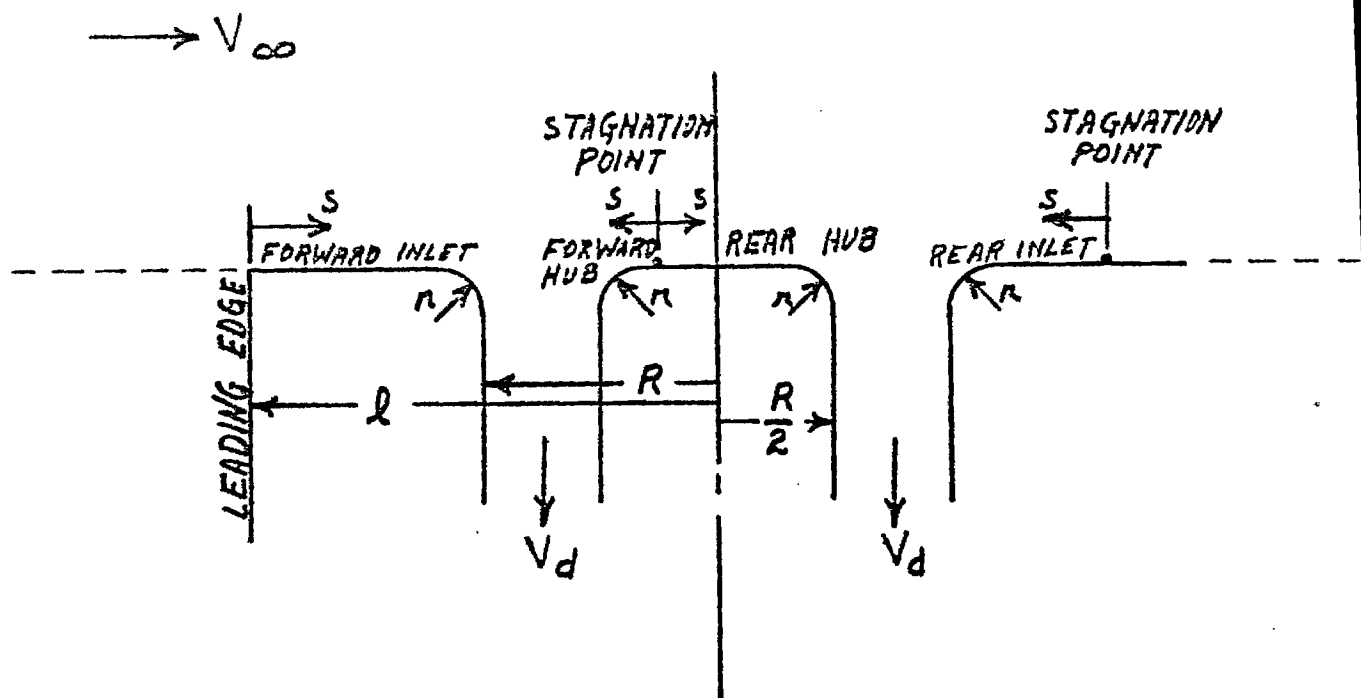
ℓ ~ Distance from simulated leading edge to duct centerline

r ~ Duct lip radius

R ~ Duct radius

s ~ Distance along surface from leading edge or stagnation point

V_d ~ Duct velocity for uniform flow

V_∞ ~ Freestream velocity at infinity
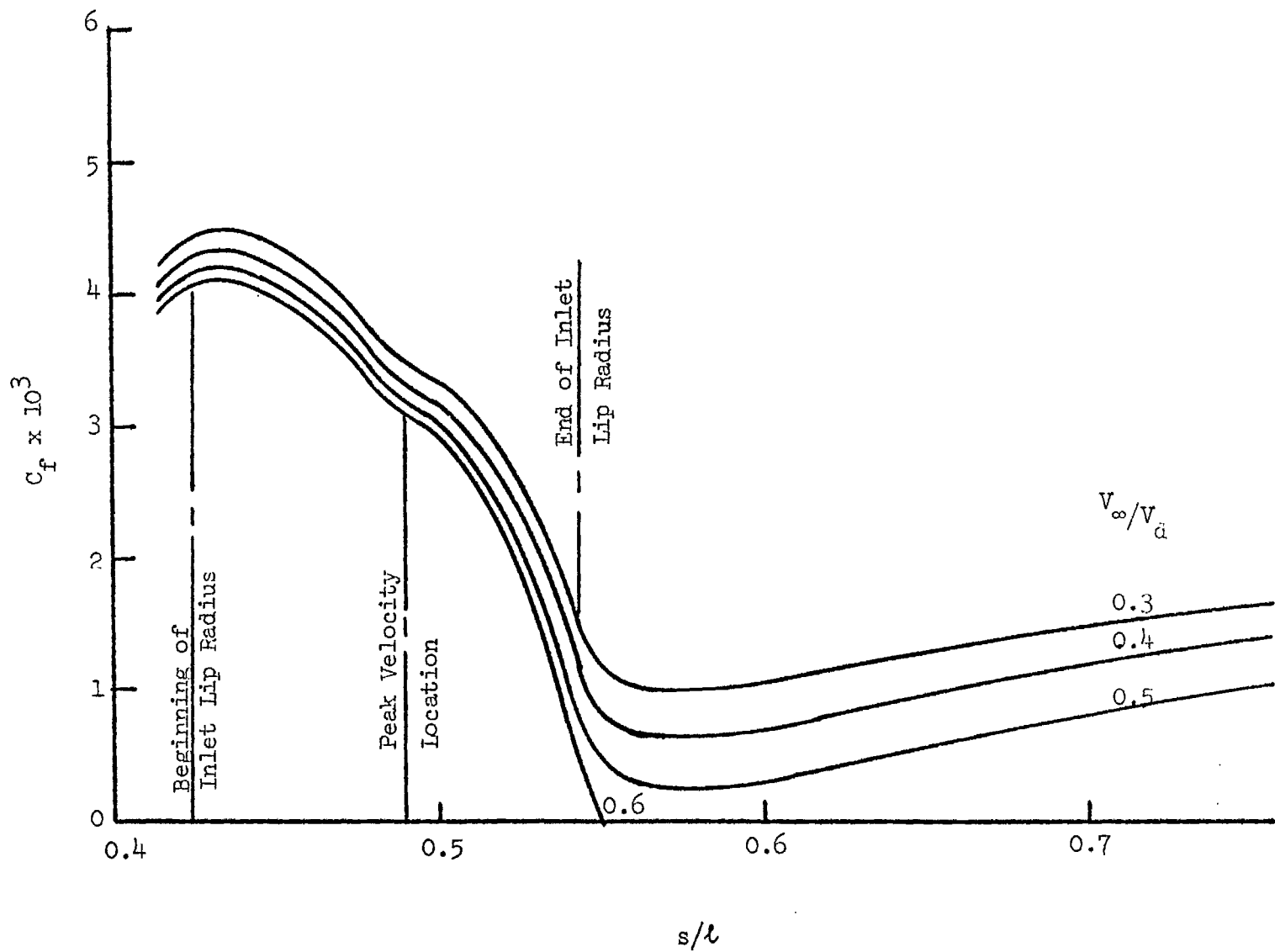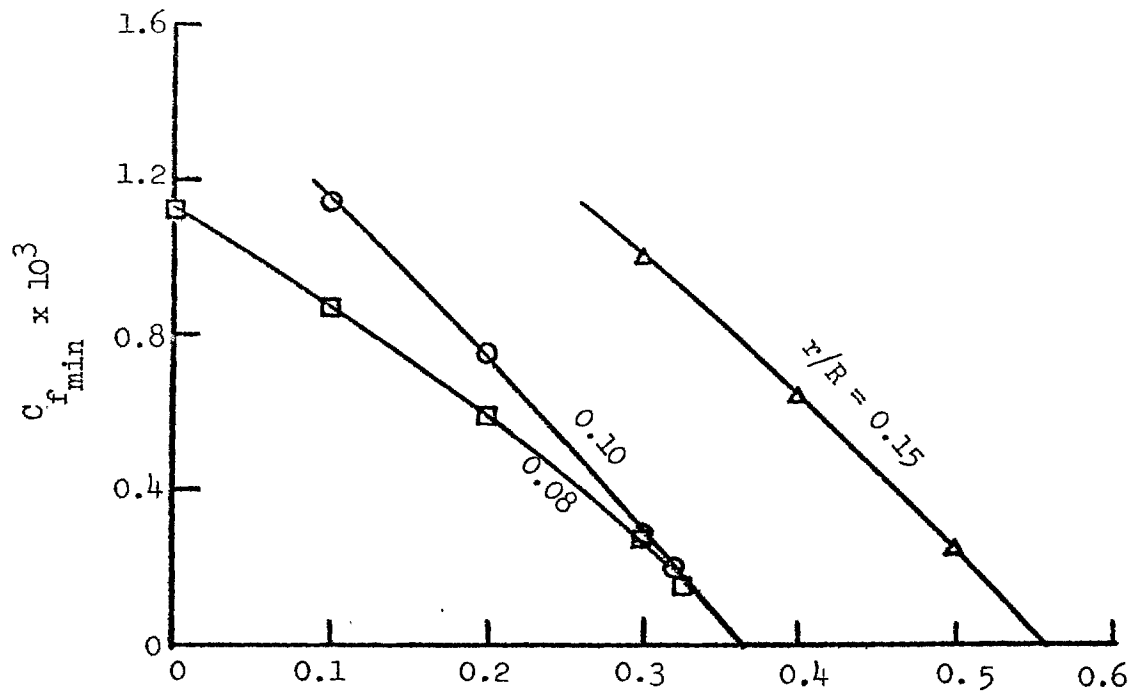
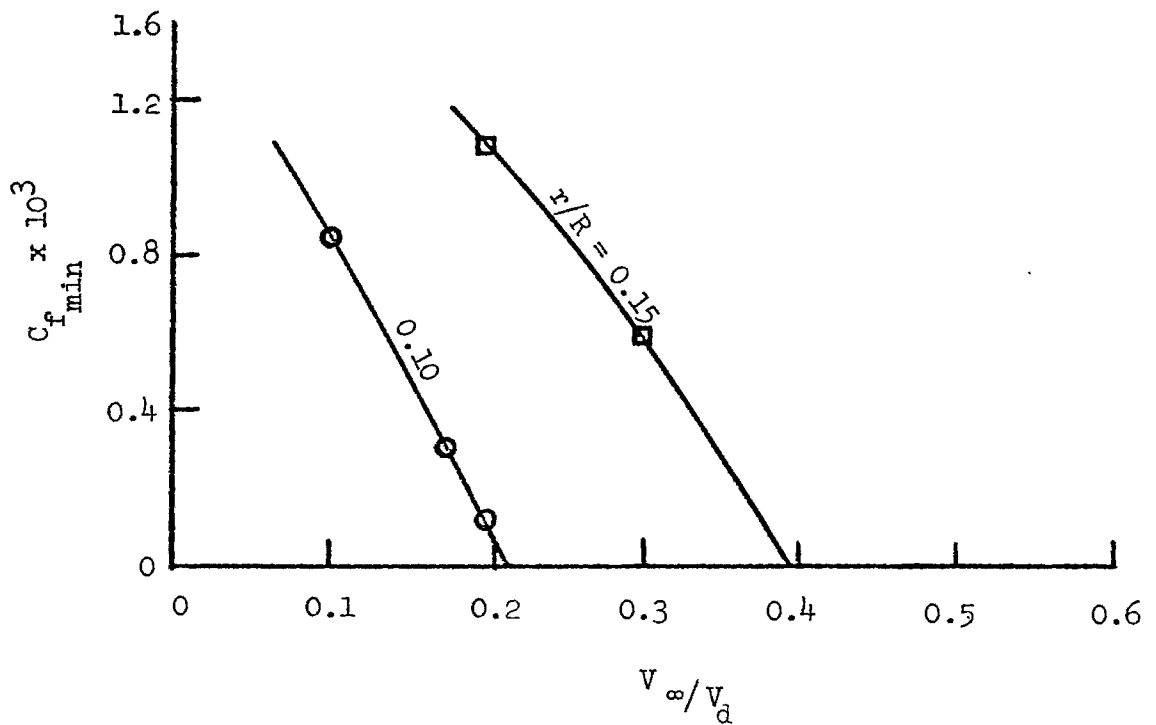Figure 18. Geometric Model for Boundary Layer Analysis

Figure 19. Variation in Friction Coefficient Along the Inlet Surface Forward Inlet Section; $r/R = 0.15$; $M_d = 0.46$; $Re_l = 14.8 \times 10^6$

a. $\mathrm{Re}_{\ell} = 14.8 \times 10^6$; $\mathrm{M_d} = 0.46$

b. $\mathrm{Re}_{\ell} = 3.17 \times 10^6$; $\mathrm{M_d} = 0.09$

Figure 20. Minimum Friction Coefficients Forward Inlet
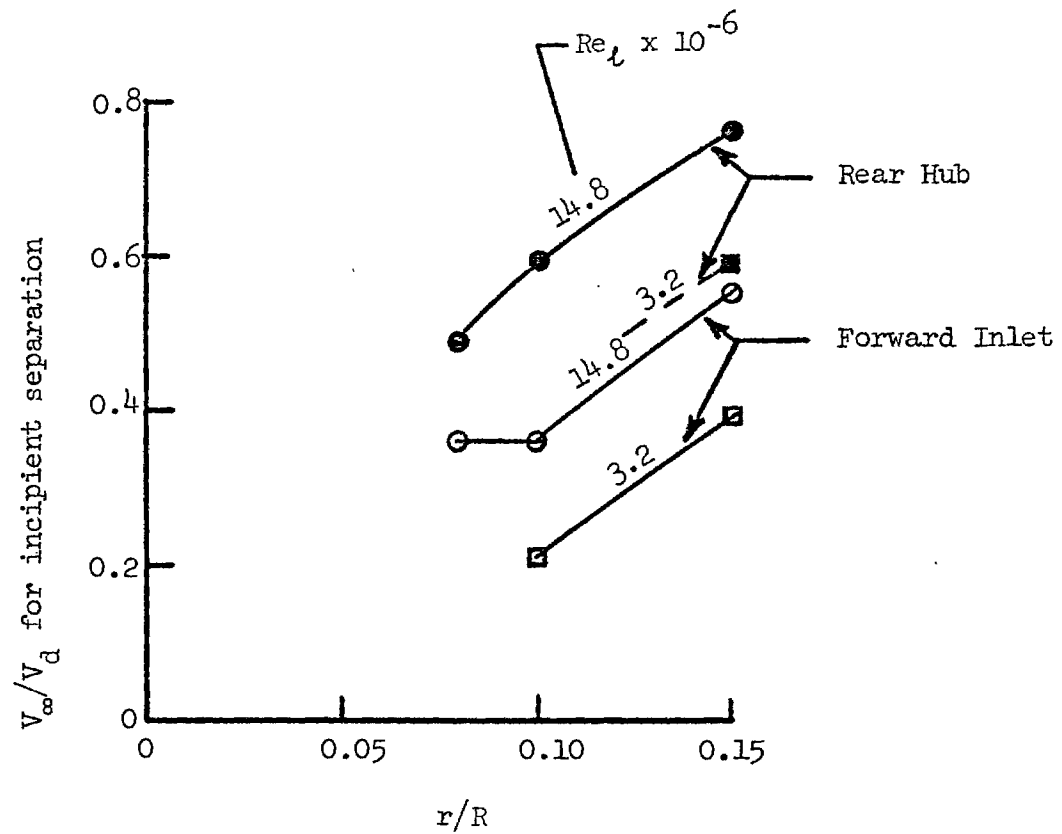Section

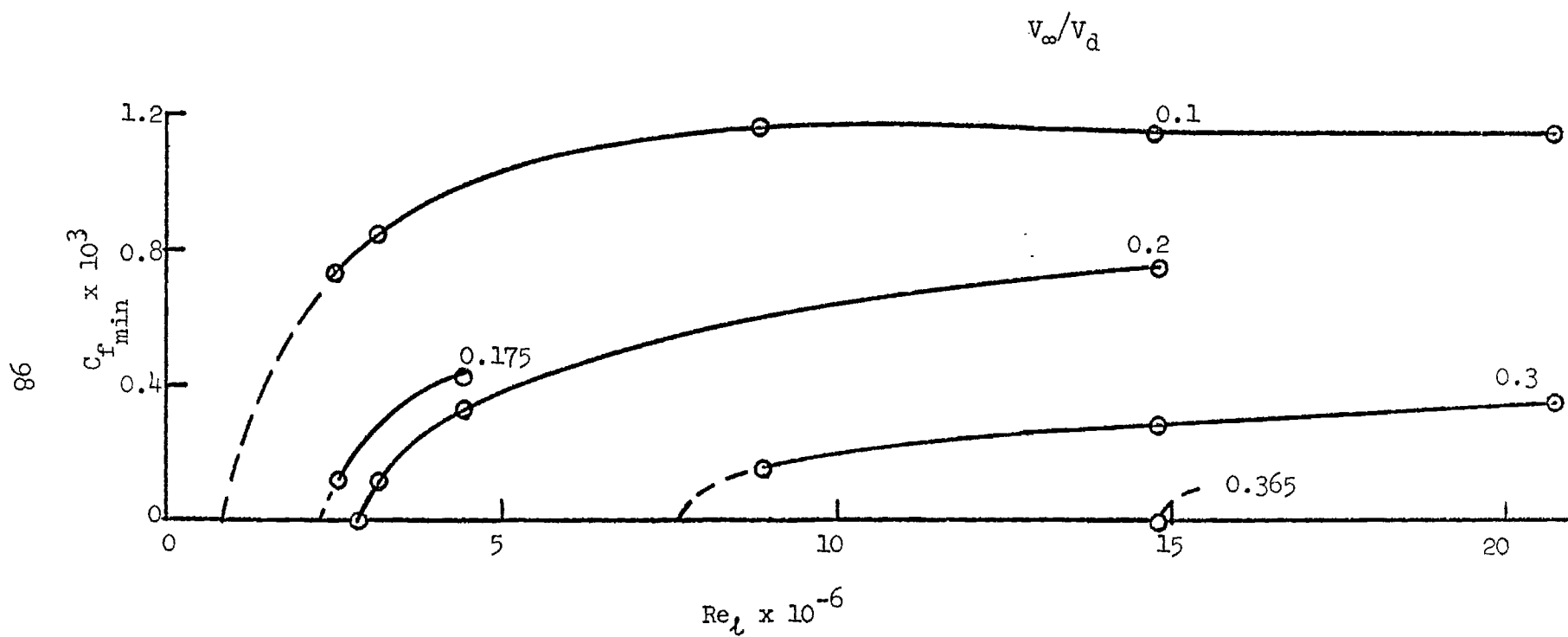Figure 21. Effects of Inlet Lip Radius on Velocity Ratio for Incipient Separation.

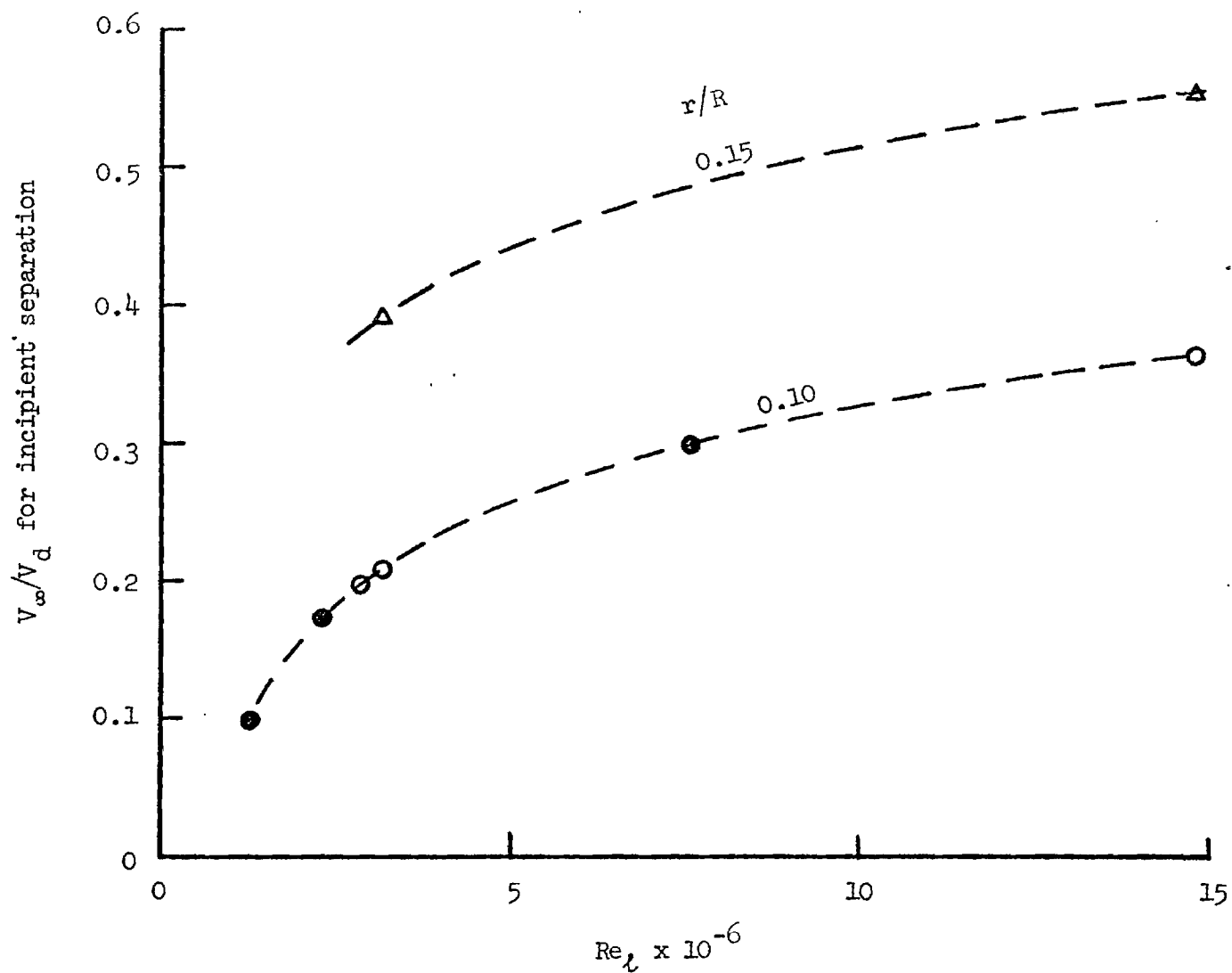Figure 22. Effects of Reynolds Number on the Minimum Friction Coefficient. Forward Inlet Section: r/R = 0.1

Figure 23. Effects of Reynolds Number on the Velocity Ratio for Incipient Separation Forward Inlet Section.

Exact Expressions for the Velocity Due to a Cylindrical Source Segment
of Constant Strength and Constant Radius.

In the cylindrical coordinate system (x,r,θ) the axial component of
the velocity induced by a cylindrical source segment of constant surface
source strength located at $r = \rho$, $\xi_1 \leq x \leq \xi_2$ is

$$u(x,r) = \sigma\rho \int_0^{2\pi} \int_{\xi_1}^{\xi_2} \frac{(x-\xi)d\xi d\theta}{[(x-\xi)^2 + r^2 + \rho^2 - 2r\rho \cos \theta]^{3/2}} \quad (A.1)$$

where σ is the source strength per unit area of the cylindrical segment.

Performing the integration with respect to ξ gives

$$u(x,r) = \sigma\rho \int_0^{2\pi} \left\{ \frac{1}{[(x-\xi_2)^2 + r^2 + \rho^2 - 2r\rho \cos \theta]^{1/2}} \right.$$

$$\left. - \frac{1}{[(x-\xi_1)^2 + r^2 + \rho^2 - 2r\rho \cos \theta]} \right\} d\theta \quad (A.2)$$

Using the change of variable $\theta = 2\beta$ and noting that the integrand in equation
(A.2) is symmetric in the interval $0 \leq \beta \leq \pi$ with respect to $\beta = \pi/2$ gives
the result

$$u(x,r) = 4\rho\sigma \left\{ \frac{1}{[(x-\xi_2)^2 + (r+\rho)^2]} \int_0^{\pi/2} \frac{d\beta}{\sqrt{1 - k_2^2 \sin^2\beta}} \right.$$

$$\left. - \frac{1}{[(x-\xi_1)^2 + (r+\rho)^2]} \int_0^{\pi/2} \frac{d\beta}{\sqrt{1 - k_1^2 \sin^2\beta}} \right\}$$

$$u(x,r) = 4\sigma\rho \left\{ \frac{K(k_2)}{[(x-\xi_2)^2 + (r+\rho)^2]} - \frac{K(k_1)}{[(x-\xi_1)^2 + (r+\rho)^2]} \right\} \tag{A-3}$$

where K is the complete elliptic integral

$$k_2^2 = \frac{4r\rho}{(x-\xi_2)^2 + (r+\rho)^2} \tag{A.4}$$

and

$$k_1^2 = \frac{4r\rho}{(x-\xi_1)^2 + (r+\rho)^2} \tag{A.5}$$

It can be easily shown that, at the mid-point of the segment, equation (A.3) gives

$$u\left(\frac{\xi_2 + \xi_1}{2}, \rho\right) = 0 \tag{A.6}$$

The radial component of velocity due to this cylindrical source segment is

$$v(x,r) = \sigma\rho \int_0^{2\pi} \int_{\xi_1}^{\xi_2} \frac{(r-\rho \cos \theta)d\xi d\theta}{[(x-\xi)^2 + r^2 + \rho^2 - 2r\rho \cos \theta]^{3/2}} \tag{A.7}$$

Performing the integration with respect to ξ gives

$$v(x,r) = -\sigma\rho \left\{ \int_0^{2\pi} \frac{(x-\xi_2)(r-\rho \cos \theta)d\theta}{[r^2+\rho^2-2r\rho \cos \theta]\sqrt{(x-\xi_2)^2+r^2+\rho^2-2r\rho \cos \theta}} \right.$$

$$\left. - \int_0^{2\pi} \frac{(x-\xi_1)(r-\rho \cos \theta)}{[r^2+\rho^2-2r\rho \cos \theta]\sqrt{(x-\xi_1)^2+r^2+\rho^2-2r\rho \cos \theta}} \right\} \tag{A.8}$$

101

Using the change of variables $\theta = 2\beta$ and noting that the integrand is symmetric with respect to $\beta = \pi/2$ in the interval $0 \leq \beta \leq \pi$, yields

$$v(x,r) = -4\sigma\rho \left\{ (x-\xi_2) \int_0^{\pi/2} \frac{(r+\rho-2\rho \cos^2\beta)d\beta}{[(r+\rho)^2-4r\rho \cos^2\beta]\sqrt{(x-\xi_2)^2+(r+\rho)^2-4r\rho \cos^2\beta}} \right.$$

$$\left. - (x-\xi_1) \int_0^{\pi/2} \frac{(r+\rho-2\rho \cos^2\beta)d\beta}{[(r+\rho)^2-4r\rho \cos^2\beta]\sqrt{(x-\xi_1)^2+(r+\rho)^2-4r\rho \cos^2\beta}} \right\} \quad (A.9)$$

Using the definition

$$n = \frac{4r\rho}{(r+\rho)^2} \qquad (A.10)$$

equation (A.9) is written as follows

$$v(x,r) = -\frac{2\sigma\rho}{r(r+\rho)^2} \left\{ \frac{(x-\xi_2)}{\sqrt{(x-\xi_2)^2 + (r+\rho)^2}} \right.$$

$$\times \left[(r^2-\rho^2) \int_0^{\pi/2} \frac{d\beta}{[1-n \cos^2\beta]\sqrt{1-k_2^2\cos^2\beta}} \right.$$

$$\left. + (r+\rho)^2 \int_0^{\pi/2} \frac{d\beta}{\sqrt{1-k_2^2\cos^2\beta}} \right] - \frac{(x-\xi_1)}{\sqrt{(x-\xi_1)^2+(r+\rho)^2}}$$

$$\times \left[(r^2-\rho^2) \int_0^{\pi/2} \frac{d\beta}{[1-n \cos^2\beta]\sqrt{1-k_1^2\cos^2\beta}} \right.$$

$$\left. \left. + (r+\rho)^2 \int_0^{\pi/2} \frac{d\beta}{\sqrt{1-k_1^2\cos^2\beta}} \right] \right\} \qquad (A.11)$$

102

This can be written in terms of $K(k)$, the complete elliptic integral of the first kind, and $\Pi(n\backslash k)$, the complete elliptic integral of the third kind, as follows

$$v(x,r) = - \frac{2\sigma\rho}{r(r+\rho)^2} \left\{ \frac{(x-\xi_2)}{\sqrt{(x-\xi_2)^2+(r+\rho)^2}} \left[(r^2-\rho^2)\Pi(n\backslash k_2)+(r+\rho)^2 K(k_2) \right] \right.$$

$$\left. - \frac{(x-\xi_1)}{\sqrt{(x-\xi_1)^2+(r+\rho)^2}} \left[(r^2-\rho^2)\Pi(n\backslash k_1)+(r+\rho)^2 K(k_1) \right] \right\} \qquad (A.12)$$

It is convenient to express $\Pi(n\backslash k)$ in terms of Heuman's Lambda function and the complete elliptic integral of the first kind by the use of the relation

$$\Pi(n\backslash k) = K(k) + \frac{\pi}{2} \delta_2 \left[1 - \Lambda_o (\epsilon\backslash k) \right] \qquad (A.13)$$

where

$$\epsilon = \sin^{-1} \left[\frac{1 - n}{1 - k^2} \right]^{1/2} \qquad (A.14)$$

$$\delta_2 = \left[\frac{n}{(1 - n)(n - k^2)} \right]^{1/2} \qquad (A.15)$$

With these substitutions, equation (A.12) is re-written as

$$v(x,r) = - \frac{\sigma\rho}{r} \left\{ \frac{4r(x-\xi_2)K(k_2)}{(r+\rho)\sqrt{(x-\xi_2)^2+(r+\rho)^2}} + \pi \frac{(x-\xi_2)(r-\rho)}{|x-\xi_2||r-\rho|} [1-\Lambda_o(\epsilon_2\backslash k_2)] \right.$$

$$\left. - \frac{4r(x-\xi_1)K(k_1)}{(r+\rho)\sqrt{(x-\xi_1)^2+(r+\rho)^2}} - \pi \frac{(x-\xi_1)(r-\rho)}{|x-\xi_1||r-\rho|} [1-\Lambda_o(\epsilon_1\backslash k_1)] \right. \qquad (A.16)$$

103

For exterior flow $(r \to \rho^+)$ the radial component of the velocity at the mid-point of the cylindrical segment is

$$v\left(\frac{\xi_2 + \xi_1}{2}, \rho\right) = \frac{2(\xi_2 - \xi_1)\, \sigma K(k)}{\sqrt{4\rho^2 + \frac{(\xi_2 - \xi_1)^2}{4}}} + 2\pi\sigma \qquad (A.17)$$

where

$$k^2 = \frac{4\rho^2}{4\rho^2 + \frac{(\xi_2 - \xi_1)^2}{4}}$$

The term $2\pi\sigma$ was predicted by Kelloggs theory.